

Diss. ETH No. 16357

*Comparative Investigation of  
Mathematical Methods for  
Modeling and Optimization of  
Common-Rail DI Diesel Engines*

A thesis submitted to the  
SWISS FEDERAL INSTITUTE OF TECHNOLOGY  
ZURICH  
for the degree of  
DOCTOR OF TECHNICAL SCIENCES

presented by  
MARCO WARTH  
Dipl. Masch.-Ing. ETH Zürich

born April 10, 1976  
Citizen of Ruswil and Gunzwil, LU

Accepted of the recommendation of  
Prof. Dr. K. Boulouchos, examiner  
Prof. Dr. Ph. Rudolf von Rohr, co-examiner

2005



# 非凡な道程へ 温故知新の心

*“To walk uncommon paths,  
one has to know the old ways  
and seek for the new ones.”*

Japanese Proverb



# *ACKNOWLEDGMENTS*

This thesis was written during my work as a research associate with the Aerothermochemistry and Combustion Systems Laboratory (LAV) at the Swiss Federal Institute of Technology in Zurich.

Above all, I would to thank Prof. Dr. Konstantinos Boulouchos - who has both promoted my interest in this topic and guided my work - for his interest, his support and for our various motivating discussions. My gratitude also goes to Prof. Dr. Philipp Rudolf von Rohr for his interest in this work and for his time and efforts acting as co-examiner.

I would also like to thank Peter Obrecht for the excellent collaboration during the development and implementation of the phenomenological models.

For providing me with a unique set of experimental engine data, the generosity and support of Dr. Andrea Bertola, Klaus Heim, Dr. German Weisser, and Dr. Georgios Bikas are greatly appreciated.

Last but not least, special thanks go to:

- Pat Kirchen for both the scientific and personal discussions, the expert proofreading of this thesis and for teaching me the canadian way of life,
- Daniel Fritsche and Dr. Marc Füre for being comrades in arms - and mind - for the past three years,
- all the colleagues from LAV for the good collaboration,
- “Rusmu & Sorsi fürs Verständnis, d’Onderschtötzig ond s’Bänzin im Bluet”
- and all those not mentioned here, who are in my mind for contributing, in any way, to the success of this work.

Marco Warth

Zurich, October 2005



# *ABSTRACT*

In the following work, a phenomenological/knowledge based model and a “black-box” approach for the simulation and optimization of Common-Rail DI diesel engines are developed and comparatively evaluated. The evaluation, which is carried out for a comprehensive sample of engines and operating conditions, focuses on the ability of both approaches to yield predictive measures of the in-cylinder combustion process, as well as the engine out exhaust emissions.

The phenomenological/knowledge based model expands an existing, simple, yet physically and chemically accurate model by implementing Evolutionary Algorithms to calibrate the model parameters. As is shown through comprehensive investigations using measurements from an automotive, a heavy-duty, and a two-stroke marine diesel engine, the new models are able to determine the qualitative and quantitative Rates Of Heat Release (ROHR), nitrogen oxide and soot emissions across an entire engine operating map within a matter of seconds. To evaluate the general applicability of the model, a version of the model calibrated to one engine (for example the heavy-duty engine) is directly applied to another engine (for example the marine diesel engine), without recalibrating the model parameters. For such a “blind try” investigation, it is seen that because the phenomenological model considers the appropriate physical and chemical processes, it is capable of providing extrapolative predictions.

In addition to evaluating the model based on a comparison of calculations and measurements from applied combustion systems, a detailed investigation of the model itself is carried out. In particular, a sensitivity analysis of the model specific parameters and statistical analyses are used to evaluate the modeling and optimization performance of the model. From such an analysis of the ROHR model, it is shown, among other things, that: (i) the accuracy of the model depends on the calibration algorithm, (ii) there are only negligible differences due to stochastic parameter initialization when using Evolutionary Algorithms, and (iii) the chemical and physical effects seen during the implementation of alternative fuels, such as diesel-water emulsions and diesel-butylal blends are correctly represented by the ROHR sub-model. Furthermore, from the detailed analysis of the emission models, a larger sensitivity of the model to small parameter changes is seen, as is a general influence of the operating conditions on the model accuracy.

Based on a comparison of engine variables, such as the cylinder pressure and temperature, nitrogen oxide and soot emissions, determined from measurement and simulation results, the ability of the phenomenological model to predict the combustion and emission formation processes is unambiguously verified. Although a wide range of engine operating conditions are considered in this comparison, only small

---

deviations (less than 10 %) are seen between the measured and calculated engine variables, with the exception of the maximum rate of pressure rise.

As an alternative to the phenomenological/knowledge based model approach, an Artificial Neural Network (ANN) is also investigated as a representative “black-box” approach. From a comparison of these two approaches, based on their abilities to predict ROHR parameters, nitrogen oxide and soot emissions, it is seen, that the ANN is more easily adapted to different engine configurations and provides better agreement with the measured calibration (i.e. training) data. However, when the models are used to predict the ROHR characteristics and exhaust emissions for operating conditions to which they were not trained, the ANN is not able to match the extrapolative ability of the phenomenological/knowledge based model, which provides better agreement with the measured values.

As is shown through the comparison of the two approaches, the phenomenological/knowledge based model and ANN have different strengths and weaknesses, and depending on the intended application, one approach will have distinct advantages over the other. The decision as to which approach is better suited will be based, in part, on the available experimental data, the overall knowledge of the system being considered, the time available for the investigation (both for the actual calculations and the development of the approach), as well as the necessity for extrapolative calculations. The phenomenological/knowledge based model approach is preferred when qualitative predictions based on fundamental knowledge are essential, while the ANN is preferred when the fast analysis of comprehensive experimental measurements, without fundamental knowledge of the physical and chemical processes, is required. Overall, the more general applicability, the more consistent qualitative results, and the possibility for extrapolative investigations make the phenomenological/knowledge based approach the more appropriate choice for the majority of applications, particularly for future engine developments.



# ZUSAMMENFASSUNG

Gegenstand der vorliegenden Arbeit ist die Herleitung und vergleichende Untersuchung eines modell-/wissensbasierten und eines “black-box” Ansatzes zur innermotorischen Simulation und Optimierung der Verbrennung sowie Schadstoffentstehung in direkt eingespritzten Common-Rail Diesel Motoren. Die hierzu entwickelten Ansätze und Modelle werden für eine umfangreiche Palette von unterschiedlichen Motoren und Betriebszustände angewandt.

Der neu entwickelte, modell-/wissensbasierte Ansatz baut auf einfachen, jedoch physikalisch und chemisch korrekten phänomenologischen Modellen auf, welche mittels evolutionärer Algorithmen kalibriert werden. Wie in umfangreichen Untersuchungen an einem Automobil-, einem Nutzfahrzeug-, und einem Schiffsantrieb erfolgreich gezeigt werden konnte, erlaubt der Ansatz die kennfeldweite, qualitative und quantitative Berechnung von Brennverläufen, Stickoxid- und Russmissionen innerhalb weniger Sekunden. Anhand von sogenannten “blinden Versuchen”, in welchen kalibrierte Modelle eines Motors ohne Anpassung der Parameter auf einen anderen Motor übertragen wurden (z.B. das für den Nutzfahrzeugmotor kalibrierte Brennverlaufsmodell wird zur Berechnung des Schiffsantriebs verwendet), konnte des weiteren gezeigt werden, dass die Verwendung geeigneter physikalisch/chemisch basierter Modelle selbst extrapolative Abschätzungen ermöglicht.

Neben den stark anwendungsorientierten Vergleichen von experimentellen und berechneten Kenngrößen für die jeweiligen Betriebspunkte wurden für alle Modelle auch detaillierte Untersuchungen (z.B. Parameter Sensitivitätsstudien) und statistische Analysen zu speziellen Modellierungs- und Optimierungsaspekten durchgeführt. Die detaillierte Analyse der Brennverlaufsmodellierung ergab dabei unter anderem eine differenzierte Abhängigkeit der Modellqualität von verschiedenen Kalibrierungsalgorithmen, vernachlässigbare Abweichungen aufgrund stochastischen Parameterinitialisierung bei evolutionären Algorithmen, sowie die korrekte Abbildung der physikalischen und chemischen Einflüsse unterschiedlicher Kraftstoffe wie Diesel-Wasser-Emulsionen oder Diesel-Butylal-Gemische. Am Beispiel der Schadstoffmodellierungen konnten ferner stark unterschiedliche Sensitivitäten der Modelle sowohl bei geringen Parameteränderungen, als auch zwischen verschiedenen Betriebspunkten im Allgemeinen, gezeigt werden.

Mittels eines Vergleichs von experimentell und numerisch ermittelten Motorprozessgrößen, wie zum Beispiel Zylinderdruck und -temperatur, Stickoxid und Russ Emissionen, wird das Potential der phänomenologischen Modelle zur Vorausberechnung motorischer Vorgänge anschaulich aufgezeigt. Über alle Betriebspunkte gesehen weisen dabei die betrachteten Kenngrößen, mit Ausnahme der maximalen Druckerhöhungen, lediglich Fehler im tiefen einstelligen Prozentbereich auf.

---

Als Gegenstück zur Untersuchung des modell-/wissensbasierten Ansatzes werden in dieser Arbeit künstliche Neuronale Netze (engl.: Artificial Neural Networks ANN), als "Schulbeispiel" für black-box Ansätze, verwendet. Am Beispiel der Modellierung und Simulation, bzw. Training und Verifikation, der Brennverlauf-scharakteristika, Stickoxid- und Russemissionen konnten sowohl eine exzellente Adaptierbarkeit der Netze für alle Motor und Modell Kombinationen, wie auch eine reduzierte Extrapolierbarkeit der trainierten Netze nachgewiesen werden. Während die Abweichungen zwischen den experimentellen und simulierten Ergebnissen für trainierte Betriebspunkte deutlich geringer ausfielen als bei den phänomenologischen Modellen, verhielt es sich bei der Verifikation, bzw. Extrapolation der Betriebspunkte gerade umgekehrt, d.h. es kommt zu einer signifikanten Verminderung der Qualität der simulierten Ergebnisse bei den künstliche Neuronalen Netzen.

Wie durch den Vergleich der beiden Ansätze gezeigt werden kann, verfügen sowohl der modell-/wissensbasierte als auch der black-box Ansatz über Stärken und Schwächen, welche abhängig vom Fokus der Untersuchung, den Ausschlag für den einen beziehungsweise anderen Ansatz geben. Die Entscheidung welcher Ansatz letztendlich besser geeignet ist, ist dabei unter anderem abhängig von den verfügbaren experimentellen Daten, den Kenntnissen vom betrachteten System, den zeitlichen Rahmenbedingungen (sowohl für die Entwicklung des Ansatzes, als auch die eigentlichen Berechnungen), und der Notwendigkeit von extrapolativen Berechnungen. Der modell-/wissensbasierte Ansatz eignet sich für qualitativ zuverlässige Vorhersagen basierend auf fundiertem Wissen, während der black-box Ansatz für schnelle Analysen von umfangreichen experimentellen Daten ohne fundierte Kenntnisse zu den physikalisch/chemischen Zusammenhängen anbietet. Die breitere Anwendbarkeit, sowie die qualitativ konstanteren Resultate und die Möglichkeit der Extrapolation der Berechnungen lassen für die meisten Anwendungen eine Präferenz hin zu wissensbasierten Modellen erkennen.

# *TABLE OF CONTENTS*

<b>ACKNOWLEDGMENTS</b> .....	<b>V</b>
<b>ABSTRACT</b> .....	<b>VII</b>
<b>ZUSAMMENFASSUNG</b> .....	<b>IX</b>
<b>TABLE OF CONTENTS</b> .....	<b>XI</b>
<b>LIST OF FIGURES</b> .....	<b>XV</b>
<b>LIST OF TABLES</b> .....	<b>XIX</b>
<b>NOMENCLATURE</b> .....	<b>XXI</b>
<b>1 INTRODUCTION</b> .....	<b>1</b>
1.1 Motivation and Objectives .....	1
1.2 Common-Rail DI Diesel Engines .....	2
1.2.1 Combustion Analysis and Modeling .....	3
1.2.2 Exhaust Emissions .....	3
1.2.3 Optimization .....	3
1.3 Approach .....	4
<b>2 STATE-OF-THE-ART</b> .....	<b>5</b>
2.1 Internal Combustion Engine Modeling .....	5
2.1.1 Empirical or Thermodynamic Models .....	5
2.1.2 Phenomenological Models .....	7
2.1.3 Detailed or Complex Models .....	8
2.2 Artificial Neural Networks .....	10
2.3 Design of Experiments (DoE) .....	12
2.4 Optimization .....	13
2.4.1 “Classic” Methods .....	14
2.4.2 “Evolutionary Computation” Algorithms .....	15
<b>3 APPROACHES AND EQUIPMENT</b> .....	<b>17</b>
3.1 System & Objectives .....	17
3.2 “Model/Knowledge Based” Approach .....	17
3.2.1 “Modeling/Optimization” Scheme .....	18
3.2.2 Application Examples .....	18
3.2.2.1 Thermodynamic Modeling .....	19
3.2.2.2 Polymer Electrolyte Fuel Cell Modeling .....	19

---

3.3	“Black-Box” Approach .....	19
3.3.1	“Artificial Neural Network” Scheme .....	20
3.4	Computational Setup .....	21
3.4.1	Thermodynamic Analysis & Simulation .....	21
3.4.2	Artificial Neural Networks .....	22
3.4.3	Optimization Algorithms .....	22
3.5	Experimental Setup .....	26
3.5.1	Engines .....	26
3.5.2	Measurement Techniques .....	28
<b>4</b>	<b>RATE OF HEAT RELEASE .....</b>	<b>31</b>
4.1	Model Description .....	31
4.1.1	Inputs & Outputs .....	32
4.1.2	Evaporation & Spray Formation .....	33
4.1.3	Ignition Delay(s) & Fuel Allocation .....	34
4.1.4	Pre-Mixed Combustion .....	35
4.1.5	Diffusion Controlled Combustion .....	36
4.1.6	Parameters .....	37
4.2	Model Parameter Sensitivity Study .....	37
4.3	Comparative Algorithm Study .....	40
4.3.1	Basic Setup .....	40
4.3.2	Algorithm Performance .....	41
4.3.3	Stochastic Initialization & Evolution .....	42
4.3.4	Summary .....	43
4.4	Model Study on Different Engine Sizes .....	43
4.4.1	“Heavy-Duty” Diesel .....	43
4.4.2	“Automotive” Diesel .....	47
4.4.3	“Marine” Diesel .....	49
4.5	Advanced Fuels Survey .....	51
4.6	Conclusions .....	53
<b>5</b>	<b>EMISSIONS OF NITROGEN OXIDE .....</b>	<b>55</b>
5.1	Model Description .....	55
5.1.1	Inputs & Outputs .....	56
5.1.2	Variable Virtual Combustion Zones .....	56
5.1.3	Reaction Mechanism .....	57
5.1.4	Kinetics of NO Formation .....	58
5.2	Model Parameter Sensitivity Study .....	58
5.3	Model Study on Different Engine Sizes .....	59
5.3.1	“Heavy-Duty” Diesel .....	60
5.3.2	“Automotive” Diesel .....	61
5.3.3	“Marine” Diesel .....	63
5.4	Conclusions .....	64

---

<b>6</b>	<b>SOOT EMISSION</b> .....	<b>67</b>
6.1	Model Description .....	67
6.1.1	Inputs & Outputs .....	67
6.1.2	“Two Step - Two Zone” Approach .....	68
6.2	Model Parameter Sensitivity Study .....	70
6.3	Model Study on Different Engine Sizes .....	71
6.3.1	“Heavy-Duty” Diesel .....	71
6.3.2	“Automotive” Diesel .....	72
6.3.3	“Marine” Diesel .....	74
6.4	Conclusions .....	75
<b>7</b>	<b>ENGINE PROCESS SIMULATIONS</b> .....	<b>77</b>
7.1	Setup .....	77
7.2	Simulations .....	78
7.2.1	Cylinder Pressure and Temperature .....	78
7.2.2	Combustion Characteristics .....	80
7.2.3	Emissions .....	82
7.3	Conclusions .....	83
<b>8</b>	<b>ARTIFICIAL NEURAL NETWORKS</b> .....	<b>85</b>
8.1	Comparative Study Setup .....	85
8.2	Rate of Heat Release .....	85
8.2.1	“Heavy-Duty” Diesel .....	86
8.2.2	“Marine” Diesel .....	88
8.3	Nitrogen Oxide & Soot Emissions .....	89
8.3.1	“Heavy-Duty” Diesel .....	89
8.3.2	“Marine” Diesel .....	90
8.3.3	“Automotive” Diesel .....	92
8.4	Conclusions .....	93
<b>9</b>	<b>CONCLUSIONS AND OUTLOOK</b> .....	<b>95</b>
9.1	Summary & Conclusions .....	95
9.2	Outlook .....	96
	<b>REFERENCES</b> .....	<b>99</b>
<b>A</b>	<b>APPENDIX</b> .....	<b>107</b>
A.1	Operating Conditions .....	107
A.1.1	“Automotive” Diesel .....	107
A.1.2	“Heavy-Duty” Diesel .....	109
A.1.3	“Marine” Diesel .....	111
A.2	Kinetics of NO Formation .....	112
A.3	Correlation & Linear Regression Statistics .....	113
A.4	Cylinder Pressures .....	114
	<b>CURRICULUM VITAE</b> .....	<b>115</b>



# LIST OF FIGURES

## 1 INTRODUCTION

## 2 STATE-OF-THE-ART

Fig. 2.1	Control Volume as Used in Single-Zone Cylinder Models.....	6
Fig. 2.2	Model of an Artificial Neuron With Interconnections .....	10
Fig. 2.3	Schematic Diagrams of (a) Multi-Layer Feedforward Neural Network and (b) Simple Recurrent Neural Network.....	11
Fig. 2.4	Iterative Optimization Scheme of Optimizer & Analyzer.....	14

## 3 APPROACHES AND EQUIPMENT

Fig. 3.1	Modeling/Optimization Scheme .....	18
Fig. 3.2	Polymer Electrolyte Fuel Cell Modeling: (a) Sketch of a Single Plate Fuel Cell, (b) Comparison Plot between the Experimental and Simulated Current-Voltage Characteristics .....	19
Fig. 3.3	Artificial Neural Network Scheme .....	20
Fig. 3.4	Error Objective Function: (a) Standard Least Square Error (LSE), (b) LSE Including Tolerance Value .....	23
Fig. 3.5	Recombination Mechanisms: (a) Intermediate, (b) Extended Line Recombination (According to [76]).....	24
Fig. 3.6	Examples of Injection Profiles (Rate of Fuel Injected): (a) Automotive Split Injection Timing and Injection Profile, (b) Measured Heavy-Duty Single Injection Profile.....	28

## 4 RATE OF HEAT RELEASE

Fig. 4.1	Phenomenological Rate of Heat Release (ROHR) Model.....	31
Fig. 4.2	ROHR Characteristics: (a) Integral and (b) Detailed Premixed & Diffusion Controlled Combustion Characteristics .....	32
Fig. 4.3	ROHR Model Output Sensitivities to $\pm 5\%$ Variations of Injection & Evaporation Parameters: (a) Integral ROHR, (b), and (c) Detailed Premixed and Diffusion Controlled Combustion Characteristics. (d) Sensitivity of $Q_{\max}$ to $\pm 50\%$ Variations in $c_{\text{SMD}}$ , $\beta$ , and $A$ .....	39
Fig. 4.4	Comparison of Experimental and Numerical ROHR Characteristics for the CMA-ES Algorithm Model Calibration: (a) Sequential Operating Conditions Plot, (b) 1-to-1 Scatter Plot.....	40
Fig. 4.5	Comparison of the 4 Algorithms Used for the ROHR Model: (a) Performance Plot, (b) 1-to-1 Scatter Plot (Best vs. Worst Algorithm) .....	41
Fig. 4.6	Comparative Algorithm Study Statistics: (a) Person's Correlation Coefficient & Linear Regression Slope (b) $\phi_{50}$ 1-to-1 Plot .....	42

Fig. 4.7	Performance and Parameter Variations of 25 Optimization Runs: (a) Error vs. # Function Evaluations (b) Single Parameter Variation .....	43
Fig. 4.8	Heavy-Duty Diesel ROHR Model Calibration & Verification: (a) Sequential Operating Conditions Plot, (b) 1-to-1 Scatter Plot.....	44
Fig. 4.9	Examples (6 out of 39) of ROHR Traces for Heavy-Duty Engine .....	45
Fig. 4.10	Extended ROHR Characteristics for the Heavy-Duty Engine: (a) Ignition Delay, (b) Premixed Combustion Ratio, (c) Maximum ROHR and (d) Location of Maximum ROHR .....	46
Fig. 4.11	Automotive Diesel ROHR Model: Calibration & Verification.....	47
Fig. 4.12	Automotive Diesel Operating Conditions With Pilot- and Main-Injection Pulses: (a) # 3, (b) # 25.....	48
Fig. 4.13	Automotive Diesel ROHR: Heavy-Duty Model Blind Try.....	48
Fig. 4.14	Marine Diesel ROHR Model Calibration & Verification (a) Sequential Operating Conditions Plot, (b) 1-to-1 Scatter Plot.....	50
Fig. 4.15	Marine Diesel Engine ROHR Model: (a) Blind Try, (b) Adjusted .....	50
Fig. 4.16	Marine Engine Comparison of Three Model Parameter Sets: (a) Pearson's Correlation Coefficient & Linear Regression Slope, (b) Linear Regression Intercept .....	51
Fig. 4.17	Heavy-Duty Advanced Fuels ROHR Model Characteristics: (a) Calibration/Verification Operating Conditions Plot, (b) 1-to-1 Scatter Plot, (c) Fuel Operating Conditions Plot, (d) Model Errors.....	52
Fig. 4.18	Heavy-Duty Advanced Fuels Blind Try ROHR Characteristics: (a) Fuel Operating Conditions Plot, (b) Model Errors .....	53

## 5 EMISSIONS OF NITROGEN OXIDE

Fig. 5.1	Variable representative air/fuel ratio function and associated in-cylinder temperature trace for NO formation.....	56
Fig. 5.2	Operating Condition Specific Variations of NO <sub>x</sub> Model Sensitivities: (a) Point of Discontinuity Combustion Progress Parameters, (b) NO Formation Mechanism Reaction Rate Constants .....	59
Fig. 5.3	Mean (Operating Condition Averaged) NO <sub>x</sub> Model Sensitivities: (a) Normalized Variations of $\lambda_{end}$ , $c_{ROHR}$ , and $\zeta_{end}$ , (b) $\pm 5\%$ Step Size Parameter Variations.....	60
Fig. 5.4	Heavy-Duty Diesel NO <sub>x</sub> Model Calibration & Verification: (a) Sequential Operating Conditions Plot, (b) 1-to-1 Scatter Plot.....	60
Fig. 5.5	Heavy-Duty Single Operating Condition: (a) Pressure History and ROHR, (b) Representative Temperature and Mass of Nitric Oxide .....	61
Fig. 5.6	Automotive Diesel NO Model: Calibration & Verification .....	62
Fig. 5.7	Automotive NO Emissions: Heavy-Duty Model Blind Try .....	62
Fig. 5.8	Marine Diesel NO Model: Calibration & Verification.....	63
Fig. 5.9	Marine NO Emissions: Heavy-Duty Model Blind Try.....	64



---

## 6 SOOT EMISSION

Fig. 6.1	Representative Heavy-Duty Engine Operating Condition: (a) ROHR, (b) Soot Formed, Oxidized and Total Mass of Soot Histories .....	68
Fig. 6.2	Equivalence Ratio - Temperature Map for Soot Formation: (a) Original Akihama et al [2], (b) Mathematical Approximation .....	69
Fig. 6.3	Operating Condition Specific Sensitivities: (a) Oxidation Activation Temperature $T_{A,ox}$ and Scaling Factor $c_{ox}$ , (b) Soot Model Mean Sensitivities for $\pm 5\%$ Step Size Parameter Variations .....	70
Fig. 6.4	Heavy-Duty Diesel Soot Model Calibration & Verification: (a) Sequential Operating Conditions Plot, (b) 1-to-1 Scatter Plot.....	71
Fig. 6.5	Automotive Diesel Soot Model Calibration & Verification.....	72
Fig. 6.6	Automotive Soot Model: Variation of Engine Load.....	73
Fig. 6.7	Automotive Soot Emissions: Heavy-Duty Model Blind Try.....	73
Fig. 6.8	Marine Diesel Soot Model Calibration & Verification .....	74
Fig. 6.9	Marine Soot Emissions: Heavy-Duty Model Blind Try .....	75

## 7 ENGINE PROCESS SIMULATIONS

Fig. 7.1	Engine Process Simulation Comparative Study Setup .....	77
Fig. 7.2	Comparison of Cylinder Pressures and ROHRs (left side), Burned Gas and Mean Temperatures (right side) for Three Selected Heavy-Duty Diesel Operating Conditions; (a) # 2, (b) # 5, and (c) # 15 .....	79
Fig. 7.3	Comparison of Engine Process Simulation Characteristics: (a) Maximum Pressure and Location of Maximum Pressure, (b) Maximum Temperature and Maximum Mean Temperature .....	80
Fig. 7.4	Comparison of Cylinder Pressures and ROHRs (left side), Burn and Mean Temperatures (right side) for Operating Condition # 9 .....	81
Fig. 7.5	Comparison of Engine Process Simulation Characteristics (left side: Absolute Values, right side: According Relative Errors): (a) Maximum Pressure and Maximum Mean Temperature (b) Exhaust Pressure and Exhaust Temperature.....	81
Fig. 7.6	Comparison of Maximum Pressure Increase and Indicated Efficiency (left side: Absolute Values, right side: According Relative Errors).....	82
Fig. 7.7	Comparison of Nitrogen Oxide Emissions (left side: Absolute Values, right side: According Relative Errors).....	82

## 8 ARTIFICIAL NEURAL NETWORKS

Fig. 8.1	Comparison of Simulation Schemes (ANN vs. Modeling).....	85
Fig. 8.2	Training vs. Verification: Overfitting Criteria .....	85
Fig. 8.3	Heavy-Duty Diesel ROHR ANN Training & Verification: (a) Sequential Operating Conditions Plot, (b) 1-to-1 Scatter Plot.....	86
Fig. 8.4	Heavy-Duty ROHR ANN: Training vs. Verification.....	87
Fig. 8.5	Comparison of Heavy-Duty Engine ROHR Simulation Methods: (a) Artificial Neural Network, (b) Phenomenological Modeling .....	87

---

Fig. 8.6	Comparison of Marine Diesel Engine ROHR Simulation Methods: (a) Artificial Neuronal Network, (b) Phenomenological Modeling .....	88
Fig. 8.7	Comparison of Blind Try Marine Diesel Engine ROHR Simulations: (a) Artificial Neuronal Network, (b) Phenomenological Modeling .....	89
Fig. 8.8	Heavy-Duty Diesel Emissions ANN Training & Verification: (a) Nitrogen Oxide Emissions, (b) Soot Emissions .....	90
Fig. 8.9	Marine Diesel Nitrogen Oxide Emission Simulation: (a) ANN Sequential Operating Conditions Plot, (b) ANN 1-to-1 Scatter Plot, (c) ANN Blind Try, (d) Phenomenological Modeling Blind Try .....	91
Fig. 8.10	Automotive NO Emissions: (a) Measurements, (b) ANN Simulation.....	91
Fig. 8.11	Automotive NO Emissions: (a) 1-to-1 Plot of Training and Verification Operating Conditions, (b) NO Emission Residuals .....	92

## 9 CONCLUSIONS AND OUTLOOK

### A APPENDIX

Fig. A.1	Comparison of Measured and Numerical Cylinder Pressures for Six Selected Heavy-Duty Diesel Operating Conditions; (a) # 2, (b) # 4, (c) # 5, (d) # 9, (e) # 15, and (f) # 18 .....	114
----------	---	-----

# *LIST OF TABLES*

## **1 INTRODUCTION**

## **2 STATE-OF-THE-ART**

Tab. 2.1	Representative ANN Based Diesel Engine Modeling Studies .....	12
----------	---	----

## **3 APPROACHES AND EQUIPMENT**

Tab. 3.1	Computational Setup .....	21
Tab. 3.2	Artificial Neural Network (ANN) Characteristics .....	22
Tab. 3.3	Objective Functions used for the Model Calibration .....	23
Tab. 3.4	Genetic Algorithm Characteristics .....	24
Tab. 3.5	Evolutionary Algorithm Characteristics .....	25
Tab. 3.6	CMA Evolutionary Strategy Characteristics .....	25
Tab. 3.7	MATLAB GADS Toolbox Characteristics .....	26
Tab. 3.8	Engine and Injection System Specifications .....	27
Tab. 3.9	Overview of Operating Condition Ranges (Minimum .. Maximum) .....	27
Tab. 3.10	Approximate Values of Errors for the Heat Release Analysis Based on In-House Experience .....	29

## **4 RATE OF HEAT RELEASE**

Tab. 4.1	ROHR Model Parameters .....	38
Tab. 4.2	Heavy-Duty Engine ROHR Model Statistics .....	44
Tab. 4.3	Automotive Engine ROHR Model Statistics for the EA Optimized and the Heavy-Duty Blind Try Case .....	49
Tab. 4.4	Advanced Fuels Properties .....	52
Tab. 4.5	Heavy-Duty Advanced Fuels ROHR Model Statistics for the EA Optimized and the Heavy-Duty Blind Try Case .....	54

## **5 EMISSIONS OF NITROGEN OXIDE**

Tab. 5.1	Nitrogen Oxide Emission Model Parameters .....	57
Tab. 5.2	Heavy-Duty Engine Calibration & Verification Statistics .....	61
Tab. 5.3	Automotive Engine: Optimized vs. Blind Try Statistics .....	63
Tab. 5.4	Marine Engine Optimized vs. Blind Try Statistics .....	64

## **6 SOOT EMISSION**

Tab. 6.1	Soot Emission Model Parameters .....	69
Tab. 6.2	Heavy-Duty Soot Model: Calibration & Verification Statistics .....	72
Tab. 6.3	Variation of Engine Load Operating Condition Data .....	73
Tab. 6.4	Automotive Optimized vs. Blind Try Soot Model Statistics .....	74
Tab. 6.5	Marine Engine Optimized vs. Blind Try Statistics .....	75

---

## 7 ENGINE PROCESS SIMULATIONS

Tab. 7.1	GT-Power Characteristics .....	78
Tab. 7.2	Selected Operating Conditions Specifications (c.f. Figure 7.2) .....	78

## 8 ARTIFICIAL NEURAL NETWORKS

Tab. 8.1	Heavy-Duty ROHR ANN: Training vs. Verification .....	87
Tab. 8.2	Heavy-Duty Engine Pearson's Correlation Coefficients $r$ .....	87
Tab. 8.3	Marine Engine Pearson's Correlation Coefficients $r$ .....	88
Tab. 8.4	Heavy-Duty Diesel Specific Soot Emission Details .....	90

## 9 CONCLUSIONS AND OUTLOOK

### A APPENDIX

Tab. A.1	Automotive Diesel Operating Conditions .....	107
Tab. A.2	Heavy-Duty Diesel Operating Conditions .....	109
Tab. A.3	Heavy-Duty Advanced Fuels Survey Operating Conditions .....	110
Tab. A.4	Marine Diesel Operating Conditions .....	111
Tab. A.5	Rate Constants for the NO Formation Mechanism .....	112
Tab. A.6	Comparative Algorithm Study Statistics: ( $r$ ) Pearson's Correlation Coefficient, ( $m$ ) Linear Regression Slope, and ( $b$ ) Linear Regression Intercept .....	113
Tab. A.7	Marine Diesel Engine ROHR Model Statistics for the EA Optimized, the Heavy-Duty Blind Try, and the Adjusted Case .....	113

# NOMENCLATURE

## *Latin Variables and Symbols*

<i>A</i>	Area	$m^2$
<i>b</i>	Linear regression intercept	-
<i>c</i>	Scaling factor, velocity, speed	-, $m/s$ , $m/s$
<i>d</i>	Diameter	$m$
<i>f, F</i>	Function, Allocation function, time delay function	-
<i>H</i>	Heating Value	$MJ/kg$
<i>k</i>	Kinetic energy, reaction rate constants	$m^2/s^2$ , -
<i>l</i>	Length	$m$
<i>m</i>	Mass, linear regression slope	$kg$ , -
<i>n, N</i>	Number	-
<i>p</i>	Pressure	$Pa$
<i>Q</i>	Energy, Rate of Heat Release (ROHR)	$J$ , $J/^\circ CA$
<i>r</i>	Pearson's correlation coefficient	-
<i>s</i>	Speed	$m/s$
<i>t, T</i>	Time, Temperature	$s$ , $K$
<i>u</i>	Velocity	$m/s$
<i>V</i>	Volume	$m^3$
<i>x</i>	Model parameters	-
<i>y</i>	Model output characteristics	-
<i>Re</i>	Reynolds number	-
<i>#</i>	Number	-

## *Greek Variables and Symbols*

$\beta$	Evaporation rate	-
$\Delta$	Difference	-
$\zeta$	Burned mass fraction	-
$\lambda, \Lambda$	Air/fuel (equivalence) ratio	-
$\xi$	Ratio	-
$\eta$	Efficiency	-
$\rho$	Density	$kg/m^3$
$\tau$	Characteristic time	$s$
$\phi$	Fuel/air (equivalence) ratio	-
$\varphi$	Angle	$^\circ$
$\chi$	Sensitivity	-

---

## *Indices*

0	Start, steady-state condition
10	10 %
50	50 %
90	90 %
A	Activation
AF	Air/Fuel mixture
Chem	Chemical
Comb	Combustion
Cyl	Cylinder
Del	Delay
Diff	Diffusion (controlled combustion)
e	Equilibrium
EO	Exhaust Valve Open
Evap	Evaporation
Exh	Exhaust
form	Formation
g	Background
<i>i</i>	<i>i</i> <sup>th</sup> Element
Inj	Injection
lam	Laminar
max	Maximum
meas	Measurement
obj	Objective
oc	Operating condition
ox	Oxidation
Prmx	Premixed (combustion)
ref	Reference
s	Soot
sim	Simulation
st	Stoichiometric
tot	Total
turb	Turbulent
Vap	Vapor

---

## *Abbreviations*

<i>ANN</i>	Artificial Neural Network
<i>aTDC</i>	after Top Dead Center (gas exchange TDC = 0 [°CA])
<i>B60</i>	Diesel-Butylal Blend (60 % Butylal by Mass)
<i>CA</i>	Crank Angle
<i>CMA-ES</i>	Covariance Matrix Adaption Evolutionary Strategy
<i>CMC</i>	Conditional Moment Closure
<i>CPU</i>	Central Processing Unit
<i>DI</i>	Direct Injection
<i>DNS</i>	Direct Numerical Simulation
<i>DoE</i>	Design of Experiments
<i>E13</i>	Water-in-Diesel Fuel Emulsion (13 % Water by Mass)
<i>E21</i>	Water-in-Diesel Fuel Emulsion (21 % Water by Mass)
<i>EA</i>	Evolutionary Algorithm
<i>EGR</i>	Exhaust Gas Recirculation
<i>EP</i>	Evolutionary Programming
<i>EPA</i>	U.S. Environmental Protection Agency
<i>GA</i>	Genetic Algorithm
<i>GADS</i>	Genetic Algorithm & Direct Search
<i>HCCI</i>	Homogeneous Charge Compression Ignition
<i>IC</i>	Internal Combustion
<i>JANAF</i>	Joint Army - Navy - Air Force
<i>LAV</i>	Aerothermochemistry and Combustion Systems Laboratory
<i>LES</i>	Large Eddy Simulation
<i>LTC</i>	Low Temperature Combustion
<i>NIST</i>	U.S. National Institute of Standards & Technology
<i>PM</i>	Particulate Matter
<i>PAH</i>	Polycyclic Aromatic Hydrocarbons
<i>RANS</i>	Reynolds-Averaged Navier-Stokes
<i>R&amp;D</i>	Research and Development
<i>ROHR</i>	Rate of Heat Release
<i>s.f.</i>	Scaling Factor
<i>SMD</i>	Sauter Mean Diameter
<i>SOC</i>	Start Of Combustion
<i>SOI</i>	Start Of Injection
<i>WEG</i>	Wärme-Entwicklungs-Gesetz (Heat Release Analysis & Simulation)





# *1 INTRODUCTION*

More than a century after the first simple petrol engine was cranked, the technology which mobilized mankind on land, sea and in the air is on the edge of a period of new developments. There might not be a change in the basic principles of internal combustion engines, but the way the future engines are going to operate will be clearly different from the ones a decade, never mind a hundred years, ago.

Even though the major advances will be electronics empowered by microchips, the pace of this change has mainly been - and will continue to be - forced by consumption, emission and emotion (i.e. power output) requirements. In a world where client satisfaction and time to market are major factors, testing and simulation have become increasingly important.

## *1.1 Motivation and Objectives*

Whereas numerical simulations were often restricted to experimental data post-processing in the past, the most stimulating factor in modern internal combustion engine research and development is the complementary interaction of advanced experimental and computational investigations. Even with the sophistication, wide variety and accuracy of the experimental methods available, the advantages of the computational methods, such as the unbounded data processing and analysis (i.e. potentially full resolution in time, space and species), the time and cost effectiveness, and the prediction capabilities, still persist.

While experimental studies are needed in order to calibrate and verify numerical simulations, computational investigations are required to interpret and complete experimental results. Facing both the exponential increase in IC engine complexity (e.g. Common-Rail direct injection, variable valve train actuation, etc.), and the stringent time and cost conditions in the global markets, integrated experimental and computational approaches are in great demand [17][37][80].

Focusing on the first phase of the engine design process, the present study compares a “model/knowledge based” and a “black-box” approach for the fast and accurate simulation and optimization of Common-Rail DI diesel engines. After an overview of the various IC engine models and optimization methods is given, the assets and drawbacks of the two approaches are systematically evaluated in a comprehensive investigation for three distinct engines; an automotive, a heavy-duty, and a two-stroke marine diesel engine.

## 1.2 Common-Rail DI Diesel Engines

Despite the significant contributions to local and global air quality problems, as well as the (potential) health effects, commercial applications are almost exclusively powered by direct injection diesel engines. In addition, due to the high efficiency, superior drivability, low life-cycle costs, the share of diesel powered passenger cars in western Europe increased from 13.8 % in 1990 to 48.2 % in 2004 [1].

In order to control/reduce the negative impacts on the environment, emission regulations specify and enforce the maximum amount of pollutants allowed to be emitted by an internal combustion engine. For common diesel engines, generally the particulate matter (PM)<sup>1</sup>, the nitrogen oxide (NO<sub>x</sub>)<sup>2</sup>, the hydrocarbons (HC), and the carbon monoxide (CO) emissions are regulated, whereas the carbon dioxide (CO<sub>2</sub>) emissions for example are subject to voluntary agreements between administrations and manufacturers.

Facing the increasingly stringent emission regulations, major engine research and development focuses on the simultaneous reduction of fuel consumption and exhaust emissions of diesel engines by combustion and cycle efficiency improvements [45]. According to [10], the various technologies developed and implemented in modern diesel engines can be classified - in a non exhaustive list - as follows:

- **FUEL INJECTION AND AIR MANAGEMENT**  
variable-rate fuel injection systems (e.g. Common-Rail), exhaust gas recirculation, variable nozzle/geometry turbocharger, two-stage turbocharging, four-valve cylinder heads, variable swirl, variable valve train actuation, etc.
- **FUEL COMPOSITION MODIFICATIONS**  
low sulphur fuels, water-in-diesel fuel emulsions, oxygenated and hydrogen enriched fuels, etc.
- **EXHAUST GAS AFTERTREATMENT**  
oxidation catalysts, diesel particulate filters, nitrogen oxides adsorber catalysts, selective catalytic reduction systems, etc.
- **COMBUSTION CONCEPT**  
Homogeneous Charge Compression Ignition (HCCI), Low Temperature Combustion (LTC), etc.

- 
1. *Particulate Matter (PM)* - both solid and liquid particles of 1 nanometre to 100 micrometres in diameter suspended in the air. IC engine PM emission mainly consist of elemental carbon (soot), unburned fuel (hydrocarbons), and various acids, with a soot content that varies from 25 % to 95 % (depending on the fuel, operating condition and type of engine used) [3].
  2. *Nitrogen Oxide (NO<sub>x</sub>)* - generic term for the various nitrogen oxides produced during combustion, such as nitric oxide (NO), nitrogen dioxide (NO<sub>2</sub>), or nitrous oxide (N<sub>2</sub>O). Nitrogen oxide formation is promoted by high temperatures and excess of oxygen.

### ***1.2.1 Combustion Analysis and Modeling***

Given that in engineering “modeling a process” has become a synonym for developing and using an appropriate combination of assumptions and equations that permit critical features of a process to be analyzed [44]. Internal combustion engine models thus range from zero-dimensional empirical model, to three-dimensional computational reactive fluid dynamic models.

An experimental combustion analysis generally includes the interpretation of global engine operating characteristics, such as performance/efficiency measures and exhaust emissions, as well as time resolved temperature and (in-cylinder) pressure data.

### ***1.2.2 Exhaust Emissions***

Diesel exhaust is a complex mixture of gases, vapors, liquid aerosols and substances made up of particles (i.e. fine particles), that has the potential to cause a range of serious health problems. Despite the controversy about the epidemiology studies used to develop health risk assessments of diesel exhaust, long-term/chronic inhalation exposure is likely to pose a lung cancer hazard to humans and short-term/acute exposures can cause irritation and inflammatory symptoms [21].

Among the more than 40 substances emitted by diesel engines that are listed as hazardous air pollutants by the U.S. Environmental Protection Agency (EPA), the nitrogen oxide and particulate matter (soot) emissions are the most important ones. Whereas the nitrogen oxide emissions (along with unburned hydrocarbons and sunlight) make for the formation of ground-level ozone<sup>1</sup> and contribute to the formation of acid rain, particulate matter emissions are mainly associated with the serious health effects mentioned above.

### ***1.2.3 Optimization***

During the IC engine design process, optimization methods are used for example, to calibrate numerical models [100], to reduce engine exhaust emissions in automated test-bed systems (i.e. electronic control unit calibration) [95], or to find the best fuel/propulsion systems in life cycle analysis studies [64]. The optimization techniques employed range from gradient-free methods, such as evolutionary algorithms or coordinate strategies, to first and second-order gradient methods, such as conjugate gradient or Newton’s method (c.f. Section 2.4 and [69]).

---

1. *Ozone (O<sub>3</sub>)* - an allotrope of oxygen (O<sub>2</sub>) consisting of three oxygen atoms, a powerful oxidizing agent, highly corrosive and poisonous.

### *1.3 Approach*

To describe the manner in which the goals outlined in Section 1.1 were attained, this thesis is structured in three parts. After a detailed survey on the current state-of-the-art IC engine modeling techniques, as well as Artificial Neural Network (ANN), Design of Experiments (DoE), and the application of optimization techniques in IC engine research and development (Chapter 2), both the model/knowledge based and the black-box modeling approach, as well as the computational and experimental setup are presented in Chapter 3.

In the second part of this thesis, a thorough investigation of the phenomenological model/knowledge based approach is given. Starting with a phenomenological Common-Rail DI diesel engine Rate Of Heat Release (ROHR) model in Chapter 4, consistent models for the simulation of nitrogen oxide and soot exhaust emissions are given in Chapters 5 and 6, respectively. In addition to the model description and parameter studies in the first two sections of Chapters 4 to 6, each model is applied to three distinct engines - an automotive, a heavy-duty and a marine diesel engine - in order to evaluate the respective model generalization capability. In addition to these main investigations, which are conducted for all three models, both a comparative algorithm study and an advanced fuels investigation are used to further evaluate the ROHR model (Chapter 4). To conclude the model/knowledge based approach part, Chapter 7 presents the application of the derived phenomenological models in various engine process simulations.

The third component of this work consists of a ANN/black box approach study on the simulation of ROHR characteristics and exhaust emissions and its comparative evaluation against the phenomenological model/knowledge based approach (Chapter 8). This is followed by a summary, general conclusions and an outlook on future work in this area (Chapter 9).

## 2 STATE-OF-THE-ART

The subsequent sections are intended to give an overview of the classic modeling approaches for internal combustion engines and two potential alternatives; the artificial neural network (ANN) and design of experiments (DoE) approaches. An outline on the various optimization techniques in engineering closes the chapter.

### 2.1 Internal Combustion Engine Modeling

The manifold tasks and applications in engine research & development (R&D) have led to various types of combustion engine simulation models. Ranging from fast and rather approximate models to exhaustive but time-consuming models, a classification into three major categories is commonly used [16][19]. Depending on the intention of the classification, the categories are either dimensional (zero-, quasi- and multi-dimensional) or complexity level based (empirical/thermodynamic, phenomenological and detailed/complex).

#### 2.1.1 Empirical or Thermodynamic Models

Derived from the first law of thermodynamics, mass balances and experimentally obtained correlations, this type of models just accounts for only temporal variations (ordinary differential equations), i.e. spatial variations in composition and thermodynamic properties are neglected. Typically, the whole combustion chamber is modeled as a homogeneously mixed zone (a.k.a. single-zone combustion models). Given these simplifications, the models are computationally efficient and easy to handle, but fail to resolve local phenomena, such as fuel spray interaction, turbulence structure and emission formation.

#### Single-Zone Cylinder Model

Defining the entire combustion chamber as control volume (c.f. Figure 2.1) and applying the conservation law for mass and energy (i.e. the first law of thermodynamics), results in the two governing equations for open thermodynamic systems:

$$\frac{dm_{\text{cyl}}}{dt} = \sum_k \frac{dm_k}{dt} = \frac{dm_{\text{in}}}{dt} + \frac{dm_{\text{exh}}}{dt} + \frac{dm_{\text{fuel}}}{dt} + \frac{dm_{\text{bb}}}{dt} \quad (2.1)$$

$$\frac{dU_{\text{cyl}}}{dt} = \frac{dQ_{\text{w}}}{dt} + \frac{dQ_{\text{chem}}}{dt} - p_{\text{cyl}} \frac{dV_{\text{cyl}}}{dt} + \sum_k h_k \frac{dm_k}{dt} \quad (2.2)$$

(presuming all flows directed into the control volume have positive signs).

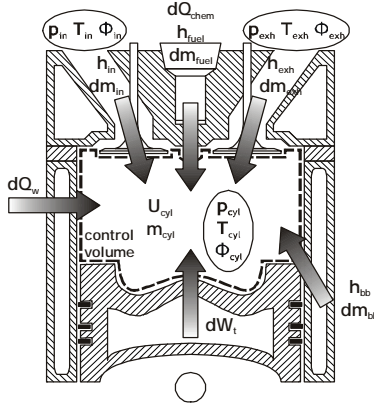


Fig. 2.1 Control Volume as Used in Single-Zone Cylinder Models

In order to solve the equations for the change in internal energy of the control volume, a series of sub-models are required, e.g. for the mass fluxes (gas exchange, fuel injection and blow-by), mechanical work (friction), heat transfer to the combustion chamber walls, ignition delay and the rate of heat release. Furthermore, to link the change of internal energy to changes in temperature and pressure, thermodynamic gas property correlations, such as the polynomials developed by Zacharias [108] or the NIST-JANAF tables [22] are needed.

### Applications & Examples

Single-zone thermodynamic models have been, and still are frequently used in internal combustion engine R&D, specifically for common investigations, such as the analysis of in-cylinder pressure data, transient powertrain simulations or control engineering applications. Therefore, this class of models comprehends numerous modeling approaches.

- **HEAT TRANSFER**

Directly derived from experimental correlations there are single equation models by Nusselt [71] and Eichelberg [28]. The widely used Woschni formula [106] - which is based on an analogy between the in-cylinder flow pattern in a combustion engine and the turbulent flow pattern in a circular tube - is another good example of this type of model.

- **RATE OF HEAT RELEASE**

Generally there is no detailed modeling of physical and chemical processes in single-zone models. Hence, mathematical “substitution” functions, derived from analytical theory and measurement approximations, such as the Vibe combustion profile [98], the polygon-hyperbola profile [84] or the two equation analytical profile [39] are widely used.

- *EMISSIONS*

Based on the in-cylinder mean temperature data of a single-zone model, Schröder [85] derived an empirical correlation (i.e. there is no chemical reaction scheme used) to model engine-out emissions of nitrogen oxide.

As for soot emissions, most global one-step equation models belong to this class of model (e.g. Khan et al. [57] or Lee [63])

### 2.1.2 Phenomenological Models

Phenomenological models aim to strike a balance between computational requirements and model accuracy. In order to overcome the deficiencies of the empirical models in handling local phenomena, the control volume (i.e. the combustion chamber) is typically divided into multiple zones characterized by different temperatures and compositions. The zoning is thereby either done sequentially, i.e. along a given time axis - such as the two-zone models by Hohlbaum [49] and Rakopoulos et al. [79], and the n-zone model by Weisser et al. [101] - or geometrically, i.e. in space - such as the “packages” model by Hiroyasu et al. [47].

Using simplified yet physically and chemically coherent models to capture the underlying local processes (i.e. spray atomization, fuel evaporation, air entrainment, ignition, etc.) phenomenological models allow for both qualitative and quantitative predictions of pollutant emissions and rates of heat release. Given the simplistic spatial resolution (the number of zones accounted for is usually in the range of two up to a few dozen), the absence of the Navier-Stokes momentum equation, as well as the spatial averaging of the turbulent flow field, these models are not able to account for example for the effects of changes in combustion chamber geometry, such as different bowl shapes, or complex interactions among different zones.

### *Applications & Examples*

Phenomenological models are typically applied in experimental data analysis, optimization of control variables, or simulations over entire engine operating maps, to bridge the gap until detailed three-dimensional models become computationally affordable. Combining low computing times (generally of the order of seconds for one operating condition) and reasonably accurate predictions for global combustion parameters, these models are best suited for conceptual studies.

- *HEAT TRANSFER*

In general, phenomenological heat transfer models distinguish between a radiative (hot gases and soot particles) and a forced convective (turbulent charge movement and gas-wall temperature gradients) component of the overall heat transferred to the combustion chamber walls. Given that the

overall heat flux is strongly dependent on the local conditions, most of the models divide the combustion chamber into sections by merging similar conditions [29][86].

- *RATE OF HEAT RELEASE*

Given the tight coupling of the physical and chemical processes present in combustion engines (e.g. fuel evaporation and air entrainment), common rate of heat release models consequently consider the whole range of in-cylinder processes. Various sub models are used to represent the injection, air entrainment, ignition, and combustion processes.

Although the aforementioned approaches may differ, they share the same phenomenological concept; the breakdown of the combustion into kinetically controlled (“premixed”) and mixing-controlled (“diffusion”) components. Recent technical advances in multiple pulse injection systems have resulted in substantial work on extending the models to account for different injection strategies [7][67][91].

- *EMISSIONS*

Based on the (extended) Zeldovich reaction mechanism for the formation of nitric oxide, models for both a “quasi” two-zone approach [42] and an n-zone approach [102] have been extensively used. Numerous versions of a two step equation approach (formation and oxidation) have been proposed to model soot emissions [48][88]. Additionally, there has also been work on integrated approaches for the rates of heat release, soot and  $\text{NO}_x$  emission modeling (e.g. [14][34][93]).

### 2.1.3 Detailed or Complex Models

Akin to empirical and phenomenological models, the governing principles for detailed/complex models are the conservation of mass, energy and momentum (a.k.a. Navier-Stokes equation). Solving these conservation laws in time and (three-dimensional) space results in a set of partial differential equations (PDEs). Furthermore the chemistry processes prevailing in combustion, as well as the interaction between the chemistry and the fluid mechanics described in three-dimensional Navier-Stokes equations increase the complexity (i.e. the numerical stiffness) of the present models.

The numerical schemes used to solve these models are commonly classified into three main categories: the rather coarse Reynolds-Averaged Navier-Stokes (RANS), intermediate resolution Large Eddy Simulations (LES) and fully resolving Direct Numerical Simulations (DNS). Concerning combustion engineering problems;



RANS simulations are currently employed in a majority of the cases for the sake of simplicity and available computation time [8], whereas predominantly LES and DNS simulations are used in fundamental research studies [33][61].

Owing to the limited understanding and the complexity of the reaction chemistry at a fundamental level, there is considerable activity in this field of research, including studies on hydrocarbon reaction mechanisms [9] or turbulence-chemistry interactions [107].

### *Applications & Examples*

Compared to empirical and phenomenological models, the generality of detailed/complex models makes it possible to comply with almost any kind of problem. Depending on the intention, and hence the level of sophistication, the models are commonly used to gain insight into the governing processes, provide information of local in-cylinder phenomena or evaluate new combustion technologies.

- *HEAT TRANSFER*

Gosman and Watkins applied computational fluid dynamic simulations for turbulent in-cylinder flows including a one-dimensional gas-wall heat transfer model [36]. Given the present LES and DNS turbulence models available, the model accuracy is no longer restricted in terms of the turbulent flow field resolution.

- *RATE OF HEAT RELEASE / COMBUSTION*

Focusing on the combustion itself, numerous approaches, such as the characteristic time scale models by Magnussen et al. [65], the flamelet approach by Peters et al. [76] or the Conditional Moment Closure (CMC) model by Bilger et al. [12] exist. Details about the advantages and disadvantages of each of these models, as well as a general survey on multidimensional combustion modeling are given by [92].

- *EMISSIONS*

As the thermal nitric oxide formation based on the Zeldovich mechanism is included in most commercially available engine simulation codes, the main emphasis in nitrogen oxide emission studies is on prompt  $NO$ ,  $NO_2$  and  $N_2O$  formation, and catalytic removal processes (e.g. Miller [68]).

There is still only a limited understanding of the fundamental governing physical and chemical processes to be considered for the modeling of engine out soot emissions [55]. Although it is derived for laminar premixed flames, the model by Frenklach and Wang [31], using detailed kinetics for acetylene pyrolysis and the growth of polycyclic aromatic hydrocarbons (PAHs), is being studied for engine applications [58].

## 2.2 Artificial Neural Networks

Inspired by biological nervous systems - such as the human brain, where information is transmitted and stored in groups of interconnected neurons<sup>1</sup> - Artificial Neural Networks (ANNs) employ clusters of small and simple information processing units (a.k.a. artificial neurons) to mimic the natural learning process and thereby acquire knowledge.

Similar to the human brain, ANNs operate like “black box” models, as they do not require detailed information about the basic system being observed. ANNs “learn” the relationship between input and output parameters by “studying” given data, and “store” the knowledge in the interconnections, or rather the associated weights (akin to the synapses efficacy in biological neural systems).

### Basic Structures & Definitions

In a simplified model of an artificial neuron, the given inputs are weighted, added up and passed through an activation function (e.g. a threshold, linear or sigmoid<sup>2</sup> function) to produce an output signal, as shown in Figure 2.2. Combining several artificial neurons in a network architecture, similar neurons are generally arranged in layers that are labeled as input, hidden and output layers (a.k.a. multi-layer network architecture). During the training mode of an ANN, an appropriate learning algorithm (e.g. backpropagation<sup>3</sup>) is used to modify the interconnection weights such that, given selected inputs, the network attempts to produce the desired outputs.

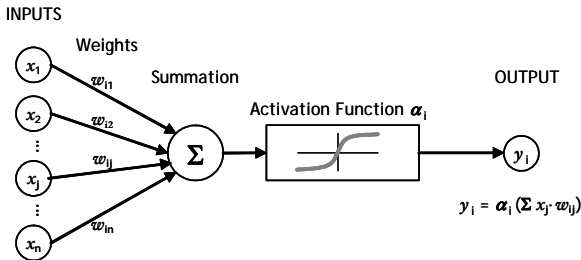


Fig. 2.2 Model of an Artificial Neuron With Interconnections

1. *Neuron* - primary cell of the nervous system, consisting of a cell body, the axon (single long activation fiber out of the cell body) and multiple dendrites (receptive nerve fibers)
2. *Sigmoid* - curved in two directions, viz. shaped like the letter S (c.f. Figure 2.2)
3. *Backpropagation* - abbreviation for “backwards propagation (of errors)”

## Types of Artificial Neural Networks

Although the modular design of ANNs allows for numerous network architectures, mainly the feed-forward and the recurrent neural network schemes are used for engineering systems [40].

- **FEED-FORWARD NEURAL NETWORKS**

The unidirectional flow of information in the distinct layered network structure - from the input to the output neurons - is the characteristic feature of feed-forward neural networks (Figure 2.3 (a)). Composed of threshold neurons<sup>1</sup> only, a single-layer network is deemed to be the bottom-of-the-line feed-forward network (a.k.a perceptron network). While single-layer neural networks are limited to linear function approximation tasks, ANNs with three or more layers are capable of approximating arbitrary continuous functions, using e.g. sigmoid and linear neurons [51].

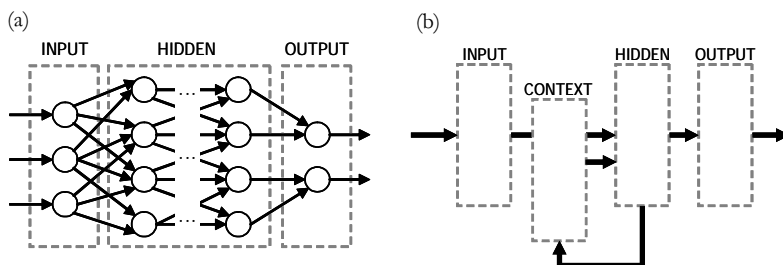


Fig. 2.3 Schematic Diagrams of (a) Multi-Layer Feedforward Neural Network and (b) Simple Recurrent Neural Network

- **RECURRENT NEURAL NETWORKS**

Unlike in feed-forward neural networks, recurrent networks have a bi-directional flow of information. For example, the simple recurrent network scheme uses an additional context layer to maintain the information of a previous state, enabling time series predictions (Figure 2.3 (b)).

## Applications

A summary on the numerous applications of ANNs in internal combustion engines, such as emissions and performance modeling, engine controller design and fault diagnosis is given in [52].

Focusing on diesel engine modeling topics only, Table 2.1 lists examples of recent studies including ANNs used in various applications.

1. *Threshold Neuron* - artificial neuron with a “threshold” activation function, i.e. given normalized inputs and weights, the output is typically 1 or -1 with a threshold value of 0

<i>AUTHORS</i>	<i>TOPIC(S)</i>
Clark et al. [23]	exhaust emission modeling (CO <sub>2</sub> , NO <sub>x</sub> ) based on engine speed & torque (incl. 1 <sup>st</sup> & 2 <sup>nd</sup> derivatives)
De Lucas et al. [24]	modeling the influences of fuel specifications (composition, cetane index, etc.) on PM emissions
Delagrammatikas et al. [25]	combination of DoE & ANNs for vehicle-level optimization studies (e.g. fuel consumption, acceleration times)
He and Rutland [41]	modeling of in-cylinder pressure, temperature, wall heat transfer, NO <sub>x</sub> and soot emissions
Hentschel et al. [43]	in-car modeling of transient exhaust emissions (opacity, NO <sub>x</sub> ) with dynamic ANNs (ECU data inputs)
Kesgin [56]	emission (NO <sub>x</sub> ) and efficiency modeling
Ouenou Gamo et al. [73]	exhaust emissions (i.e. opacity) modeling
Papadimitriou et al. [74]	automatically selected neural networks for engine calibration in control-oriented applications
Traver et al. [96]	transient emission modeling (NO <sub>x</sub> , CO, CO <sub>2</sub> and HC) using in-cylinder combustion pressure data

*Tab. 2.1 Representative ANN Based Diesel Engine Modeling Studies*

## 2.3 Design of Experiments (DoE)

The (statistical) Design Of Experiments (DoE) offers a range of procedures and methods for planning experiments, so that it is possible to analyze, predict and optimize the influence of one or more input variables on the output variable(s) of an experiment.

According to the “Engineering Statistics Handbook” [70], the key steps in a DoE study are the:

1. *SPECIFICATION OF OBJECTIVES & ASSUMPTIONS*  
depending on the intention of the design<sup>1</sup>, i.e. whether a comparative (choose between alternatives), screening (identify significant input/output variables) or modeling study is planned
2. *SELECTION OF INPUT & OUTPUT VARIABLES*  
including all relevant but no dispensable variables
3. *SELECTION OF EXPERIMENTAL DESIGN*  
depending on the number of variables and the objectives chosen

---

1. (*Experimental Design* - a detailed planing prior to the execution of an experiment, in order to yield valid and objective conclusions from the experimental data obtained.

4. *EXECUTION OF THE DESIGN (EXPERIMENT)*
5. *DATA CONSISTENCY CHECK WITH ASSUMPTIONS*  
are the results reproducible?
6. *ANALYSIS & MODELING OF THE RESULTS*

examine the results for outliers, typographical errors and obvious problems, create the model from the data, check the model residuals and use the results to answer the questions set in the objectives

Using (simple) mathematical functions (a.k.a. regression functions) to model the effects of the input variables on the output of the system, the DoE response surface models differ significantly from other approaches, such as ANNs or phenomenological models. Both ANN and DoE approaches use “black-box” concepts to model the system behavior, and while ANN models are capable of approximating any continuous function describing the input/output correlations, DoE models are not.

### *Applications & Examples*

Despite the limitations in generality, given the structured procedure and the possibility to reduce the number of experiments necessary, DoE approaches are commonly used in industrial applications, such as combustion engine R&D [18]. Examples range from comparative studies of engine components and injection strategies for an automotive DI diesel engine [13], to screening and modeling studies of the in-cylinder flow field and combustion chamber geometry for a medium-duty DI diesel engine [77].

## *2.4 Optimization*

Optimization can be defined as the search for the best possible solution(s) to a given problem. In general, the n-dimensional optimization problem is expressed by

$$\begin{cases} \min(f(\mathbf{x})) \\ g_i(\mathbf{x}) = 0, i = 1, \dots, p, \\ h_j(\mathbf{x}) \leq 0, j = 1, \dots, q \end{cases} \quad (2.3)$$

where  $\mathbf{x} \in \mathfrak{R}^n$  is the parameter vector minimizing<sup>1</sup> the (single-)objective function  $f(\mathbf{x}) \in \mathfrak{R}$ , subject to the equality  $g_i(\mathbf{x})$  and inequality  $h_j(\mathbf{x})$  constraints given. Additionally, the limits (high/low) for the parameter vector values are defined as  $x_k^l \leq x \leq x_k^h$ ,  $k = 1, \dots, n$ , where  $l$  stands for the lower and  $h$  for the higher limit respectively.

---

1. In practice, the optimum is generally defined as the minimum of an objective function. Maximum optimization problems are therefore transformed into minimization problem using  $\max(f(\mathbf{x})) = -\min(-f(\mathbf{x}))$ .

Given that in engineering applications, e.g. gas turbine design [20], multiple (conflicting) objectives have to be optimized, the result of an optimization is a set of “trade-off” solutions (i.e. pareto optimal set<sup>1</sup>), rather than one single best solution. A mutual comparison of at least two solutions from the pareto set thereby shows, that both of them are better and worse in at least one objective at the same time [97].

Various solutions exist to tackle the optimization problem, most of them sharing the iterative concept of splitting-up the parameter vector estimation (optimizer) and the parameter vector evaluation (analyzer) as in Figure 2.4

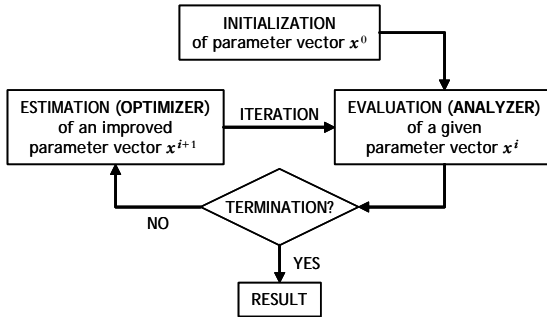


Fig. 2.4 Iterative Optimization Scheme of Optimizer & Analyzer

The classification of single-objective optimization algorithms is based on whether a method requires information from the objective function’s first and second order derivatives, or only from the objective function. Additionally, a distinction is made between stochastic and deterministic methods. Using information from only the objective function (i.e. direct), in combination with stochastic processes e.g. in the reproduction and variation of the parameter vectors, the evolutionary computation algorithms are classified as direct-stochastic optimization methods. In contrast, the classic coordinate strategy may serve as an example for the direct-deterministic group of optimization methods [69].

### 2.4.1 “Classic” Methods

In general, the classic algorithms of gradient descent, deterministic hill climbing and purely random search (with no heredity) perform poorly when applied to nonlinear optimization problems. As there exists no algorithm solving for all optimization problems, that on average performs superior to any other algorithm (according to the no-free-lunch theorem [104]), the classic algorithms outperform advanced and complex algorithms in solving linear, quadratic or unimodal problems.

1. *Pareto optimality* - the parameter vector  $\mathbf{x}^i \in \mathfrak{R}^n$  is pareto optimal if and only if there is no vector  $\mathbf{x}$  such that  $f_j(\mathbf{x}) \leq f_j(\mathbf{x}^i)$  for all  $i \in \{1, 2, \dots, n\}$  with at least once strict inequality.

## 2.4.2 “Evolutionary Computation” Algorithms

The mutual basis of all regular approaches in evolutionary computation, specifically genetic algorithms, evolution strategies and evolutionary programming, is the implementation of the evolution principle: reproduction, random variation, competition and selection of contending individuals<sup>1</sup> in a population<sup>2</sup>. Thus, the general characteristics outlining any evolutionary algorithm are the collective learning process of a population of individuals, the randomized processes intended to model mutation<sup>3</sup> and recombination<sup>4</sup> and the assignment of a measure of quality or fitness value to an individual [5].

Translated into a pseudo-program-code, the general scheme of an evolutionary algorithm look as follows:

```

initialize the population
evaluate the initial population
REPEAT
  recombine the individuals to produce an offspring
    population
  mutate the individuals of the offspring population
  evaluate the solutions for the offspring population
  assign a measure of quality to the individuals
  select the (best) individuals for the next generation
UNTIL some convergence criteria is satisfied
  
```

Utilizing the size of the parent and offspring population, as well as the characteristics for the recombination, mutation, evaluation and selection processes (also referred to as strategy parameters) as inputs, the evolutionary algorithm iteratively converges towards the optimum solution.

### Genetic Algorithms (GAs)

Three features distinguish GAs from other evolutionary algorithms:

- *BINARY REPRESENTATION (ENCODING)*  
Various subsequent implementations of the original GA<sup>5</sup> use real-valued representation schemes instead of the bitstring encoding (i.e. the parameter vector consists of 0's and 1's only) to be more easily applied to the problem being tackled.

---

1. *Individual* - single parameter vector, representing (encoding) a search point in the space of potential solutions to a given problem
2. *Population* - a pool of individuals
3. *Mutation* - modification in transmission of (genetic) information from one generation to the next
4. *Recombination* - creation of one or more offspring given at least two individuals (parents)
5. A simple GA using bit-string encoding, crossover recombination and mutations [50]

- *PROPORTIONAL (PROBABILISTIC) SELECTION METHOD*  
Because of the high selective pressure<sup>1</sup> associated with it, the probabilistic selection of individuals according to their fitness value runs the risk of premature convergence of a population. That is, the “best” individuals become dominant and hence start to inbreed<sup>2</sup>.
- *CROSSOVER RECOMBINATION*  
Crossover recombination randomly swaps single values (bits) or segments of the parameter vectors of two dissimilar individuals, aiming to combine the best features from both individuals and thus creating a better offspring. Although most GAs use mutation along with crossover recombination, almost exclusively crossover recombination is used to assure the diversity and broadening of the population.

### *Evolution Strategies (ESs)*

Using normally distributed mutations to modify the real-valued parameter vectors, the emphasis in ESs is equally placed on mutation and recombination as search operators. Moreover, the simultaneous adjustment (extended optimization) of the strategy parameters and the parameter vector itself further distinguishes the ESs from other GAs.

Unlike in GAs, the selection operators in ESs are deterministic and the parent and offspring population sizes usually differ from each other. That is, the number of parents is less or equal the number of offspring and thus the worst performing individuals (i.e. the ones with the lowest measure of quality) of an offspring generally don't procreate.

### *Evolutionary Programming (EP)*

Similar to ESs, the EP algorithms use normally distributed mutations and extend the evolutionary process to the strategy parameters as well. Emphasizing mutation while neglecting the recombination of individuals, EP algorithms drop the implicit assumption that the fitness value is linked to parts of the parameter vector, as is usually assumed for GAs and ESs.

Further studies on applications, advantages and disadvantages of the various optimization algorithms used in EP are given in [6][30][89], whereas [35][50][60][81] provide the fundamentals for the various approaches.

- 
1. *Selective Pressure* - probability of the best individual being selected compared to the average probability of selection of all individuals
  2. *Inbreeding* - mating of nearly identical individuals, reduces the diversity of the population and hence increases the risk of premature convergence.



## 3 *APPROACHES AND EQUIPMENT*

After briefly defining the system and introducing the objectives of the study, detailed information on both the “model/knowledge based” and “black-box” approaches are given in the first part of this chapter. The second part subsequently documents the equipment used, i.e. both computer soft-/hardware and the three distinct IC engines and utilized measurement techniques.

### 3.1 *System & Objectives*

The combustion of a Common-Rail DI diesel engine, as characterized by the rate of heat release and the nitrogen oxide and soot emissions, serves as a measure for the subsequently described comparative investigation. Given the general engine and operating condition specifications as inputs, the actual ROHR and specific  $\text{NO}_x$  and soot emissions are defined as outputs.

The objectives of the study are the fast and reliable prediction of the system outputs for three distinct types of engines, more specifically an automotive, a heavy-duty and a two-stroke marine diesel engine. Additionally, the investigation includes the comparison of two dissimilar approaches for modeling; the “model or knowledge based” and “black-box” approaches. As there are at least two optimization sequences necessary to get from initiation to an optimized simulated engine operating map, a concept for the interaction of modeling and optimization is derived.

### 3.2 *“Model/Knowledge Based” Approach*

The model or knowledge based approach in this context refers to a physical and chemical description of the underlying system, derived from both fundamental theory and phenomenological experience. As stated in the objectives, the description of the system (i.e. the basic models) should allow for fast and reliable predictions of the system outputs. In other words: the models used in this approach need to be as complex as necessary and as simple as possible at the same time. Hence, given the restrictions and requirements, only phenomenological models (c.f. Section 2.1.2, p. 7) are used in this study.

Physical and chemical models - phenomenological ones in particular - inherently need to be calibrated to fit the actual system. The model or knowledge based approach hence consists of two optimization parts, the model calibration (a.k.a. model optimization) and the system or process optimization. The quality of the

model calibration thereby significantly affects the outcome of the subsequent search for the system optimum.

### 3.2.1 “Modeling/Optimization” Scheme

Based on experience from joint experimental and numerical combustion engine R&D projects, such as [59] and [83], a fundamental modeling and optimization scheme is derived to profit from the mutual advantages of both subjects. Along with the distinction between modeling and optimization, the strict subdivision of experimental data into calibration and verification parts thereby assures the formal correctness of the approach. Although the objectives of the two optimization parts in the scheme, the “model calibration” and the “system optimization”, differ, the optimization algorithms do not need to be dissimilar.

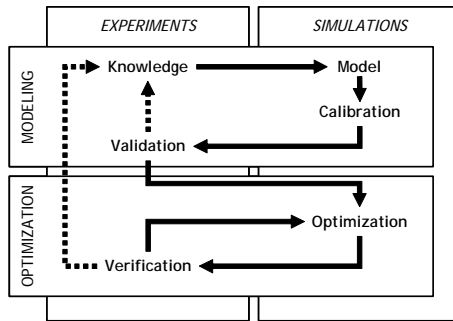


Fig. 3.1 Modeling/Optimization Scheme

Starting from available (experimental) knowledge of the system, there is an iterative process of modeling, calibration and verification to derive an appropriate model of the system. Given an appropriate model, the iteration between the numerical optimization and the experimental validation allows for both the optimization of the system outcome and a profound understanding of the application (Figures 3.1).

### 3.2.2 Application Examples

As the proposed modeling/optimization scheme by itself is not restricted to diesel engine combustion systems only, it has successfully been applied to other applications using the same procedures, e.g. evolutionary algorithms as optimization method.

### 3.2.2.1 Thermodynamic Modeling

Similar to the approach used to model the nitrogen oxide and soot emissions from Common-Rail DI diesel engines (c.f. Chapters 5 and 6), Lämmle [62] uses the scheme to model knock<sup>1</sup> phenomena in SI natural gas engines.

Using computational reactive fluid dynamic simulations of HCCI<sup>2</sup> phenomena in diesel engines, Barroso [9] applied the scheme to determine the kinetic parameters for the governing reactions in a hydrocarbon combustion mechanism.

### 3.2.2.2 Polymer Electrolyte Fuel Cell Modeling

Using evolutionary algorithms for parameter optimization, a phenomenological 1+1 dimensional model for Polymer Electrolyte Fuel Cells (PEFCs) [32] was calibrated according to the modeling/optimization scheme.

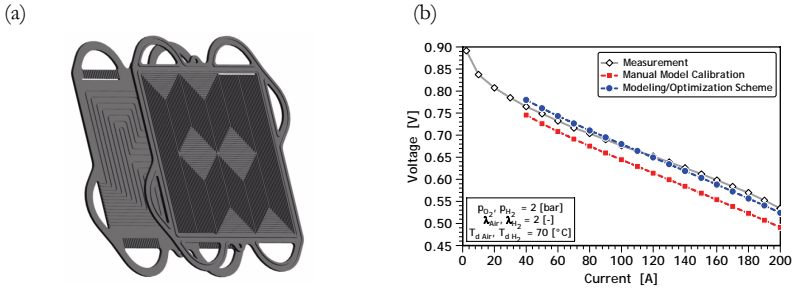


Fig. 3.2 Polymer Electrolyte Fuel Cell Modeling: (a) Sketch of a Single Plate Fuel Cell, (b) Comparison Plot between the Experimental and Simulated Current-Voltage Characteristics

Comparing the model calibration accuracy for the global current-voltage characteristics of a single plate fuel cell, the modeling/optimization scheme with evolutionary algorithms exceeds the classic manual model calibration.

## 3.3 “Black-Box” Approach

The generic term black-box approaches commonly stands for a variety of methods, such as Artificial Neural Networks (ANNs), statistical regression or fuzzy logic models, which do not contain physical or chemical models. The omission of physical or chemical models to describe the interdependence of the system inputs and out-

1. *Knock* - pressure waves/fluctuations associated with autoignition of a portion of the air-fuel mixture ahead of the advancing flame front
2. *HCCI* - Homogeneous Charge, Compression Ignition

puts is the major advantage and disadvantage of the black-box approaches at the same time. Considering that there is little or no a priori knowledge of the system necessary, the approach is best suited for systems where there is a lack of fundamental understanding. Alternatively, given a system where fundamental knowledge on the system behavior is available, black-box approaches tend to be less efficient than model/knowledge based approaches. Partial black-box approaches, a.k.a. grey-box methods<sup>1</sup>, are one way to compensate for this drawback, using fundamental knowledge in the form of phenomenological models where available.

### 3.3.1 “Artificial Neural Network” Scheme

In the present study an Artificial Neural Network (ANN) scheme is used as an alternative example to the phenomenological modeling/optimization scheme (c.f. Section 3.2.1). Similar to the modeling/optimization scheme, the ANN process consists of two basic phases; network training and system optimization (Figure 3.3). Unlike in the modeling phase of the modeling/optimization scheme though (Figure 3.2), there are generally no iterations needed in the network training phase.

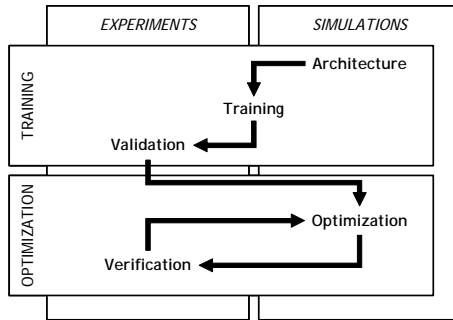


Fig. 3.3 Artificial Neural Network Scheme

Starting from a particular ANN architecture and a set of corresponding input and output data (training data), a learning algorithm modifies the interconnection biases and weights such that the network attempts to reproduce the behavior of the system. Once the network is trained, the subsequent system optimization phase is analog to the one in the modeling/optimization scheme (Figures 3.2 and 3.3).

1. *Grey-box methods* - systems or modules are defined by external interfaces, as black-box methods, and a partially resolved internal structure based on knowledge

### 3.4 Computational Setup

As the objectives for the present study include a comparative investigation of two approaches for modeling, identical experimental (Section 3.5) and computational setups (Section 3.4) are used. Table 3.1 lists the main characteristics of the computational setup while details on the selected software packages are provided in Section 3.4.1 et sqq.

<i>OPERATING SYSTEM</i>	Windows XP <sup>®</sup> SP2
<i>CPU / MEMORY</i>	Intel Pentium <sup>®</sup> P4, 3 GHz, 1 GB RAM
<i>SOFTWARE PACKAGES</i>	MATLAB <sup>®</sup> R14 SP2, WEG R10, GT-Suite <sup>™</sup> 6.1

Tab. 3.1 Computational Setup

#### 3.4.1 Thermodynamic Analysis & Simulation

The in-house thermodynamic software package WEG is used to analyze experimental pressure data and predict combustion characteristics using various models simultaneously [72].

In addition to the classic one- and two-zone approaches for thermodynamic analyses, WEG also allows for an arbitrary number of so-called virtual combustion zones. Directly coupled to a characteristic constant or variable air/fuel-ratio, the virtual combustion zones are intended to reproduce particular combustion phenomena, such as the oxygen deficiency at high engine loads or local emission formation. Given experimental pressure data and engine/operating condition specifications<sup>1</sup>, WEG calculates the apparent burn rate, overall engine heat transfer, rate of heat release and gas temperatures.

In order to predict the diesel combustion characteristics and exhaust emissions (i.e. the thermodynamic simulation), WEG contains three phenomenological models: a rate of heat release (Chapter 4), a nitrogen oxide emission (Chapter 5) and a soot emission model (Chapter 6). Employing the above described modeling/optimization scheme, the external dynamic data exchange<sup>2</sup> interface furthermore allows the WEG thermodynamic simulation models to be used as server applications in the programming language MATLAB. Thus, all optimization algorithms and ANNs used in the present study are programmed in MATLAB.

---

1. *Engine Specifications* - e.g. bore, stroke, compression ratio, inlet/exhaust valve diameter, etc.  
*Operating Condition Specifications* - e.g. engine speed, load, SOI, rate of fuel injected, etc.  
2. *Dynamic Data Exchange (DDE)* - standard communication & command interface between multiple applications (e.g. MATLAB and WEG) in Windows operating systems

### 3.4.2 Artificial Neural Networks

Featuring a modular network representation for commonly used network architectures and a comprehensive set of training functions, the MATLAB Neural Network Toolbox 4.0.5 [66] is used to design and simulate the ANNs in this study.

Based on the universal approximation theorem by Hornik et al. [51] and following the successful applications in IC engine combustion modeling (e.g. [26][41]), a multi-layer feed forward network architecture is chosen. Three different networks are designed to approximate the ROHR combustion characteristics and the specific nitrogen oxide and soot exhaust emissions as a function of seven key operating condition parameters. An outline of the configuration of the ANN, as well as the parameters used is provided in Table 3.2 .

<i>ARCHITECTURE</i>	Multi-layer feed forward network
<i>TRAINING</i>	Levenberg-Marquardt algorithm with back-propagation
<i>INITIALIZATION</i>	Nguyen-Widrow method
<i>ACTIVATION FUNCTION</i>	Sigmoid (hidden neurons) & linear (output neurons)
<i>INPUTS</i>	$c_m, \text{BMEP}, p_{\text{Inj}}, \Delta t_{\text{Inj}}, \varphi_{\text{SOI}}, x_{\text{EGR}}, \lambda_{\text{global}}$
<i>OUTPUTS</i>	ROHR Characteristics: $\varphi_{\text{SOC}}, \varphi_{10}, \varphi_{50}, \varphi_{90}, Q_{\text{max}}, \dots$ NO <sub>x</sub> and soot emissions

Tab. 3.2 Artificial Neural Network (ANN) Characteristics

### 3.4.3 Optimization Algorithms

Given an engineering problem, the definition of an appropriate fitness or objective function, as well as the physical or technical constraints of the system parameter values, are crucial to all optimization algorithms.

#### Constraints

Parameters in engineering systems, for example the valve timing, laminar flame speed or global A/F-ratio in an IC engine, are subject to physical or technical constraints. As the present study deals with phenomenological models based on physical and chemical parameters (e.g. pressure values, temperatures, velocities, etc.), the chosen optimization algorithms need to account for equality and inequality parameter constraints. Given these constraints, the variable size of the search dimensions (asymmetric search space) generally has an impact on the search strategy and accordingly the efficiency of the optimization algorithms. Details on the different model parameters and their corresponding size ranges are given in Chapter 4 et sqq.

## Fitness/Objective Functions

In order to handle both single (nitrogen oxide and soot emission) and multiple (rate of heat release) objective optimization tasks with identical algorithms, a single objective approximation function is used to describe the multi objective pareto optimality<sup>1</sup> [90].

Given that the optimization task in the calibration part of the modeling/optimization scheme is the search for the “best” set of model parameters, that is the set of model parameters which produces the smallest deviations from the measurements (e.g. least square errors), the single objective approximation function is defined as the weighted sum of the individual multiple objectives (Table 3.3).

ROHR	$f_{obj} = \sum_i c_i f_{obj}^i = c_1 \Delta^2(\varphi_{SOC}) + c_2 \Delta^2(\varphi_{10}) + c_3 \Delta^2(\varphi_{50}) + c_4 \Delta^2(\varphi_{90}) + \dots$ $c_5 \Delta^2(m_{pmx}) + c_6 \Delta^2(Q_{max}) + c_7 \Delta^2(\varphi_{Q_{max}}) + c_8 \Delta^2(\varepsilon_Q)$
NO <sub>X</sub>	$f_{obj} = \Delta^2(\text{NO}_x)$
SOOT	$f_{obj} = \Delta^2(m_{soot})$

Tab. 3.3 Objective Functions used for the Model Calibration

To account for the accuracy of the experimental data used in the model calibration, a tolerance value is assigned to each objective (output) of the model prior to the calculation of the objective function (Figure 3.4).

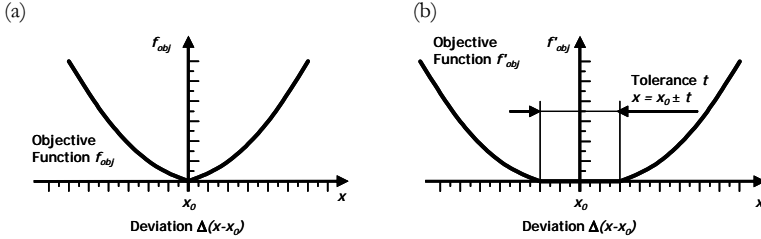


Fig. 3.4 Error Objective Function: (a) Standard Least Square Error (LSE), (b) LSE Including Tolerance Value

## Genetic Algorithm

The classic genetic algorithm (GA) [35] notwithstanding, the in-house developed GA uses real value parameter encoding, mutation, as well as a simulated annealing<sup>2</sup> mechanism in addition to the standard crossover mechanism for reproduction (Table 3.4).

1. *Pareto optimality* - a.k.a. indifference curves, best solutions to a multi objective problem that could be achieved without disadvantaging at least one of the objectives
2. *Simulated Annealing* - probabilistic “neighbourhood” search method, inspired by the annealing technique in metallurgy (heating up and controlled cooling of a material)

After the stochastic initialization of the population (1<sup>st</sup> generation) and the subsequent evaluation of the objective function, reproduction mechanisms are applied to the population, using statistical probabilities of crossover, transition and mutation. To select the individuals that are allowed to propagate to the next generation, a roulette wheel algorithm<sup>1</sup> in combination with a guaranteed survival of the best individuals (i.e. elitist survival) is used.

ENCODING	Real value encoding (constrained)
PARAMETERS	$n_{pop}$ , $P_{xover}$ , $P_{trans}$ , $P_{mut}$ , $n_{elit}$ (constant over generations)
INITIALIZATION	Stochastic initialization of population (1 <sup>st</sup> generation)
REPRODUCTION	Crossover, transition (simulated annealing), mutation
SELECTION	Roulette wheel selection, elitist survival

Tab. 3.4 Genetic Algorithm Characteristics

### Evolutionary Algorithm

Unlike classic GAs, the evolutionary algorithm (EA) used in this work employs crossover, intermediate and extended line recombination algorithms for the reproduction of the individuals (Figure 3.5). Furthermore, strategic algorithm parameters are modified during the optimization, such as the range of the extended line recombination  $r_{line}$ , which is reduced in order to increase the (local) optimization efficiency towards the end of an optimization run. Both tournament<sup>2</sup> and stochastic selection mechanisms are used to choose the individuals that propagate to the next generation (Table 3.5).

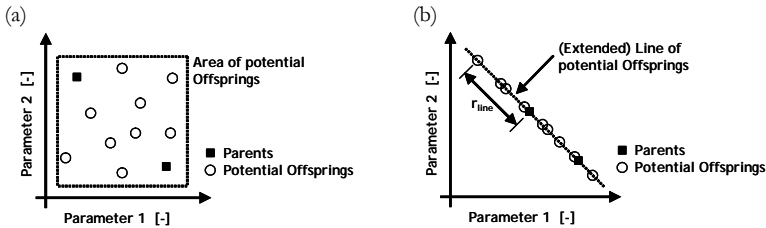


Fig. 3.5 Recombination Mechanisms: (a) Intermediate, (b) Extended Line Recombination (According to [78])

1. *Roulette Wheel Algorithm* - the probability of selection is proportional to the objective value, i.e. the higher the objective value, the higher the probability of selection
2. *Tournament Selection* - the best individual amongst a group of individuals (i.e. the tournament) is selected; the size of the tournament determines the selection pressure (ratio of the best individual's selection probability to the average selection probability of all individuals)



<i>ENCODING</i>	Real value encoding (constrained)
<i>PARAMETERS</i>	$n_{\text{pop}}, n_{\text{parent}}, n_{\text{offspring}}, P_{\text{xover}}, P_{\text{line}}, \alpha_{\text{line}}, r_{\text{line}}, P_{\text{inter}}, \alpha_{\text{inter}}, P_{\text{mut}}, P_{\text{tour}}$ (adapted/modified during search)
<i>INITIALIZATION</i>	Stochastic initialization of population (1 <sup>st</sup> generation)
<i>REPRODUCTION</i>	Crossover, (extended) line & intermediate recombination, mutation
<i>SELECTION</i>	Tournament, stochastic

Tab. 3.5 Evolutionary Algorithm Characteristics

### “Covariance Matrix Adaptation” Evolutionary Strategy

The  $(\mu, \lambda)$  Covariance Matrix Adaptation Evolutionary Strategy (CMA-ES) presented by Hansen et al. [38] determines the  $k^{\text{th}}$  offspring of the generation  $(g+1)$ ,  $x_k^{(g+1)}$ , given the center of mass of the selected individuals  $\langle x \rangle_{\mu}^{(g)}$ , the global step size  $\sigma^{(g)}$  and the random vectors  $B^{(g)}D^{(g)}z_k^{(g+1)}$  according to Equation (3.1):

$$x_k^{(g+1)} = \langle x \rangle_{\mu}^{(g)} + \sigma^{(g)} [B^{(g)}D^{(g)}z_k^{(g+1)}], k = 1, \dots, \lambda \quad (3.1)$$

where  $\mu$  is the number of parents,  $\lambda$  the number of offspring, and  $\sigma$  the initial step size. The symmetric positive definite  $n \times n$  covariance matrix  $C^{(g)}$  of the random vectors  $B^{(g)}D^{(g)}z_k^{(g+1)}$  is used to approximate the (local) search space. The global step size used in the derandomized correlated mutation is deterministically adapted during the search process (Table 3.6).

The assets of the CMA-ES are its adaptability to arbitrary optimization problems, small number of parameters, and computational efficiency, including a highly parallel processing architecture.

<i>ENCODING</i>	Normalized real value encoding
<i>PARAMETERS</i>	$n_{\text{offspring}} = \lambda, n_{\text{parent}} = \mu, \sigma_{\text{initial}}$ (adapted during search)
<i>INITIALIZATION</i>	Fixed object variable start points
<i>REPRODUCTION</i>	Derandomized correlated mutation
<i>SELECTION</i>	No selection mechanism, individuals are adapted

Tab. 3.6 CMA Evolutionary Strategy Characteristics

### “Genetic Algorithm & Direct Search” MATLAB Toolbox

Apart from the direct search tools - which are not used in this investigation - the MATLAB Genetic Algorithm & Direct Search (GADS) Toolbox 1.0.3 offers a set of common GA mechanisms with numerous options for initialization, fitness scaling, selection, crossover and mutation.

This study employs normalized real value encoding, stochastic initialization, standard crossover and mutation reproduction mechanisms, and uses truncation<sup>1</sup> as a selection criteria (Table 3.7).

<i>ENCODING</i>	Normalized real value encoding
<i>PARAMETERS</i>	$n_{\text{pop}}$ , $P_{\text{xover}}$ , $P_{\text{mut}}$ , $c_{\text{threshold}}$ (constant over generations)
<i>INITIALIZATION</i>	Stochastic initialization of population (1 <sup>st</sup> generation)
<i>REPRODUCTION</i>	Crossover, mutation
<i>SELECTION</i>	Truncation

Tab. 3.7 *MATLAB GADS Toolbox Characteristics*

### 3.5 Experimental Setup

Extensive experimental data from investigations on three turbocharged, Common-Rail DI diesel engines - representing automotive, heavy-duty and two-stroke marine diesel applications, respectively - have been provided for this study. The following section briefly summarizes and compares the key engine specifications, operating conditions and utilized measurement techniques.

#### 3.5.1 Engines

The three engines employed cover a broad spectrum of specifications: two- and four-stroke operating cycles, specific displacement volumes of 0.5 to 600 [l/cyl], engine speeds from 60 to 4000 [rpm] and engine outputs of 120 to 8500 [kW] (corresponding to torques of 340 to 750<sup>0</sup>000 [Nm]) as outlined in Table 3.8. Although the injection systems differ in fuel pumps, electronics and injectors used, all of them offer flexible injection pressures and injection timings.

The selected operating conditions vary in injection pressure, start of injection and exhaust gas recirculation rate (EGR). In addition to these standard engine control unit (ECU) parameter variations, the fuel composition (i.e. reference diesel, water-in-diesel emulsion and diesel-butylal blend) is altered for the heavy-duty diesel engine, which is selected as the base engine for all subsequent investigations. The variations in engine speed and load either cover the standard engine operating map (automotive and marine diesel engine) or correspond with the official regulations for heavy-duty diesel engine testing in Europe, the so called European Stationary Cycle (ESC)

---

1. *Truncation selection* - selects the best (according to the objective function value)  $c_{\text{threshold}}$  number of individuals

	“AUTOMOTIVE”	“HEAVY-DUTY”	“MARINE”
<i>Type</i>	5 Cyl., 4-Stroke	4 Cyl., 4-Stroke	4 Cyl., 2-Stroke
<i>Bore</i>	81.0 [mm]	122 [mm]	580 [mm]
<i>Stroke</i>	93.2 [mm]	142 [mm]	2416 [mm]
<i>Compress. Ratio</i>	17.5 [-]	17.2 [-]	17.9 [-]
<i>Turbocharger</i>	Garrett VNT	KKK	ABB Turbo Systems
<i>Max. Power</i>	120 [kW] @ 4000 [min <sup>-1</sup> ]	183 [kW] @ 2100 [min <sup>-1</sup> ]	8500 [kW] @ 105 [min <sup>-1</sup> ]
<i>Max. Torque</i>	340 [Nm] @ 1750 [min <sup>-1</sup> ]	1060 [Nm] @ 1540 [min <sup>-1</sup> ]	7.73 · 10 <sup>5</sup> [Nm] @ 105 [min <sup>-1</sup> ]
<i>Injection System</i>	Common-Rail Direct Injection	Common-Rail Direct Injection	Common-Rail Direct Injection
<i>Fuel Pump</i>	BOSCH 2 <sup>nd</sup> Generation	ETH/LVV Development	Sulzer RT-flex Development
<i>Injectors</i>	BOSCH 2 <sup>nd</sup> Generation	Common-Rail Technologies AG	Sulzer RT-flex Development
<i>Max. Inj. Pressure</i>	1600 [bar]	1600 [bar]	1100 [bar]
<i>Nozzle Tips</i>	5 x 0.166 [mm]	8 x 0.200 [mm]	confidential

Tab. 3.8 Engine and Injection System Specifications

test. A total of  $n_{oc}$  operating conditions is investigated for each engine, employing their respective ECU, application limitations and minimum exhaust emission settings (c.f. Table 3.9).

	“AUTOMOTIVE”	“HEAVY-DUTY”	“MARINE”
$n_{oc}$	[-]	57	39 + 40
<i>Fuel</i>	[-]	Diesel	Diesel, Emulsion, Butylal Blend
$c_m$	[m/s]	3.10 .. 13.02	5.92 .. 8.71
<i>BMEP</i>	[bar]	0.50 .. 18.11	4.35 .. 19.64
$p_{Inj}$	[bar]	380 .. 1600	350 .. 1600
<i>SOI</i>	[°CA]	317/342 .. 351/361	346 .. 357
<i>EGR</i>	[%]	0 .. 44.5	0 .. 43

Tab. 3.9 Overview of Operating Condition Ranges (Minimum .. Maximum)

A stringent classification of the operating conditions into two parts, one for model calibration/training and the other for a subsequent verification and extrapolation beyond experimental variation limits (for example higher and lower injection pressures), helps to ensure accurate evaluation of the investigated optimization methods (Table A.1 - Table A.4).

Besides the start of injection, the temporal profile of the injection, i.e. the rate of fuel injected, significantly affects the combustion process. The experimental injection profiles used in this study are determined from either the ECU injection parameters (start of injection SOI and duration  $t$ ), as was the case with the automotive engine; or they were measured directly on an injector test bench, as was the case with the heavy-duty engine. An example of these methods is given in Figure 3.6 (a) and (b) for the automotive and heavy-duty engine, respectively.

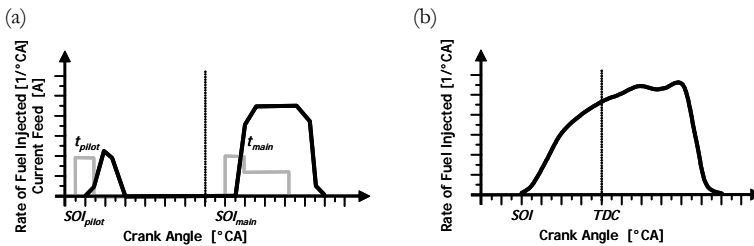


Fig. 3.6 Examples of Injection Profiles (Rate of Fuel Injected):  
 (a) Automotive Split Injection Timing and Injection Profile,  
 (b) Measured Heavy-Duty Single Injection Profile

### 3.5.2 Measurement Techniques

Standard measurement techniques have been applied to acquire the experimental data used within this study. In addition to the global steady-state engine measurements (e.g. performance, exhaust emissions, etc.), the time resolved in-cylinder pressure data were recorded in at least one cylinder of each of the engines.

#### Rate of Heat Release

As there is no direct measurement technique to record the rates of heat release, the so called “measured” rates of heat release are derived from indicated in-cylinder pressure data using standard thermodynamic heat release analysis. Measurement errors hence may arise from the piezoelectric pressure sensor data (e.g. due to sensor deformation, deposits on sensor, or drift of the signal [103]), the top dead centre allocation (temporal shift of the data), or the assumptions used for the heat release analysis (e.g. reference pressure, thermodynamic state at intake valve closing, isentropic compression/expansion, etc. [75]). As an indication of the errors to be taken into account, Table 3.10 lists values based on in-house experience.

VALUES		ERROR
Peak pressure $p_{max}$	[bar]	$\pm 1$ % of absolute value
Maximum pressure increase $(dp/d\phi)_{max}$	[bar/°CA]	$\pm 5$ % of absolute value
Top dead centre (TDC) allocation	[°CA]	$\pm 1$ increment (e.g. 0.2 °CA)
ROHR characteristics (e.g. $\phi_{SOC}$ , $\phi_{50}$ , ...)	[°CA]	$\pm 2$ increments (e.g. 0.4 °CA)
Peak ROHR $Q_{max}$	[J/°CA]	$\pm 5$ % of absolute value

Tab. 3.10 Approximate Values of Errors for the Heat Release Analysis Based on In-House Experience

## Nitrogen Oxide Emissions

The nitrogen oxide emission measurements are conducted using standard, heated chemiluminescence detectors (e.g. Pierburg CLD PM 2000 for the heavy-duty engine [10]), with a relative error smaller than 3.5 % of the maximum value. Taking into account the uncertainties in the specific power output determination, an absolute error of less than 0.50 [g/kWh] for the specific nitrogen oxide emission data has to be considered.

## Soot Emissions

The specific mass of soot (a.k.a. mass of particulate matter PM) is derived using both gravimetric (automotive and heavy-duty engine) and filter smoke number (marine diesel engine) measurements. Although the gravimetric and the filter smoke number measurement techniques use mass and light extinction as measures respectively, both account for the total organic and elementary carbon fractions of the particles. In order to have a consistent set of data, the filter smoke number measurements are converted to specific mass data given an in-house experimental correlation.

The accuracy of the data is influenced by both the relative errors of the measurement devices ( $\pm 0.1$  % of maximum value) and the experimental repeatability due to deviations in engine operation, particularly for operating conditions with soot emissions less than 0.05 [g/kWh]. As a rule of thumb, errors on the order of  $\pm 0.03$  [g/kWh] have to be taken into account for the automotive and heavy-duty diesel engine soot mass measurements.

Recent studies on two-stroke marine diesel engines show that there are discrepancies between filter smoke number and gravimetric measurements, such as simultaneous increases of the filter smoke numbers and decreases of gravimetric mass during engine load variations [4]. The experimental correlation used to convert between FSN and gravimetric measurements is hence assumed to introduce errors on the order of  $\pm 0.04$  [g/kWh].



# 4 RATE OF HEAT RELEASE

In order to simulate or predict both combustion performance and pollutant emissions of a combustion engine, a model to derive the actual rate of heat release (ROHR) is needed. Based on this model,  $\text{NO}_x$  or soot emissions, as well as combustion noise, mechanical strains, etc., can be computed via independent (sub-)models.

## 4.1 Model Description

Adapted from an approach developed by Barba et al. [7], an enhanced phenomenological model is used to predict C.I. combustion rates of heat release. The development is thereby forced by demands for a both accurate and computationally efficient model, capable of correctly predicting the rates of heat release for engine process simulation programs.

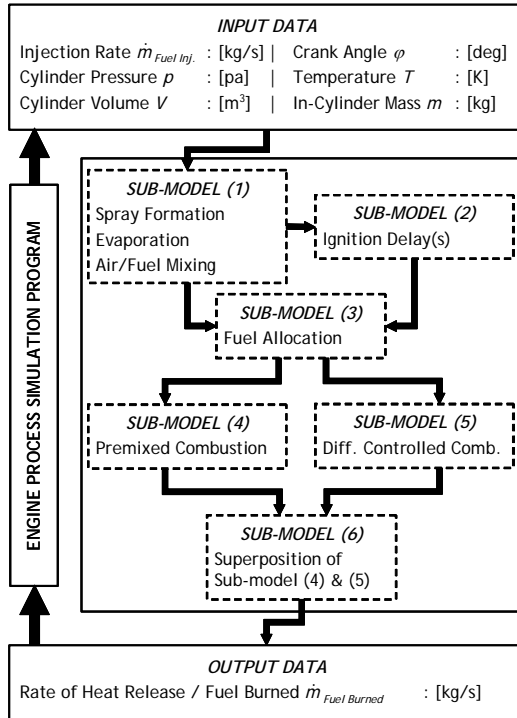


Fig. 4.1 Phenomenological Rate of Heat Release (ROHR) Model

Based on the six fundamental sub-models (c.f. Figure 4.1)

- (1) Spray Formation, Evaporation and Air/Fuel Mixing,
- (2) Ignition Delay(s),
- (3) Fuel Allocation between Premixed and Diffusion Controlled Combustion,
- (4) Premixed Combustion,
- (5) Diffusion Controlled Combustion, and
- (6) Superposition of Premixed and Diffusion Controlled Combustion;

the new model, in combination with an engine process simulation program, allows for reliable predictions of the in-cylinder pressures, emission formation and oxidation within seconds across the entire engine operating map.

### 4.1.1 Inputs & Outputs

As only the high pressure combustion phase of the engine cycle is considered, i.e. the time between the intake valve(s) closing and exhaust valve(s) opening, the model requires as inputs the engine and operating condition specifications, the thermodynamic variables of state (pressure, volume, mass and temperature), the composition of the gas trapped in the cylinder and the crank angle at intake valve closing.

The output of the model is the rate of heat released (ROHR) or rate of mass of fuel burned (a.k.a. burning rate). Integral characteristics, such as the time (measured as degree crank angle) of the start of combustion  $\varphi_{SOC}$ , 10, 50 and 90 % energy release ( $\varphi_{10}$ ,  $\varphi_{50}$ ,  $\varphi_{90}$ ) are used to compare different ROHRs. To enhance the characterization of the rates of heat released, the present study also compares the ROHR maxima for premixed and diffusion controlled combustion  $Q_{max,p}$  and  $Q_{max,d}$  along with the according times  $\varphi_{Qmax,p}$  and  $\varphi_{Qmax,d}$  as well as the masses of fuel burnt  $m_{pmx}$  and  $m_{diff}$  (c.f. Figure 4.2).

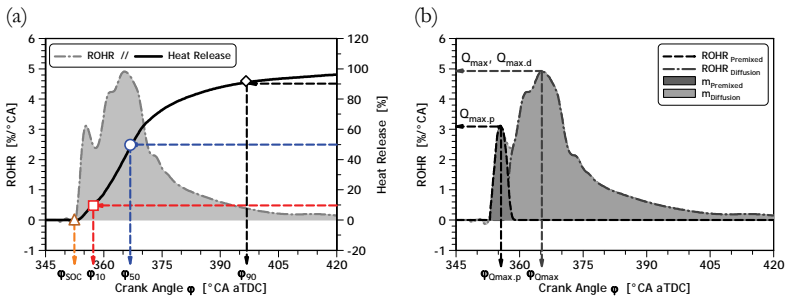


Fig. 4.2 ROHR Characteristics: (a) Integral and (b) Detailed Premixed & Diffusion Controlled Combustion Characteristics



## 4.1.2 Evaporation & Spray Formation

The temporal behavior of the model is predominantly defined by the rates of fuel injected (a.k.a. injection rates) and the rates of fuel evaporated. Thus, both mass of fuel injected per time-step and spray formation and evaporation modeling are the crucial elements in ensuring the exactness of the simulation results. As shown later on, simple, yet physically/chemically coherent descriptions of these mechanisms can fulfill these demanding requirements.

### Spray Formation

The mass of fuel injected per time-step is split into  $n$  identical droplets. The primary diameter of these droplets is assumed to be the Sauter Mean Diameter (SMD) according to Kamimoto [53]

$$d_{\text{SMD}} = c_{\text{SMD}} \cdot 47 \cdot d_{\text{Nozzle}} \cdot Re_{\text{Air}}^{-0.5} \cdot \left( \frac{\rho_{\text{Air}}}{\rho_{\text{Fuel}}} \right)^{0.25}, \quad (4.1)$$

where  $d_{\text{Nozzle}}$  is the effective nozzle diameter (geometric diameter  $\times$  coefficient of contraction  $\mu$ ), and  $Re_{\text{Air}}$  is the Reynolds number of the air trapped in the cylinder. The number of droplets  $n$  is given by the mass of fuel injected, the specific density of the fuel  $\rho_{\text{Fuel}}$  and the SMD.

### Evaporation / Wall Contact

The rate of evaporation is given by means of the common, single liquid droplet vaporization equation with the empirical rate constant  $\beta$  (a.k.a. “d<sup>2</sup>-law”)

$$d_{\text{Droplet}}^2 = d_{\text{SMD}}^2 - \beta \cdot t \quad (4.2)$$

Given the in-cylinder geometry, the impingement of droplets on the piston head or cylinder liner is modeled as build-up and evaporation of a wall-applied fuel film (i.e. transient fuel storage)

$$\dot{m}_{\text{FuelFilm}} = \frac{m_{\text{FuelFilm}}}{\tau_{\text{FuelFilm}}} - c_{\text{FuelFilm}} \cdot \dot{m}_{\text{FuelVapWall}}, \quad (4.3)$$

where  $m_{\text{FuelFilm}}$  is the actual mass of fuel stored in the film,  $m_{\text{FuelVapWall}}$  is the mass of vaporized fuel reaching the piston or cylinder liner, and  $\tau_{\text{FuelFilm}}$  and  $c_{\text{FuelFilm}}$  are the characteristic fuel film evaporation time and build-up scaling factor, respectively.

### Air/Fuel Mixing

The mixing of vaporized fuel with surrounding fresh mixture - composed of intake air and residual gas - is assumed to take place at a constant mixing ratio during the entire fuel injection process. Thus, the mass of fresh mixture in the premixed zone is given as

$$m_{\text{PrmxFM}} = A \cdot \lambda_{\text{st}} \cdot m_{\text{FuelVap}} \quad (4.4)$$

where  $A$  is the default equivalence ratio after evaporation and  $\lambda_{\text{st}}$  is the stoichiometric air/fuel ratio.

The mixing of vaporized fuel with fresh gas after either start of combustion or end of injection leads to a dilution of the premixed zone. Assuming spherical premixed zones (surface area  $A_{\text{Zone}}$  and diameter  $d_{\text{Zone}}$ ) for each injector orifice, this diffusion of vaporized fuel out off these zones is described as

$$\frac{dm_{\text{FuelVap}}}{dt} = c_1 \cdot Re_{\text{Air}}^{c_2} \cdot A_{\text{Zone}} \cdot \frac{\rho_{\text{FuelVap}}}{d_{\text{Zone}}} \quad (4.5)$$

### 4.1.3 Ignition Delay(s) & Fuel Allocation

Ignition, and thus start of combustion (SOC), occur at the time at which the so-called ignition delay integral exceeds a value of 1:

$$\int_0^t \frac{1}{\tau_{\text{IgnDel}}} dt \geq 1 \quad (4.6)$$

The effective ignition delay  $\tau_{\text{IgnDel}}$  itself is given as the sum of both the physical ignition delay, which is a function of the droplet diameter  $d_{\text{Nozzle}}$  and the velocity  $u_0$ , as well as the chemical ignition delay, defined by the in-cylinder pressure  $p$  and temperature  $T$ , the reaction activation temperature  $T_A$  and the air/fuel ratio  $\lambda_{\text{Prmx}}$ .

$$\tau_{\text{IgnDel}} = c_1 \cdot u_0^{-1.68} \cdot d_{\text{Nozzle}}^{0.88} + c_2 \cdot \left(\frac{p}{p_0}\right)^{c_3} \cdot \lambda_{\text{Prmx}}^{c_4} \cdot e^{T_A/T} \quad (4.7)$$

Even after start of combustion, vaporized fuel is added to the premixed combustion zone by means of an allocation function  $F_{\text{PrmxDiff}}$ . Resulting from droplets already existing within the premixed zone, the amount of vaporized fuel being added is determined by considering the mass of fuel burnt in premixed combustion  $m_{\text{BurntPrmx}}$  and the mass of fuel vaporized at start of combustion  $m_{\text{FuelVap0}}$ .

$$F_{\text{PrmxDiff}} = f(m_{\text{BurntPrmx}}, m_{\text{FuelVap0}}) \quad (4.8)$$

Hence the actual mass of fuel in premixed and diffusion controlled combustion zones  $m_{\text{FuelVapPrmx}}$  and  $m_{\text{FuelVapDiff}}$  are given as

$$\dot{m}_{\text{FuelVapPrmx}} = (1 - F_{\text{PrmxDiff}}) \cdot \dot{m}_{\text{FuelEvap}}, \text{ and} \quad (4.9)$$

$$\dot{m}_{\text{FuelVapDiff}} = F_{\text{PrmxDiff}} \cdot \dot{m}_{\text{FuelEvap}} \quad (4.10)$$

Considering operating conditions with multiple pulse injection profiles (e.g. pilot, main and post injection) that result in a “staged” combustion (c.f. Chapter 4.4.2), a new ignition delay integral is used everytime the combustion of an injection pulse is completed prior to the start of a subsequent injection.

#### 4.1.4 Pre-Mixed Combustion

Premixed combustion is affected by two competing mechanisms: (1) the single-point ignition turbulent flame propagation and (2) the time-scale driven, multi-point ignition turbulent combustion. Both mechanisms are based on the turbulent flame speed  $s_{\text{turb}}$ , which is assumed to be a function of the laminar flame speed  $s_{\text{lam}}$  given by Rhodes and Keck [82], and the mean piston velocity  $c_m$ .

$$s_{\text{turb}} = s_{\text{lam}} \cdot \left( 1 + 1.6 \cdot \left( \frac{c_m}{s_{\text{lam}}} \right)^{0.8} \right) \quad (4.11)$$

##### Single-Point Ignition Combustion

Given a homogeneous air/fuel mixture, the rate of fuel converted in a single-point ignition turbulent combustion  $\dot{m}_{\text{FuelBurn I}}$  can be written as

$$\dot{m}_{\text{FuelBurn I}} = c_1 \cdot \rho_{\text{AF}} \cdot s_{\text{turb}} \cdot A_{\text{Flame}} \quad (4.12)$$

where  $\rho_{\text{AF}}$  is the homogeneous mixture density,  $s_{\text{turb}}$  is the turbulent flame speed and  $A_{\text{Flame}}$  is the flame front surface.

##### Multi-Point Ignition Combustion

With the higher in-cylinder temperatures and pressures due to the single-point ignition flame propagation, the probability for further ignition points in the unburned air/fuel mixture increases. This multi-point ignition combustion  $\dot{m}_{\text{FuelBurn II}}$  (a.k.a. second phase premixed combustion) is modeled as characteristic time-scale driven turbulent combustion

$$\dot{m}_{\text{FuelBurn II}} = c_2 \cdot \frac{m_{\text{FuelVapPrmx}}}{\tau_{\text{Prmx}}} \quad (4.13)$$

where the characteristic mixing time  $\tau_{\text{Prmx}}$  is a function of the characteristic length scale  $l_{\text{Prmx}}$  and the premixed combustion ratio of fresh air to fuel  $\xi_{\text{PrmxAir}}$

$$\tau_{\text{Prmx}} = \xi_{\text{PrmxAir}}^2 \cdot \frac{l_{\text{Prmx}}}{s_{\text{turb}}} \quad (4.14)$$

##### Superposition

The overall premixed combustion burning rate follows from a superposition of the single-point and multi-point combustion mechanisms described above.

$$\dot{m}_{\text{FuelBurnPrmx}} = \frac{\dot{m}_{\text{FuelBurn I}} \cdot \dot{m}_{\text{FuelBurn II}}}{\dot{m}_{\text{FuelBurn I}} + \dot{m}_{\text{FuelBurn II}}} \quad (4.15)$$

### 4.1.5 Diffusion Controlled Combustion

Using a frequency based approach, the characteristics of the diffusion controlled combustion are defined by the mixing time  $\tau_{\text{Diff}}$  and the mass of vaporized fuel  $m_{\text{FuelVapDiff}}$  available.

$$\dot{m}_{\text{FuelBurnDiff}} = c_3 \cdot \frac{m_{\text{FuelVapDiff}}}{\tau_{\text{Diff}}}, \quad (4.16)$$

The mixing time  $\tau_{\text{Diff}}$  is defined as the ratio of the characteristic diffusion length scale  $l_{\text{Diff}}$  and the mass transfer velocity  $u'$

$$\tau_{\text{Diff}} = \frac{l_{\text{Diff}}}{u'} \quad (4.17)$$

where the characteristic length scale  $l_{\text{Diff}}$  is given as a function of the instantaneous in-cylinder volume  $V_{\text{Cyl}}$ , the number of injection nozzle orifices  $n_{\text{Nozzle}}$ , and the specific air/fuel ratio for the transferred mass  $\lambda_{\text{Diff}}$ .

$$l_{\text{Diff}} = \left( \frac{V_{\text{Cyl}}}{\lambda_{\text{Diff}} \cdot n_{\text{Nozzle}}} \right)^{1/3} \quad (4.18)$$

As a function of the actual air/fuel ratio at SOC  $\lambda_{\text{SOC}}$  and the burned mass fraction  $\zeta$ , the specific air/fuel ratio for the transferred mass  $\lambda_{\text{Diff}}$  mainly accounts for the decreasing mass of oxygen available during combustion.

$$\lambda_{\text{Diff}} = f(\lambda_{\text{SOC}}, \zeta) \quad (4.19)$$

Given that the mixing of air and fuel during diffusion controlled combustion is a highly turbulent process, a velocity  $u'$  derived from the instantaneous turbulence intensity is used as characteristic velocity for calculations concerning the mass transfer. Assuming a spatially homogeneous in-cylinder turbulence distribution at all times, five key effects contribute to an increase in turbulent kinetic energy: intake flow, swirl, quench flow, injection and combustion.

As a common approximation, the contributions of the intake and quench flows, as well as the swirl to the turbulence intensity are taken to be proportional to the square of the mean piston velocity  $c_m$  (a.k.a. background turbulence). The characteristic velocity  $u'$  is thus defined as

$$u' = \sqrt{c_g \cdot c_m^2 + c_{\text{Inj}} \cdot k_{\text{Inj}} + c_{\text{Comb}} \cdot k_{\text{Comb}}} \quad (4.20)$$

where the effects of injection and combustion on the turbulent kinetic energy are described as functions of the rate of fuel injected  $m_{\text{FuelInj}}$ , the nozzle exit velocity  $u_0$ , the in-cylinder mass  $m_{\text{Cyl}}$  and the burning rate  $m_{\text{FuelBurn}}$ .

$$\frac{dk_{\text{Inj}}}{dt} = c_{\text{InjF}} \cdot f_{\text{Formation}}(\dot{m}_{\text{FuelInj}}) - c_{\text{InjD}} \cdot f_{\text{Dissipation}}(k_{\text{Inj}}, l_{\text{Inj}}) \quad (4.21)$$

$$\frac{dk_{\text{Comb}}}{dt} = c_{\text{CombF}} \cdot f_{\text{Formation}}(\dot{Q}_{\text{Chem}}) - c_{\text{CombD}} \cdot f_{\text{Dissipation}}(k_{\text{Comb}}, l_{\text{Comb}}) \quad (4.22)$$

### *Superposition of Premixed and Diffusion Controlled Combustion*

Assuming that the premixed and diffusion controlled combustion start simultaneously, a time delay function  $F$  is used to postpone the rate of fuel burnt during diffusion controlled combustion, accounting for the delayed chemical reactions governing the diffusion controlled combustion immediately after SOC.

$$\dot{m}_{\text{FuelBurn}} = \dot{m}_{\text{FuelBurnPrmx}} + F \cdot \dot{m}_{\text{FuelBurnDiff}} \quad (4.23)$$

$$F = (\zeta_{\text{Prmx}})^{c_{\text{Delay}}} = \left( \frac{m_{\text{FuelBurnPrmx}}}{m_{\text{FuelVapPrmx}}} \right)^{c_{\text{Delay}}} \quad (4.24)$$

#### *4.1.6 Parameters*

Along with the above mentioned input data, the ROHR model parameters listed in Table 4.1 (including the size range for each parameter) are needed to calculate the actual rate of fuel burnt (output). The actual values for the parameters are determined using various approaches (c.f. Chapter 3).

## *4.2 Model Parameter Sensitivity Study*

In order to estimate the relative importance of the individual ROHR model parameters, a sensitivity study is performed considering 19 heavy-duty engine operating conditions (“calibrating” operating conditions Table A.2).

Defining  $\mathbf{x}$  as a vector containing all ROHR model parameters, and  $\mathbf{y}$  as a vector containing the model output characteristics (Section 4.1.1), the ROHR model for each of the  $n_{\text{oc}}$  operating conditions can be written as

$$\mathbf{y} = f_{\text{ROHR}}(\mathbf{x}) \quad (4.25)$$

with

$$\mathbf{x} = [c_{\text{SMD}}, \beta, c_{\text{Spray}}, \dots] \quad \text{and} \quad \mathbf{y} = [\varphi_{\text{SOC}}, \varphi_{10}, \varphi_{50}, \dots]. \quad (4.26)$$

Given a set of base values  $\mathbf{x}_0$ , each parameter  $\mathbf{x}_i$  is independently varied in steps of  $\pm 5\%$  within its respective size range (c.f. Table 4.1). The sensitivity  $\chi$  of an output characteristic  $\mathbf{y}_i$  on the model parameter  $\mathbf{x}_i$  is defined as average over the relative changes in  $\mathbf{y}_i$  normalized with the imposed variations in  $\mathbf{x}_i$ .

$$\chi_{(\mathbf{y}_i, \mathbf{x}_i)} = \frac{1}{n_{\text{oc}}} \cdot \sum_{n_{\text{oc}}} \frac{\Delta \mathbf{y}_i}{\Delta \mathbf{x}_i} = \frac{1}{n_{\text{oc}}} \cdot \sum_{n_{\text{oc}}} \frac{|\mathbf{y}_i - \mathbf{y}_0|}{|\mathbf{x}_i - \mathbf{x}_0| / \mathbf{x}_0} \quad (4.27)$$

	<i>PARAMETER</i>		<i>UNIT</i>	<i>SIZE RANGE</i>
<i>INJECTION &amp; EVAPORATION</i>	$c_{\text{SMD}}$	Sauter Mean Diameter scaling factor (s.f.)	[-]	0.1 .. 10
	$\beta$	Empirical evaporation rate	[-]	$1 \cdot 10^{-9} \dots 1 \cdot 10^{-6}$
	$c_{\text{FuelFilm}}$	Wall-applied fuel film build-up scaling factor	[-]	0.0 .. 1.0
	$\tau_{\text{FuelFilm}}$	Characteristic fuel film evaporation time	[s]	$1 \cdot 10^{-5} \dots 1 \cdot 10^{-3}$
	$A$	Equivalence ratio after evaporation	[-]	0.4 .. 1.0
	$c_1$	Diffusion caused dilution scaling factor	[-]	$1 \cdot 10^{-5} \dots 1 \cdot 10^{-3}$
<i>IGNITION DELAY(S)</i>	$c_2$	Reynolds number exponential factor	[-]	0.0 .. 1.0
	$c_1$	Physical ignition delay scaling factor	[-]	0.0 .. 10
	$c_2$	Chemical ignition delay scaling factor	[-]	$0.0 \dots 1 \cdot 10^4$
	$c_3$	Cylinder pressure exponential factor	[-]	0.0 .. 5.0
	$c_4$	Air/fuel ratio exponential factor	[-]	0.0 .. 1.0
	$T_A$	Activation temperature	[K]	1000 .. 10'000
<i>COMBUSTION</i>	$c_1$	Single-point ignition combustion s.f.	[-]	0.0 .. 10
	$c_2$	Multi-point ignition combustion s.f.	[-]	0.0 .. 10
	$c_3$	Diffusion controlled combustion s.f.	[-]	0.0 .. 10
	$c_g$	Background turbulence intensity s.f.	[-]	0.0 .. 10
	$c_{\text{Inj}}$	Injection induced turbulence scaling factor	[-]	0.0 .. 10
	$c_{\text{Comb}}$	Combustion induced turbulence s.f.	[-]	0.0 .. 10
	$c_{\text{InjF}}$	Injection turbulence formation scaling factor	[-]	0.0 .. 1.0
	$c_{\text{InjD}}$	Injection turbulence dissipation s.f.	[-]	0.0 .. 1.0
	$c_{\text{CombF}}$	Combustion turbulence formation s.f.	[-]	0.0 .. 1.0
	$c_{\text{CombD}}$	Combustion turbulence dissipation s.f.	[-]	0.0 .. 1.0
	$c_{\text{Delay}}$	Superposition exponential delay factor	[-]	0.0 .. 50

*Tab. 4.1 ROHR Model Parameters*

As an example, Figure 4.3 (a),(b) and (c) shows the sensitivities of the global ROHR characteristics ( $\varphi_{\text{SOC}}/\varphi_{10}/\varphi_{50}/\varphi_{90}/Q_{\text{max}}/\varphi_{Q_{\text{max}}}$ ) and the detailed premixed and diffusion combustion characteristics ( $Q_{\text{max,p}}/\varphi_{Q_{\text{max,p}}}/Q_{\text{max,d}}/\varphi_{Q_{\text{max,d}}}/m_{\text{prmx}}/m_{\text{diff}}$ ) on 5 % variations in injection and evaporation parameter values.

Except for three, all sensitivities, given the 5 % variation in model parameters, are lower than one; in other words, 5 % parameter variations generally result in less than 5 % changes in model output characteristics. Furthermore, some of the variations in parameter values affect the model outcomes by less than a factor of  $10^{-5}$ , i.e. a 5 %

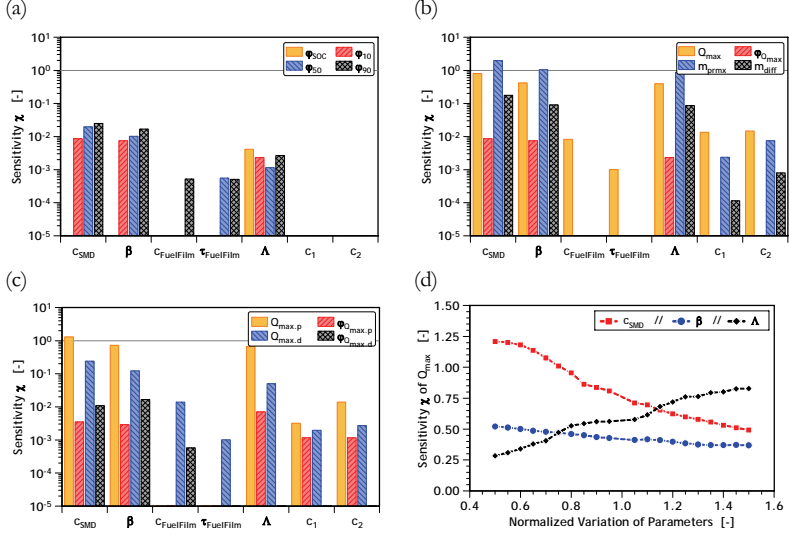


Fig. 4.3 ROHR Model Output Sensitivities to  $\pm 5\%$  Variations of Injection & Evaporation Parameters: (a) Integral ROHR, (b), and (c) Detailed Premixed and Diffusion Controlled Combustion Characteristics. (d) Sensitivity of  $Q_{max}$  to  $\pm 50\%$  Variations in  $c_{SMD}$ ,  $\beta$ , and  $A$

variation of the parameter value (e.g. the dilution caused diffusion scaling factor  $c_1$ ) results in a less than  $5 \cdot 10^{-5}\%$  change in model outputs (e.g.  $\varphi_{SOC}$  or  $\varphi_{50}$ ).

The different sensitivities of particular parameters represent the governing structures of the model. The characteristic wall-applied fuel film evaporation time  $\tau_{FuelFilm}$  for example - although affecting the global 50 & 90% energy released characteristics - has neither an effect on the start of combustion nor on the maximum of the premixed combustion ROHR  $Q_{max,p}$ . This is explained as a direct consequence of the inherent delay between the fuel film build-up and evaporation processes (the wall-applied fuel film build-up starts with the first droplet of an injection spray impinging the wall).

Figure 4.3 (d) shows the sensitivity of the maximum rate of heat release to a variation of the Sauter Mean Diameter  $c_{SMD}$ , evaporation rate  $\beta$ , and equivalence ratio after evaporation  $A$  in the range of  $\pm 50\%$ . Whereas the influence of the variation size on the sensitivity of the evaporation rate  $\beta$  is almost negligible, the influence on  $c_{SMD}$  and  $A$  are both non-linear and oppositional in trend (a decrease in parameter variation leads to a decrease and an increase in  $A$  and  $c_{SMD}$  sensitivity at the same time).

The sensitivities, and hence the relative importance of the model parameters, not only indicate which parameters have little influence on the model outcome, they also

indicate the need for an advanced calibration algorithm due to the inherent non-linearity of the model (e.g. variable sensitivities over variation step size).

### 4.3 Comparative Algorithm Study

Given that there is no algorithm solving for all optimization problems, that on average performs superior to any other algorithm [105], a comparative study on the four algorithms mentioned in Section 3.4.3, the Genetic Algorithm (GA), the Evolutionary Algorithm (EA), the Covariance-Matrix-Adaption Evolutionary Strategy (CMA-ES) and the Matlab Genetic Algorithm & Direct Search (GADS) is carried out.

#### 4.3.1 Basic Setup

In order to compare the performance of the algorithms, each of the four is used to calibrate the ROHR model (single objective approximation function, Section 3.4.3) based on a set of heavy-duty diesel engine operating conditions (“calibration” operating conditions Table A.2). To verify the performance of the calibration, the models are validated using the “verification” operating conditions given in Table A.2. To reduce the inherent statistical randomness of the algorithms, multiple optimization (calibration) runs on four identical desktop computers are performed.

The sum of the deviations between experimental and numerical ROHR output characteristics  $\varphi_{SOC}$ ,  $\varphi_{10}$ ,  $\varphi_{50}$ , and  $\varphi_{90}$  is used as a measure to estimate the performance of the calibrated models. To visualize the performance, experimental and numerical ROHR characteristics of both calibration and verification operating conditions are plotted sequentially (Figure 4.4 (a)). In addition to the sequential operating condition representation, a “1-to-1” scatter plot of measured against simulated characteristics is used to visualize the statistical correlation (Figure 4.4 (b)).

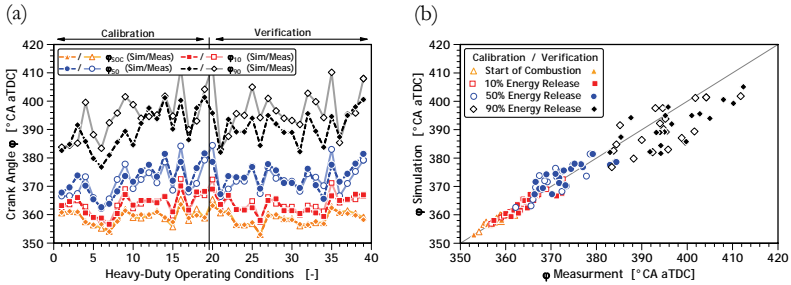


Fig. 4.4 Comparison of Experimental and Numerical ROHR Characteristics for the CMA-ES Algorithm Model Calibration: (a) Sequential Operating Conditions Plot, (b) “1-to-1” Scatter Plot



### 4.3.2 Algorithm Performance

To visualize the temporal performance of the algorithms, the average error from ten consecutive optimization runs is plotted against the number of ROHR model function evaluations<sup>1</sup> (Figure 4.5 (a)). After large initial errors, followed by similar performance characteristics at approximately 7'500 function evaluations, the four algorithms investigated vary in both temporal performance and final error (the optimizations are stopped after a specific CPU-time).

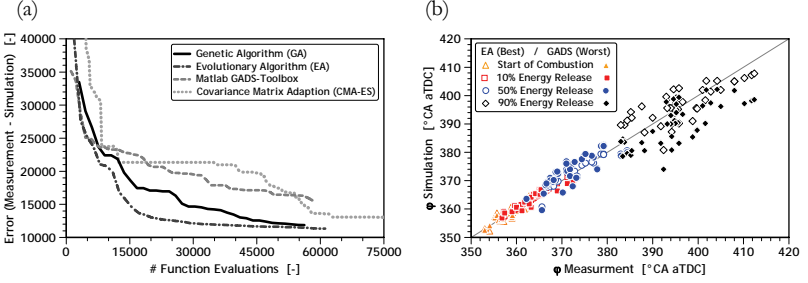


Fig. 4.5 Comparison of the 4 Algorithms Used for the ROHR Model: (a) Performance Plot, (b) “1-to-1” Scatter Plot (Best vs. Worst Algorithm)

Whereas the GA and GADS algorithms show a linear - however different in slope - performance improvement, the EA and CMA-ES feature exponential and stepwise improvements respectively. While EA and GADS final optimization errors may differ by nearly 40 % ( $f_{\text{Error.EA}} = 11'200$  vs.  $f_{\text{Error.GADS}} = 15'600$ ), the only significant deviations found in global ROHR characteristics are at  $\varphi_{50}$  and  $\varphi_{90}$  (Figure 4.5 (b)).

Analyzing the four calibrated models using both the Pearson's correlation coefficients<sup>2</sup> and the linear regression slopes<sup>3</sup>, yields similar results for the GA, EA and CMA-ES algorithm (Figure 4.6 (a)). The correlation coefficients for the  $\varphi_{\text{SOC}}$ ,  $\varphi_{10}$  and  $\varphi_{50}$  characteristics determined using these three algorithms are of the order of 0.9, while the  $\varphi_{90}$  correlation coefficients are slightly worse (0.75 to 0.8). The correlation coefficients for the GADS algorithm drop almost linearly from 0.9 ( $\varphi_{\text{SOC}}$ ) to 0.55 ( $\varphi_{90}$ ).

1.  $n_{\text{Eval}}$  (# function evaluations) =  $n_{\text{oc}}$  (# operating conditions) \*  $n_{\text{CallsAlgorithm}}$  (# function calls by the algorithm)
2. Pearson's correlation coefficient  $r$  - measure of how well a linear equation describes the relation between two variables  $x$  and  $y$ ; defined as the covariance of  $(x, y)$  and the product of the standard deviations,  $r = \text{cov}(x, y) / (\sigma_x \sigma_y)$ ,  $-1 \leq r \leq 1$  ( $r = 1$  : perfect linear correlation)
3. Linear regression slope  $m$  - slope of best-fit line plotted through  $x$  and  $y$  using the method of “least squares”;  $y = mx + b$  (c.f. Figure 4.6 (b))

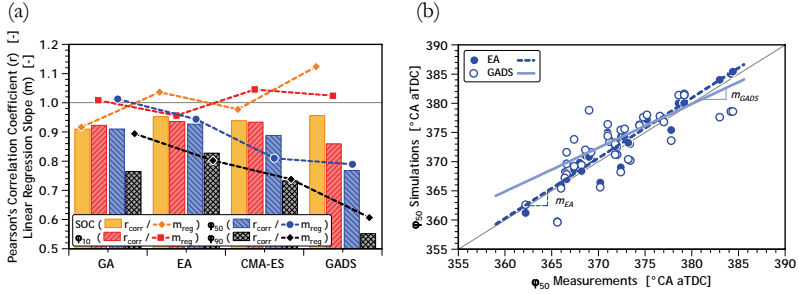


Fig. 4.6 Comparative Algorithm Study Statistics: (a) Person's Correlation Coefficient & Linear Regression Slope (b)  $\phi_{50}$  "1-to-1" Plot

All four algorithms investigated have linear regression slopes  $m$  of approximately unity for the  $\phi_{SOC}$  and  $\phi_{10}$  characteristics, whereas the values for the  $\phi_{50}$  and  $\phi_{90}$  characteristics are significantly lower than 1, specifically for both the CMA-ES and GADS algorithm. As an example, Figure 4.6 (b) compares the  $\phi_{50}$  data obtained from both the GA and GADS calibrated ROHR models, visualizing the effects measured by the linear regression slope  $m$ . A slope  $m$  which is lower than unity refers to a reduced sensitivity of the simulation output, i.e. while low measurement values are over predicted by the simulation, higher values are under predicted.

### 4.3.3 Stochastic Initialization & Evolution

In order to determine the influence of a stochastic initialization on the performance of evolutionary algorithms, 25 consecutive ROHR model calibrations are performed using the EA algorithm.

As shown in Figure 4.7 (a), the initial variations caused by the stochastic initialization decrease with the number of function evaluations ( $\Delta f_{\text{ERROR}}$  at initialization: 24'600; after 50'000 function evaluations: 1'700). Furthermore, neither the optimization case with the best nor the worst stochastic parameter initialization remains the best nor worst case at the end of the optimization. Thus, although there is a significant influence on the initial phase of the optimization, the stochastic manipulations used during the evolutionary processes (i.e. recombination and mutation) have a larger impact on the optimization outcome.

To illustrate the influence of stochastic initialization on the individual model parameters, Figure 4.7 (b) shows the development of the combustion induced turbulence scaling factor  $c_{\text{Comb}}$  for the 25 consecutive optimization runs. Whereas initial values are randomly distributed, the solutions tend to approach the best overall value with an increasing number of function evaluations (similar to the performance value variation decrease).

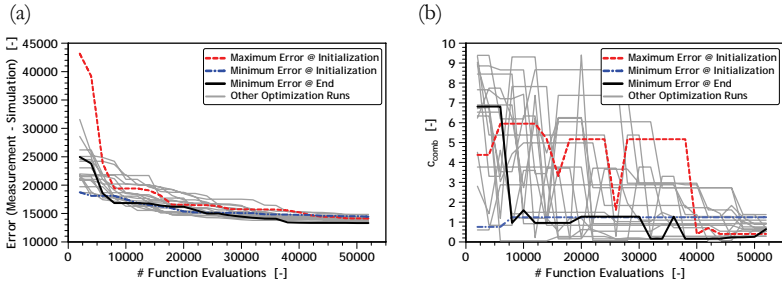


Fig. 4.7 Performance and Parameter Variations of 25 Optimization Runs: (a) Error vs. # Function Evaluations (b) Single Parameter Variation

### 4.3.4 Summary

Although the four algorithms show similar global performances (except for the minor deviations in  $\varphi_{50}$  and  $\varphi_{90}$ ), the exponential temporal performance improvement of the EA makes it the preferred algorithm. Hence, the EA is used as parameter calibration algorithm in all subsequent investigations and studies.

## 4.4 Model Study on Different Engine Sizes

To evaluate the general applicability of the proposed ROHR model, the three engines employed in this study cover both major application areas of modern Common-Rail DI diesel engines (automotive, heavy-duty and marine, specifications c.f. Section 3.5.1) and a wide range of operating conditions (c.f. Appendix A). Using the heavy-duty engine as the reference engine, in addition to the calibration of the model to each specific engine, the heavy-duty engine specific model is also applied to the automotive and marine diesel engine, without any parameter modifications (i.e. “bind try”).

### 4.4.1 “Heavy-Duty” Diesel

Figure 4.8 shows the results using an EA (Evolutionary Algorithm) with a population size  $n_{\text{pop}}$  of 100 ( $n_{\text{parent}} = 50$ ,  $n_{\text{offspring}} = 150$ ) to calibrate the 23 ROHR model parameters given in Table 4.1. With a mean model calculation time of one-third of a second, approximately 12 hours are required to calibrate the ROHR model based on the 19 operating conditions.

Evident from an engineering point of view is the excellent prediction of the relative variations between two arbitrary operating conditions (hereafter referred to as “trends”) for the four ROHR characteristics, as well as the small deviations of the

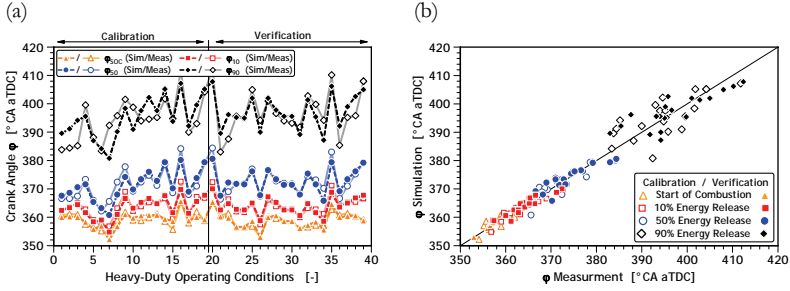


Fig. 4.8 Heavy-Duty Diesel ROHR Model Calibration & Verification: (a) Sequential Operating Conditions Plot, (b) “1-to-1” Scatter Plot

absolute values of the start of combustion  $\phi_{SOC}$  and the positions of 10% and 50% energy release ( $\phi_{10}$ ,  $\phi_{50}$ ). Otherwise, the differences between the measured and simulated positions of 90 % energy release  $\phi_{90}$  are up to 10 °CA. As a result of the small energy release rates near the end of combustion, minor inaccuracies in the energy release cause significant deviations in the temporal locations, (e.g. an error of  $\pm 1\%$  in absolute energy released changes the location by almost 5 °CA).

The correlation statistics for  $\phi_{SOC}$ ,  $\phi_{10}$ ,  $\phi_{50}$ , and  $\phi_{90}$  given in Table 4.2 confirm the “graphical” interpretations from Figure 4.8. Whereas the  $\phi_{SOC}$ ,  $\phi_{10}$ , and  $\phi_{50}$  correlation coefficients are of the order of 0.9 for both calibration and verification, the  $\phi_{90}$  coefficients are significantly lower (approximately 0.7 and 0.8 respectively). Furthermore, the linear regression slope  $m$  (smaller than unity) and the intercept  $b$  (larger than zero) indicate the slightly reduced sensitivity of the simulation data on operating condition variations during both calibration and verification.

		$\phi_{SOC}$	$\phi_{10}$	$\phi_{50}$	$\phi_{90}$	
Calibration	<b>Pearson’s Correlation Coefficient <math>r</math></b>	[-]	0.8970	0.9248	0.9005	0.7111
	<b>Linear Regression Slope <math>m</math></b>	[-]	0.84	0.86	0.85	0.67
	<b>Linear Regression Intercept <math>b</math></b>	[-]	-0.08	0.31	1.65	11.75
Verification	<b>Pearson’s Correlation Coefficient <math>r</math></b>	[-]	0.9465	0.9194	0.9174	0.8178
	<b>Linear Regression Slope <math>m</math></b>	[-]	0.95	0.82	0.77	0.62
	<b>Linear Regression Intercept <math>b</math></b>	[-]	0.01	0.71	2.83	14.17

Tab. 4.2 Heavy-Duty Engine ROHR Model Statistics

To illustrate the broad range of operating conditions used, the heat release traces from six operating conditions, arbitrarily selected from the 39 heavy-duty engine operating conditions given in Table A.2, are compared in Figure 4.9. Although the

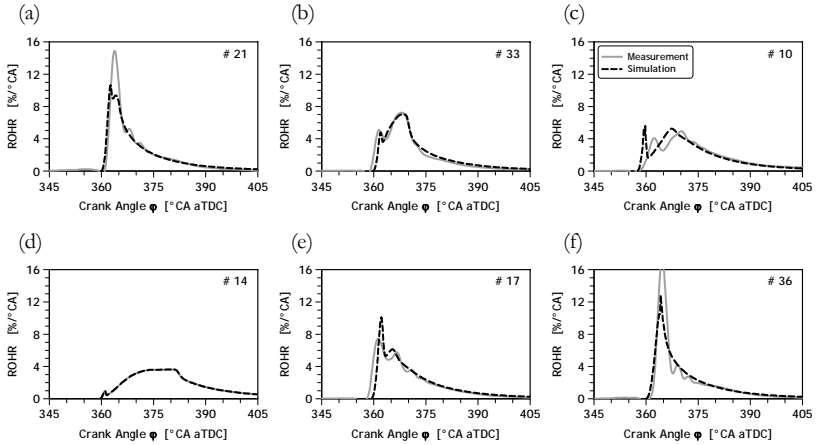


Fig. 4.9 Examples (6 out of 39) of ROHR Traces for Heavy-Duty Engine

deviations between absolute measurement and simulation values for the 90% energy release locations  $\phi_{90}$  seem to be significant (Figure 4.8), the actual rates of heat release plotted against the crank angle (Figure 4.9) do not show substantial discrepancies after 375 [°CA aTDC].

In addition to the global ROHR characteristics given in Figure 4.8, the ignition delay, the premixed combustion ratio, as well as the location and magnitude of the maximum (peak) ROHR are further crucial factors in IC engine research and development. The location and magnitude of the peak heat release rate are often used as a first approximation to estimate both the peak pressure in, and the combustion noise from modern DI diesel engines with advanced turbocharging, high-pressure injection systems and high compression ratios.

Given the process flow of the implemented phenomenological combustion model (Figure 4.1), the accuracy of the simulation depends on the first three sub-models: (1) spray formation (2) evaporation and (3) air/fuel mixing, ignition delay, fuel allocation. A closer look at the ignition delay (Figure 4.10 (a)) for example shows an excellent correlation between measured and simulated values (maximum deviation is less than 1.5 °CA).

The comparison of calculated and measured premixed combustion ratios is a measure for the prediction quality of the fuel allocation, premixed combustion, and spray formation, evaporation and air/fuel mixing sub-models (Figure 4.10 (b)). Calculated premixed combustion ratios generally under-predict their experimentally determined counterparts, which is partially due to shorter ignition delays in the simulation (e.g. # 1-3), and/or errors introduced by the non-deterministic distinction between experimental premixed and diffusion controlled combustion (c.f. [72]).

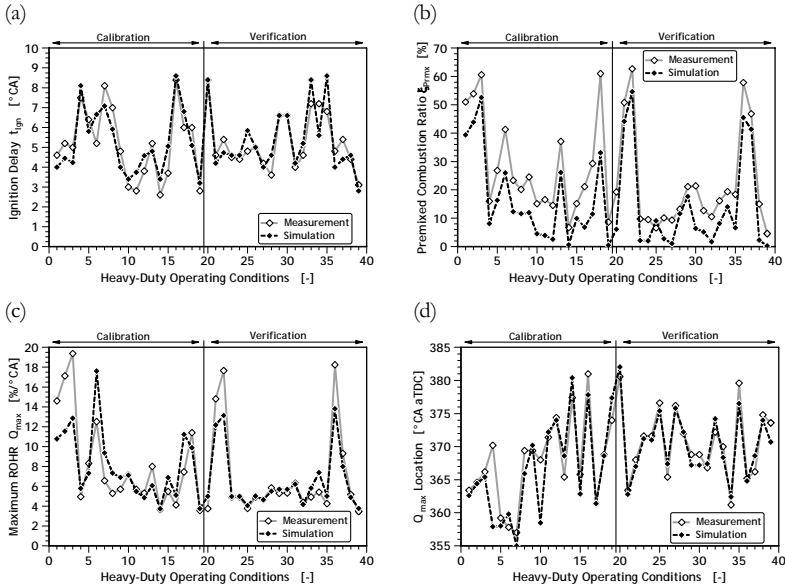


Fig. 4.10 Extended ROHR Characteristics for the Heavy-Duty Engine: (a) Ignition Delay, (b) Premixed Combustion Ratio, (c) Maximum ROHR and (d) Location of Maximum ROHR

Although more demanding in terms of model performance, the numerical results obtained for both maximum ROHR  $Q_{max}$  and location of maximum ROHR  $\phi_{Qmax}$  match experimental data trends, even though deviations in absolute values are present (Figure 4.10 (c) and (d)). The largest errors are at operating conditions with high premixed combustion ratios ( $\zeta_{Pmix} > 40\%$ , e.g. # 1-3, 21-22, 36) and mainly originate from the simplifications used for droplet formation and evaporation modeling (Section 4.1.2, assuming one representative primary droplet diameter per time-step) and two-phase premixed combustion (Section 4.1.4, single-/multi-point ignition combustion). Furthermore, the over-prediction of the maximum ROHR for operating conditions # 6 and 17 for example, are primarily caused by an elongated ignition delay in the simulation, resulting in a larger amount of fuel evaporated and ignitable at SOC, as seen in Figure 4.9 (e).

Apart from the inaccuracies at operating conditions with nearly identical maximum premixed and diffusion controlled ROHRs - such as # 4 and 10 (c.f. Figure 4.9 (c)) - the numerical locations of maximum ROHR match experimental data within an error of  $\pm 3^\circ$  CA.

#### 4.4.2 “Automotive” Diesel

An identical EA as in Section 4.4.1 is used to calibrate the ROHR model using 20 (calibration) out of the 57 representative operating conditions given in Table A.1. Due to the fact that all operating conditions except two (# 20 and 55) feature two injection pulses (i.e. pilot and main injection), the algorithm is modified to consider two independent sets of ignition delay parameters (c.f. Section 4.1.3). Thus, a total of 28 (23+5) model parameters are calibrated by the modified EA.

The ROHR characteristics ( $\varphi_{\text{SOC}}$ ,  $\varphi_{10}$ ,  $\varphi_{50}$ , and  $\varphi_{90}$ ) from the calibration and verification calculations are shown in Figure 4.11. Regarding the calibration and verification operating condition sets, similar deviations between measured and simulated characteristics, as well as similar trends, i.e. the variation of characteristics between single operating conditions, are observed. In general, deviations for  $\varphi_{\text{SOC}}$ ,  $\varphi_{10}$  and  $\varphi_{50}$  are smaller than 3 °CA, and for  $\varphi_{90}$  less than 10 °CA. The 10 % energy release location errors  $\varphi_{10}$  add up to 5 °CA for operating conditions with a mean piston velocity  $c_m$  in the range of 7 to 10.5 [m/s] (# 13-18 and 41-51), which is related to the staged combustion phenomenon<sup>1</sup>, or rather the ignition delay of the second injection.

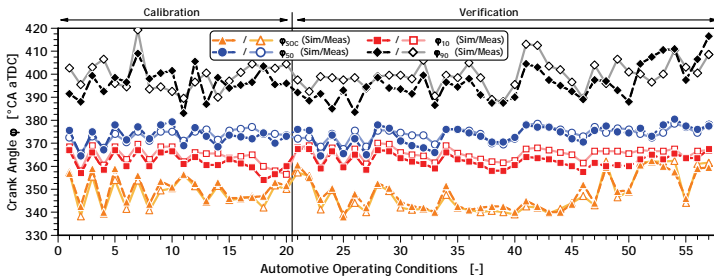


Fig. 4.11 Automotive Diesel ROHR Model: Calibration & Verification

Two distinct injection schemes (early/late pilot injection) and their respective measured and simulated ROHRs are given in Figure 4.12 as an example for staged combustion phenomena. Although differences between measured and simulated ROHR are present, the model captures the major characteristics of the two combustion stages or events.

In order to evaluate the general applicability of the proposed ROHR model, the model calibrated for the heavy-duty engine is used to simulate automotive operating conditions without changing any parameters (i.e. blind try). To account for the two

1. *Staged combustion* - multiple sequential combustion events resulting from distinct injection pulses (here: 2 combustion events resulting from 2 injection pulses)

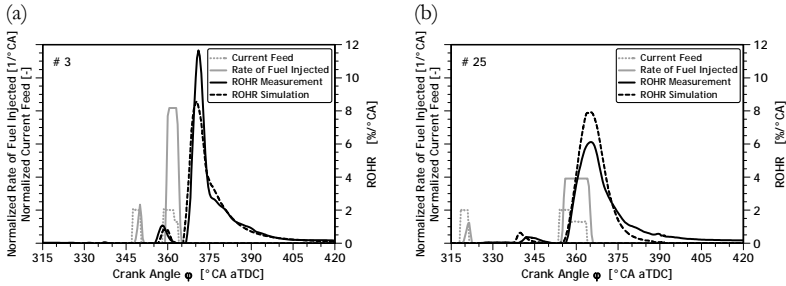


Fig. 4.12 Automotive Diesel Operating Conditions With Pilot- and Main-Injection Pulses: (a) # 3, (b) # 25

pulse injection schemes, both first and second injection delay parameters are set to the single pulse injection parameters obtained from the heavy-duty calibration.

Although absolute errors between simulated and measured characteristics are significant (c.f. Figure 4.13, Table 4.3), the trends between individual operating conditions are correctly reproduced. Given this, qualitative predictions of ROHR characteristics are feasible for a different engine size and application, using the phenomenological model without parameter recalibration.

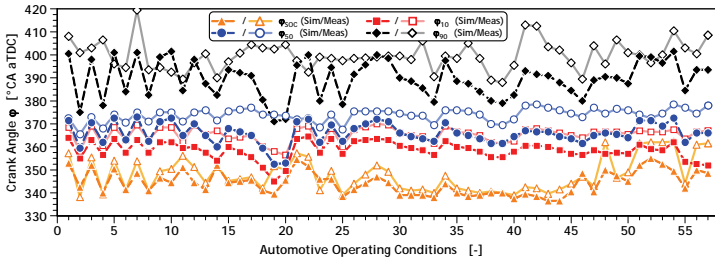


Fig. 4.13 Automotive Diesel ROHR: Heavy-Duty Model Blind Try

When considering the statistics of the ROHR characteristics for both heavy-duty (Table 4.2) and automotive (Table 4.3) optimized (calibrated) models, it is apparent that the automotive  $\varphi_{50}$  and  $\varphi_{90}$  correlation coefficients are approximately 0.2 lower than the respective heavy-duty values, while the linear regression statistics are comparable. When the automotive (optimized) and heavy-duty (blind try) model statistics are considered, the blind try correlation coefficients  $r$  ( $\varphi_{SOC}$ ,  $\varphi_{10}$  and  $\varphi_{90}$ : approx. -0.15,  $\Delta\varphi_{50}$ : -0.4!) and linear regression slopes  $m$  ( $\varphi_{SOC}$ : -0.3,  $\varphi_{50}$ : -0.4, and  $\varphi_{90}$ : -0.15) are significantly lower. The statistics hence indicate, that in order to obtain valid quantitative predictions, the model must to be recalibrated to a small subset of operating conditions (e.g. 10-20 operating conditions), given that the blind try parameters only yield qualitative results.



		$\varphi_{SOC}$	$\varphi_{10}$	$\varphi_{50}$	$\varphi_{90}$	
<i>Optimized</i>	<i>Pearson's Correlation Coefficient <math>r</math></i>	[-]	0.9631	0.8501	0.7810	0.5128
	<i>Linear Regression Slope <math>m</math></i>	[-]	0.89	0.86	1.07	0.59
	<i>Linear Regression Intercept <math>b</math></i>	[-]	-0.15	-2.03	-1.37	12.64
<i>Blind Try</i>	<i>Pearson's Correlation Coefficient <math>r</math></i>	[-]	0.8692	0.7049	0.3864	0.3838
	<i>Linear Regression Slope <math>m</math></i>	[-]	0.60	0.84	0.66	0.45
	<i>Linear Regression Intercept <math>b</math></i>	[-]	-8.26	-5.65	-2.65	13.15

Tab. 4.3 Automotive Engine ROHR Model Statistics for the EA Optimized and the Heavy-Duty Blind Try Case

### 4.4.3 “Marine” Diesel

A scaled-down version of the EA used to calibrate the ROHR model for the heavy-duty engine (Section 4.4.1) is applied to 12 (calibration) out of the 26 representative operating conditions given in Table A.4. As the mean model calculation time for the marine diesel is about 0.5 seconds, the adapted EA using a population size  $n_{pop}$  of 50 ( $n_{parent} = 25$ ,  $n_{offspring} = 75$ ) needs approximately five hours to calibrate the 23 ROHR model parameters.

To ensure the confidentiality of the marine diesel data, the ROHR characteristics shown in Figure 4.14 and Figure 4.15 are normalized using operating condition # 15 data as reference ( $\varphi_{SOI,meas} = 0$  and  $\varphi_{90,meas} = 100$ ).

The deviations between the measured and simulated ROHR characteristics are generally within measurement accuracy at  $\varphi_{SOC}$ ,  $\varphi_{10}$  and  $\varphi_{50}$ , and  $\pm 8\%$  of the normalized value at  $\varphi_{90}$  for the calibration and verification operating conditions alike (Figure 4.14). Concerning  $\varphi_{50}$  deviations, the two outliers (# 7 and 17) are low speed, low injection pressure operating conditions with an end of injection before 50 percent of the total energy is released. Because of this, the injection induced turbulence is reduced and the diffusion or mixing controlled combustion ROHR is lowered, resulting in a shift of the  $\varphi_{50}$  normalized time.

In order to evaluate the general applicability of the proposed ROHR model even for large, two-stroke engines, the heavy-duty calibrated model is applied to the marine diesel operating conditions in a blind try, i.e. without parameter recalibration. The comparison of the measured and blind try simulated ROHR characteristics in Figure 4.15 (a) points out, that despite short combustion durations - and thus errors in absolute  $\varphi_{10}$ ,  $\varphi_{50}$  and  $\varphi_{90}$  values - the blind try model accurately predicts trends and variations (c.f. Pearson's correlation coefficients  $r$ , Figure 4.16 (a)). While the simulated  $\varphi_{SOC}$  characteristics match the measurements within the experimental

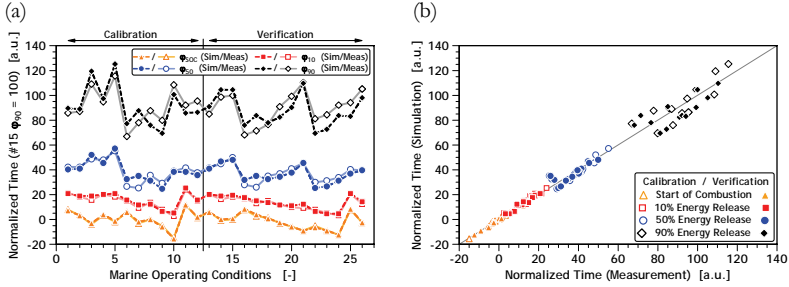


Fig. 4.14 Marine Diesel ROHR Model Calibration & Verification: (a) Sequential Operating Conditions Plot, (b) “1-to-1” Scatter Plot

accuracy, the simulated overall combustion duration is only approximately 75 % of the measured overall combustion duration (e.g. # 15:  $\varphi_{90.sim} = 72$  [a.u.]).

From an engineering point of view, the heavy-duty and marine diesel engine have well-known differences in the range of operating conditions (speed, EGR rate, ...), in-cylinder flow field (swirl, turbulence, ...), and injection system (configurations, fuel properties, ...). In order to account for this expert knowledge, an adjusted (blind try) model with a recalibrated empirical evaporation rate scaling factor  $\beta$  (fuel properties), as well as background  $c_g$  and injection induced  $c_{Inj}$  turbulence intensity scaling factors (flow field and injection system configuration) was developed, the results of which are shown in Figure 4.15 (b). Other than the the  $\varphi_{SOC}$  characteristics already matched using the blind try model, the adjusted model is capable of predicting the  $\varphi_{10}$ ,  $\varphi_{50}$ , and  $\varphi_{90}$  characteristics as well.

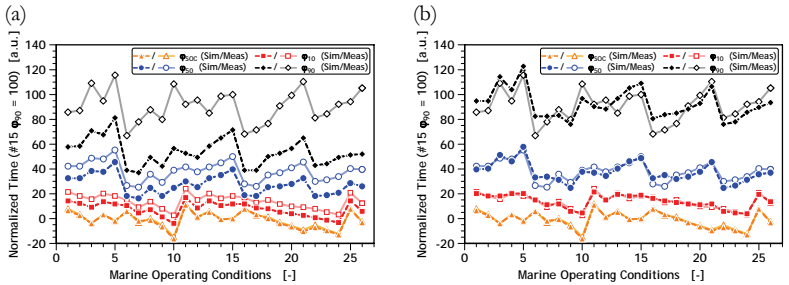


Fig. 4.15 Marine Diesel Engine ROHR Model: (a) Blind Try, (b) Adjusted

In order to visualize the differences between the three models or parameter sets employed (optimized, blind try and adjusted), Figure 4.16 shows the comparison of the linear regression statistics (c.f. Table A.7). While there are only small variations in correlation coefficients and regression slopes (except for the blind try  $\varphi_{90}$  regression slope), the variations in linear regression intercepts confirm the temporal offset (delay) of the  $\varphi_{10}$ ,  $\varphi_{50}$ , and  $\varphi_{90}$  characteristics for the blind try model.

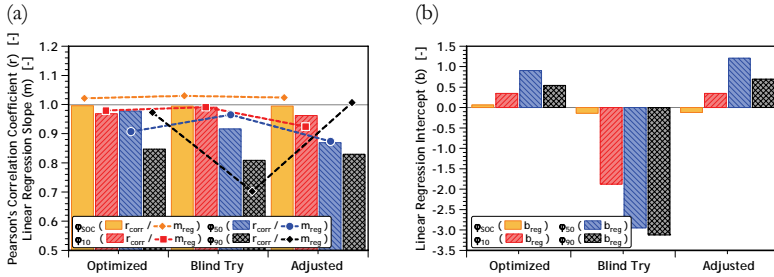


Fig. 4.16 Marine Engine Comparison of Three Model Parameter Sets: (a) Pearson's Correlation Coefficient & Linear Regression Slope, (b) Linear Regression Intercept

When comparing absolute measures of the marine diesel optimized model statistics with the heavy-duty (Table 4.2) and automotive (Table 4.3) optimized models, the quality of the marine diesel calibration even seems to be superior to the heavy-duty and automotive calibrations. This effect however is put into perspective by considering the limited range of the variations and the number of operating conditions employed (marine diesel engine: 26 operating conditions without EGR variations).

## 4.5 Advanced Fuels Survey

An advanced fuels survey is conducted to gain further information about the general applicability of the proposed ROHR model. The heavy-duty diesel engine is therefore operated at various conditions using reference diesel fuel, two water-in-diesel fuel emulsions (13 % and 21 % water by mass) and a diesel-butylal blend (c.f. Table 4.4). Bertola et al. [11] provides further information on the specifications of the fuels used and their effects on engine-out emissions.

To recalibrate the ROHR model parameters, the identical EA used for the heavy-duty engine (Section 4.4.1) is applied using 20 (calibration) out of the 40 representative operating conditions given in Table A.3. As both the calibration and verification subsets feature operating conditions with different fuels, two indices for referring the operating conditions are introduced; Arabic numerals to divide calibration/verification, and Roman numerals to divide diesel/emulsions/butylal fuels.

The resulting ROHR characteristics  $\phi_{SOC}$ ,  $\phi_{10}$ ,  $\phi_{50}$ , and  $\phi_{90}$  of this study are shown in calibration/verification order in Figure 4.17 (a) (Arabic numerals), and are also plotted against the decreasing share in diesel fuel in Figure 4.17 (c) (Roman numerals). Comparing the two figures, neither significant differences between calibration and verification model quality nor influences due to the type of fuel used

	REFERENCE DIESEL	EMULSION 13%	EMULSION 21%	BUTYLAL <sup>a</sup> 60%
<b>Lower Heating Value</b> $H_u$ [MJ/kg]	43.14	37.98	34.96	38.25
<b>Stoichiometric A/F Ratio</b> $\Lambda_{st}$ [kg/kg]	14.64	12.98	12.38	12.57
<b>Density</b> $\rho$ [kg/m <sup>3</sup> ]	819	851	862	829
<b>Water Content</b> $m_{H_2O}/m_{tot}$ [%]	0	12.89	20.89	0
<b>Oxygen Content</b> $m_{O_2}/m_{tot}$ [%]	0	10.15	15.36	11.98

Tab. 4.4 Advanced Fuels Properties

a. Butylal - Acetal (C<sub>9</sub>H<sub>20</sub>O<sub>2</sub>), high cetane number (> 73.7), oxygenate for diesel fuel

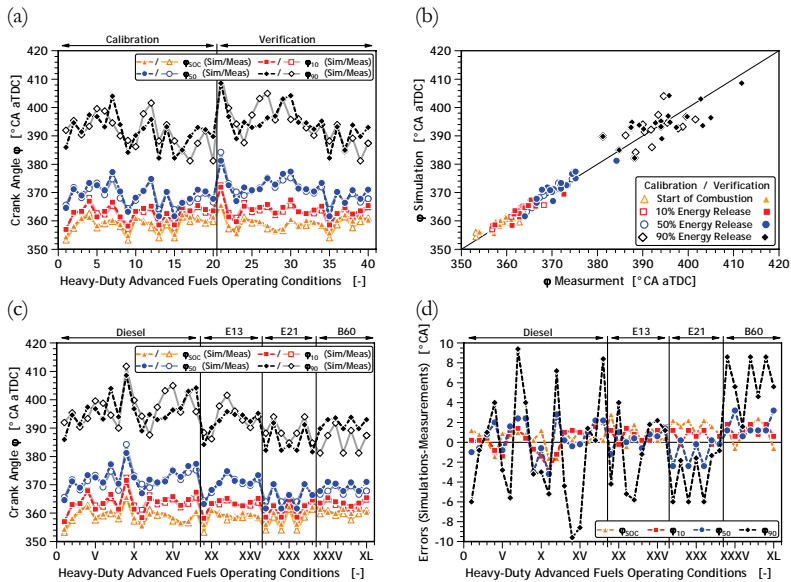


Fig. 4.17 Heavy-Duty Advanced Fuels ROHR Model Characteristics: (a) Calibration/Verification Operating Conditions Plot, (b) “1-to-1” Scatter Plot, (c) Fuel Operating Conditions Plot, (d) Model Errors

(e.g. diesel-butylal blend  $\phi_{90}$ ) are observed. To visualize the influence of the type of fuel on the deviations between measured and simulated characteristics, the absolute errors ( $\Delta\phi = \phi_{sim} - \phi_{meas}$ ) are plotted against fuel type ranked operating conditions

(Figure 4.17 (d)). While no trends are obvious for the errors when the reference fuel is utilized, the combustion duration is generally too short and too long for the water-in-diesel emulsions (e.g. emulsion 21 % :  $\varphi_{90} < -1$  °CA) and diesel-butylal blends ( $\varphi_{90} > +1$  °CA), respectively. Nevertheless, a remarkable overall accuracy of the results is obtained for the four different fuels used in this survey by only accounting for the different chemical and thermodynamic fuel properties in the proposed phenomenological ROHR model (Table 4.4).

In addition to the recalibration of the ROHR model parameters, the model calibrated for the base - reference diesel only - heavy-duty engine is used to simulate the operation with advanced fuels in a blind try attempt (Figure 4.18). Although the absolute errors between the simulated and measured ROHR characteristics are slightly higher (e.g.  $\pm 2$  °CA in  $\varphi_{90}$  for emulsions, c.f. Figure 4.17 (c),(d)), the overall performance of the blind try model allows for qualitative and quantitative predictions alike.

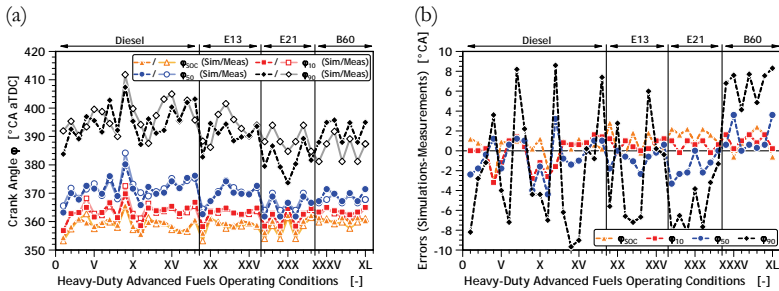


Fig. 4.18 Heavy-Duty Advanced Fuels Blind Try ROHR Characteristics: (a) Fuel Operating Conditions Plot, (b) Model Errors

When the optimized and blind try advanced fuel model statistics (Table 4.5) are compared with the statistics for the optimized heavy-duty ROHR model using reference diesel fuel (Table 4.2), the most notable differences are the reduced  $\varphi_{90}$  correlation coefficients  $r$  (0.1 and 0.15 the optimized and blind try model, respectively).

## 4.6 Conclusions

The combination of an enhanced phenomenological ROHR model with an Evolutionary Algorithm for the model calibration is successfully applied to three distinct diesel engines; an automotive, a heavy-duty, and a two-stroke marine diesel engine.

As shown in the sensitivity study of the model parameters, there is a need for an advanced calibration algorithm in order to handle the non-linear and conflicting influences of the parameters on the model output. Besides the differences in the temporal performance improvement, the comparison of four of these advanced

		$\varphi_{SOC}$	$\varphi_{10}$	$\varphi_{50}$	$\varphi_{90}$	
<i>Optimized</i>	<i>Pearson's Correlation Coefficient r</i>	[-]	0.9214	0.9538	0.9252	0.6655
	<i>Linear Regression Slope m</i>	[-]	0.83	0.91	1.01	0.58
	<i>Linear Regression Intercept b</i>	[-]	0.46	0.79	0.26	13.93
<i>Blind Try</i>	<i>Pearson's Correlation Coefficient r</i>	[-]	0.8918	0.9161	0.8876	0.6070
	<i>Linear Regression Slope m</i>	[-]	0.74	0.81	0.91	0.52
	<i>Linear Regression Intercept b</i>	[-]	0.36	0.82	0.18	14.21

*Tab. 4.5 Heavy-Duty Advanced Fuels ROHR Model Statistics for the EA Optimized and the Heavy-Duty Blind Try Case*

algorithms demonstrates the practical application of these methods for calibration of phenomenological models.

An excellent agreement between the measured and simulated ROHR characteristics is shown, inspite of the wide range of engine and operating condition setups used in this study. Furthermore, considering the heavy-duty engine calibrated model as example, the general applicability of the ROHR model is confirmed with blind trials on both the automotive and the marine diesel engines. Despite the deviations in absolute values, both blind trials correctly reproduce the variations among single operating conditions, and can be adjusted to yield correct absolute values using basic knowledge of the tested engine or a few experimental operating conditions for a recalibration.

An advanced fuels survey further shows, that both the re-calibrated and the blind try ROHR models are capable of predicting the effects of water-in-diesel emulsions and diesel-butylal blended fuels on ROHR characteristics correctly.

# 5 EMISSIONS OF NITROGEN OXIDE

Based on the ROHR model proposed in Chapter 4, a phenomenological model to determine the emissions of nitrogen oxide is given below. Combined with the soot emissions model presented in Chapter 6, one of the most pressing topics in current diesel engine research & development can be addressed: the simultaneous reduction of both nitrogen oxide and soot emissions to meet stringent emission regulations.

## 5.1 Model Description

Collectively referred to as emissions of nitrogen oxide ( $\text{NO}_x$ ), nitric oxide (NO) nominally accounts for approximately 90 % of the total  $\text{NO}_x$  emissions during regular diesel engine operation. However, for light-load, low-speed operating conditions, the share of nitrogen dioxide ( $\text{NO}_2$ ) formed may increase up to 30% of the total amount of  $\text{NO}_x$  emissions [44].

Given the low content of nitrogen in commercial fuels and the predominantly diffusion controlled combustion in standard diesel engines, the governing source for nitric oxide formation is the oxidation of molecular nitrogen contained in the combustion air (a.k.a. thermal NO formation). Moreover, for cases with high energy release fractions during the premixed combustion phase, or for cases with  $\text{NO}_x$  emission concentrations lower than 100 [ppm], prompt nitrogen oxide formation (a.k.a. Fenimore  $\text{NO}_x$ ) becomes a significant source for nitrogen oxide.

When fast calculations are to be made across an entire engine operating map, a computationally reliable and efficient mechanism for the exhaust gas NO concentration is needed. Because of both the complexity of the reaction scheme (and thus increase in computation time) and the low impact of the Fenimore  $\text{NO}_x$  formation mechanism on the total  $\text{NO}_x$  emissions, the present study follows a commonly used restriction and considers only thermal NO formation.

Weisser [102] shows for various operating conditions of a 4-stroke medium-size, medium-speed Common-Rail DI diesel engine, that reducing the mechanism complexity results in a decrease in prediction accuracy for NO emissions as well as a substantial reduction in computational time (especially for the 0-dimensional models).

The present model calculates the NO concentration using the established and computationally efficient extended Zeldovich reaction mechanism [109] along with a CHEMKIN [54] chemical equilibrium solver. This novel implementation links the characteristic in-cylinder temperature traces driving the NO formation to a representative air/fuel ratio function in a consistent way (c.f. Section 5.1.2, Figure 5.1).

### 5.1.1 Inputs & Outputs

Intended as an emission submodel in an engine process simulation program, the NO model uses the temporal state of the process (ROHR, temperature, pressure, etc.), the reaction chemistry kinetics (Section 5.1.3) and a representative air/fuel ratio function (Section 5.1.2) as inputs. As an output, the model provides the temporal NO formation and reduction rates.

### 5.1.2 Variable Virtual Combustion Zones

By means of a “virtual” combustion zone with variable stoichiometry (computed in the thermodynamic combustion process simulation), the dominant localized NO formation phenomena, such as hot spots in the fuel-lean post-combustion gases, are captured. As an attempt to include the nitrogen oxide emissions resulting from the fuel-rich components next to the flame front position, a richer-than-stoichiometric phase in the representative air/fuel ratio function is used during initial stages of combustion (Figure 5.1 (a)).

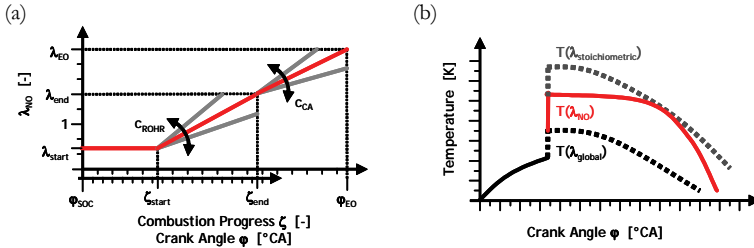


Fig. 5.1 Variable representative air/fuel ratio function and associated in-cylinder temperature trace for NO formation

After the initial constant air/fuel ratio  $\lambda_{start}$  (from  $\phi$  SOC to  $\zeta_{start}$ ), the presented model uses an air/fuel ratio proportional to the increasing combustion progress to account for characteristic diesel combustion effects (e.g. transition of unburned fuel-rich to burned fuel-lean gases). The final phase of the representative air/fuel ratio function is modeled as a crank angle proportional leaning (maximum  $\lambda_{global}$ ) of burned gases until the exhaust valves open at  $\lambda_{EO}$  and  $\phi_{EO}$ . The associated intermediate temperature trace  $T(\lambda_{NO})$ , which lies between the thermodynamic maximum process temperature  $T(\lambda_{stoichiometric})$  and the mean process temperature  $T(\lambda_{global})$ , is determined using the rate of heat release analysis software WEG, based on the variable representative air/fuel ratio function (Figure 5.1). A list of the seven model parameters used to model the representative air/fuel ratio function is given in Table 5.1.



PARAMETER		UNIT	SIZE RANGE
$\lambda_{\text{start}}$	1 <sup>st</sup> point of discontinuity : air/fuel ratio	[-]	0.4 .. 1.0
$\zeta_{\text{start}}$	1 <sup>st</sup> point of discontinuity : combustion progress	[-]	0.0 .. $\mathbf{x}^a$
$\lambda_{\text{end}}$	2 <sup>nd</sup> point of discontinuity : air/fuel ratio	[-]	1.0 .. $\mathbf{y}^b$
$\zeta_{\text{end}}$	2 <sup>nd</sup> point of discontinuity : combustion progress	[-]	$\mathbf{x}$ .. 1.0
$\lambda_{\text{EO}}$	Air/fuel ratio at exhaust valve opening (EO)	[-]	$\mathbf{y}$ .. $\lambda_{\text{global}}^c$
$c_{\text{ROHR}}$	ROHR proportional progress slope scaling factor	[-]	0.0 .. 10
$c_{\text{CA}}$	Crank angle proportional progress slope s.f.	[-]	0.0 .. 10

Tab. 5.1 Nitrogen Oxide Emission Model Parameters

- a.  $\mathbf{x}$  - variable (max. 1.0), ensures that the 1<sup>st</sup> point of discontinuity is previous to the 2<sup>nd</sup>  
 b.  $\mathbf{y}$  - variable (max.  $\lambda_{\text{global}}$ ), ensures that  $\lambda_{\text{end}}$  is lower than  $\lambda_{\text{EO}}$   
 c.  $\lambda_{\text{global}}$  - global (in-cylinder) air/fuel ratio

### 5.1.3 Reaction Mechanism

The three basic reactions of the extended Zeldovich mechanism describing the formation (and reduction) of NO from atmospheric nitrogen are



The rate of formation of nitric oxide (NO) hence can be written as

$$\frac{d[NO]}{dt} = \frac{k_1^+[O][N_2] + k_2^+[N][O_2] + k_3^+[N][OH] - k_1^-[NO][N] - k_2^-[NO][O] - k_3^-[NO][H]}{\quad}, \tag{5.2}$$

where  $k_i^+$  and  $k_i^-$  are the forward and reverse reaction rate constants respectively, and  $[ ]$  denote species mass concentrations.

Assuming that the combustion and NO formation processes in IC engines are decoupled (postflame NO formation generally dominates any flame-front-produced NO given the geometrically thin flame reaction zone and the short residence times), the engine-out concentrations of  $O$ ,  $O_2$ ,  $OH$ ,  $H$  and  $N_2$  can be approximated by their equilibrium concentrations  $[ ]_e$  (c.f. [44]). Using the notations

$$\begin{aligned}
 R_1 &= k_1^+[O]_e[N_2]_e = k_1^-[NO]_e[N]_e \\
 R_2 &= k_2^+[N]_e[O_2]_e = k_2^-[NO]_e[O]_e \\
 R_3 &= k_3^+[N]_e[OH_2]_e = k_3^-[NO]_e[H]_e
 \end{aligned} \tag{5.3}$$

for the equilibrium state, and by substituting the equilibrium concentrations  $[ ]_e$  for the instantaneous concentrations  $[ ]$  in (5.2), the rate of NO formation  $d[NO]/dt$  can be expressed as:

$$\frac{d[NO]}{dt} = \frac{2 \cdot R_1 \cdot \{1 - ([NO]/[NO]_e)^2\}}{1 + ([NO]/[NO]_e) \cdot R_1/(R_2 + R_3)} \quad (5.4)$$

### 5.1.4 Kinetics of NO Formation

When predictions of NO concentrations using established reaction rate constant  $k_i^+$  and  $k_i^-$  data from different sources are compared (c.f. Section A.2), discrepancies of more than 20 % may result for constant pressure and temperature problems [42]. Furthermore, Weisser [102] shows that the order of the reaction scheme, i.e. the number of equations considered, has less influence on the accuracy of the predictions than the set of reaction rate constants chosen.

Given that the present NO model uses the NO formation implementation scheme proposed by Heywood [44], the subsequent investigations are conducted using the corresponding reaction rate constants data (Section A.2).

## 5.2 Model Parameter Sensitivity Study

In order to estimate the relative influence of the individual NO model parameters on the model outcome, a sensitivity study on 19 heavy-duty engine operating conditions is performed (“calibrating” operating conditions Table A.2). Similar to the ROHR model parameter sensitivity study discussed in Section 4.2, the sensitivity  $\chi$  of the model parameter  $x_i$  on the mass of nitric oxide  $m$  (Table 5.1) is thereby defined as average of the relative changes in mass of NO normalized with the imposed variations in  $x_i$ :

$$\chi_{(m, x_i)} = \frac{1}{n_{oc}} \cdot \sum_{n_{oc}} \frac{\Delta m}{\Delta x_i} = \frac{1}{n_{oc}} \cdot \sum_{n_{oc}} \frac{|m - m_0|/m_0}{|x_i - x_0|/x_0} \quad (5.5)$$

As an example of the sensitivity of the NO emissions to both the operating conditions and a positive/negative step size variation, Figure 5.2 (a) shows the  $\pm 5$  % variations of the point of discontinuity combustion progress parameters  $\zeta_{start}$  and  $\zeta_{end}$  plotted against operating conditions. Whereas the mean sensitivities are approximately 1.5 and 0.025 for  $\zeta_{start}$  and  $\zeta_{end}$  respectively, single operating condition sensitivities vary from 0.05 to 10 ( $\zeta_{start}$ ) and 0.005 to 0.1 ( $\zeta_{end}$ ), indicating the dependence of the model on operating conditions, such as temperatures, EGR rate and engine load. The differences between positive and negative step size variations

of one order of magnitude furthermore are a sign of the non-linear influence of the model parameters (c.f. Figure 5.2 (a)).

As the Heywood reaction rate constants are used for all subsequent investigations, Figure 5.2 (b) only illustrates the influence of the numerous reaction rate constants on the model output, comprehensive investigation are given in [42] and [59].

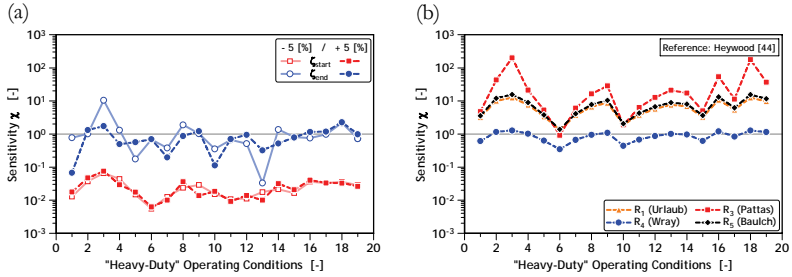


Fig. 5.2 Operating Condition Specific Variations of  $NO_x$  Model Sensitivities: (a) Point of Discontinuity Combustion Progress Parameters, (b) NO Formation Mechanism Reaction Rate Constants

Figure 5.3 (a) shows the mean (operating condition averaged) model sensitivities for normalized variations of  $\lambda_{end}$ ,  $c_{ROHR}$  and  $\zeta_{end}$ . While the sensitivity to  $\zeta_{end}$  is approximately constant over the range of the parameter variations (i.e. a change in  $\zeta_{end}$  linearly affects the model outcome), the sensitivities of  $\lambda_{end}$  and  $c_{ROHR}$  strongly depend on the parameter variation step size (i.e. changes in  $\lambda_{end}$  or  $c_{ROHR}$  have non-linear effects on model outcomes).

To visualize the relative importances of the NO model parameters, the mean sensitivities to  $\pm 5\%$  variation of all seven parameters are given in Figure 5.3 (b). Given that a mean sensitivity of unity represents an equal (i.e. proportional) variation in model outputs as imposed on model parameters, the NO model parameters can be classified into “exponential” ( $\lambda_{end}$ ,  $c_{ROHR}$ ), “inverse exponential” ( $\zeta_{start}$ ,  $c_{CA}$ ) and “linear” parameters ( $\lambda_{start}$ ,  $\lambda_{EO}$ ,  $\zeta_{end}$ ).

### 5.3 Model Study on Different Engine Sizes

Similar to the model study using different engine sizes with the ROHR model (c.f. Section 4.4), the proposed NO model is applied to all three engines employed in this investigation in order to evaluate its general applicability. The heavy-duty engine is used as the reference or base engine. In addition to engine specific model calibrations for the automotive and marine diesel engines, the heavy-duty model is applied to both engines without modifications (i.e. blind try).

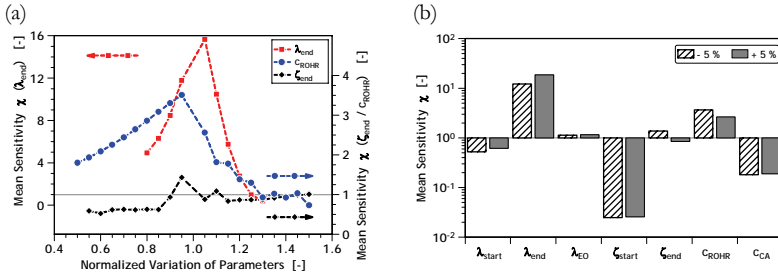


Fig. 5.3 Mean (Operating Condition Averaged)  $NO_x$  Model Sensitivities: (a) Normalized Variations of  $\lambda_{end}$ ,  $c_{ROHR}$ , and  $\zeta_{end}$ , (b)  $\pm 5\%$  Step Size Parameter Variations

### 5.3.1 “Heavy-Duty” Diesel

Figure 5.4 shows the results using an Evolutionary Algorithm with a population size  $n_{pop}$  of 30 ( $n_{parent} = 15$ ,  $n_{offspring} = 50$ ) to calibrate the seven  $NO$  model parameters (Table 5.1). Given a mean model calculation time of about two seconds (due to time-consuming equilibrium reaction calculations), the calibration based on the 19 operating conditions takes approximately ten hours.

As shown in Figure 5.4, the correlation between the measured and simulated  $NO$  emissions for both the calibration and verification is excellent. Except for the operating conditions # 36 (low speed, low load and high EGR rate) and # 39 (high speed, high load and high EGR rate), the calibrated model accurately predicts the measured  $NO$  emissions over a range spanning almost two orders of magnitude ( $m_{NO} = 0.25$  to  $14.2$  [g/kWh]).

The high Pearson’s correlation coefficients  $r$ , in combination with linear regression slopes  $m$  equal to unity and low intercepts  $b$  (c.f. Table 5.2), confirm the excellent “visual” correlations show in Figure 5.4.

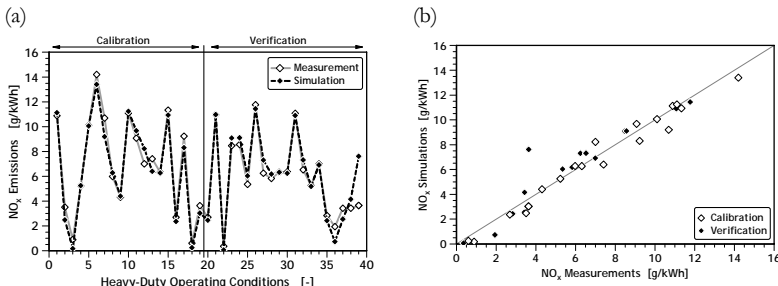


Fig. 5.4 Heavy-Duty Diesel  $NO_x$  Model Calibration & Verification: (a) Sequential Operating Conditions Plot, (b) “1-to-1” Scatter Plot

CALIBRATION VERIFICATION			
Pearson's Correlation Coefficient $r$	[-]	0.9859	0.9488
Linear Regression Slope $m$	[-]	1.00	1.00
Linear Regression Intercept $b$	[-]	-0.29	0.24

Tab. 5.2 Heavy-Duty Engine Calibration & Verification Statistics

Figure 5.5 shows the in-cylinder pressure history and associated ROHR (a), as well as the representative NO temperature and temporal NO mass history (b) for the heavy-duty operating condition # 10. The temporal resolved history of NO formation indicates that the NO formation takes place from approximately 360 to 380 [°CA aTDC], while almost no reduction of NO is detectable..

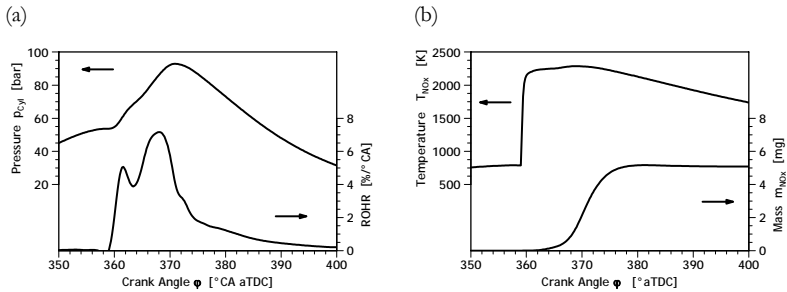


Fig. 5.5 Heavy-Duty Single Operating Condition: (a) Pressure History and ROHR, (b) Representative Temperature and Mass of Nitric Oxide

### 5.3.2 “Automotive” Diesel

The identical Evolutionary Algorithm as implemented in Section 5.3.1 ( $n_{pop} = 30$ ,  $n_{parent} = 15$ ,  $n_{offspring} = 50$ ) is used to calibrate the NO model based on 20 out of the 57 representative automotive diesel engine operating conditions given in Table A.1.

While deviations between measured and calculated NO emissions for calibration operating conditions are almost negligible, several verification operating conditions show significant deviations of up to 4 to 8 [g/kWh] (c.f. # 56). In general, trends among the different operating conditions are correctly reproduced (Figure 5.6).

When comparing specific NO emissions, the accuracy of the engine performance measures must be taken into account. Given the operating condition # 56 for example, underpredicting the engine output by 0.3 kWh causes a error (i.e. drop) of 5.5 [g/kWh] in measured specific NO emissions, and hence a reduction in the deviation from 8 to 2.5 [g/kWh].

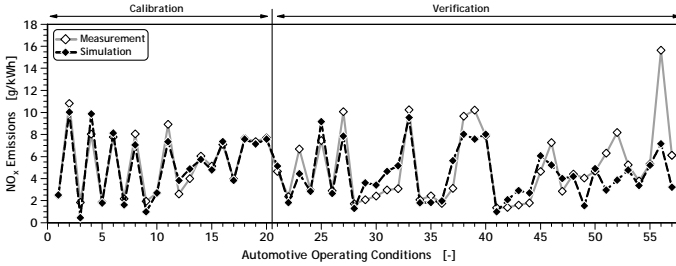


Fig. 5.6 Automotive Diesel NO Model: Calibration & Verification

To further estimate the general applicability of the proposed NO model, the model calibrated for the heavy-duty diesel engine is used to simulate automotive operating conditions without changing any model parameter (blind try).

Though absolute errors between simulated and measured specific NO emissions are significant (c.f. Figure 5.7, Table 5.3), the trends among single operating conditions are well reflected. Thus, qualitative predictions of NO emissions for a different engine sizes and applications, using a phenomenological model without a parameter re-calibration, are feasible. Similar to the optimized model calibration and verification, the largest deviations are at low load, high speed operating conditions (e.g. # 51, 52, 56 or 57).

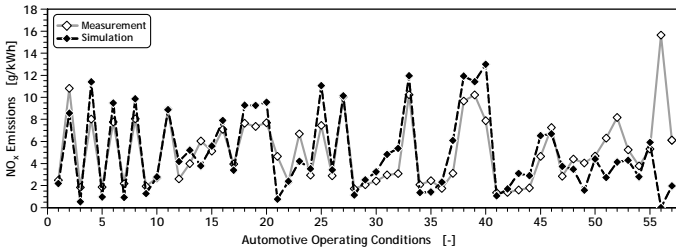


Fig. 5.7 Automotive NO Emissions: Heavy-Duty Model Blind Try

Identical correlation statistics ( $r \approx 0.95$ ,  $m = 1.0$  and  $b \approx 0.0$ ) are noted, when considering the statistics of the NO emission modeling for both the heavy-duty (Table 5.2) and automotive (Table 5.3) calibrations. Furthermore, significantly lower correlation statistics are observed when comparing the automotive verification statistics with the calibration statistics, even if the statistical outlier operating condition # 56 is excluded ( $r' = 0.84$ ,  $m' = 0.78$  and  $b' = 0.81$ ).

Regarding the automotive optimized (calibration/verification) and heavy-duty blind try model statistics, both the blind try correlation coefficient ( $r = 0.65$ ) and linear regression intercept ( $b = 2.38$ ) indicate a significantly lower correlation between the simulated and measured specific NO emissions for the blind try case (although the linear regression slope  $m$  is equal to one).

		Calibration	Verification	Blind Try
Pearson's Correlation Coefficient $r$	[-]	0.9593	0.7428	0.6510
Linear Regression Slope $m$	[-]	0.99	0.52	1.02
Linear Regression Intercept $b$	[-]	-0.09	1.80	2.38

Tab. 5.3 Automotive Engine: Optimized vs. Blind Try Statistics

### 5.3.3 “Marine” Diesel

A scaled down version of the EA used to calibrate the NO model for the heavy-duty engine is applied using 12 of the 26 representative two-stroke marine diesel engine operating conditions given in Table A.4 ( $n_{\text{pop}} = 20$ ,  $n_{\text{parent}} = 10$ ,  $n_{\text{offspring}} = 40$ ).

To ensure the confidentiality of the marine diesel data (as requested by the industry partner), the NO emissions shown in Figure 5.8 and Figure 5.9 are normalized using operating condition # 15 as reference ( $\text{NO}_{\text{meas.}\#15} = 100$  [a.u.]).

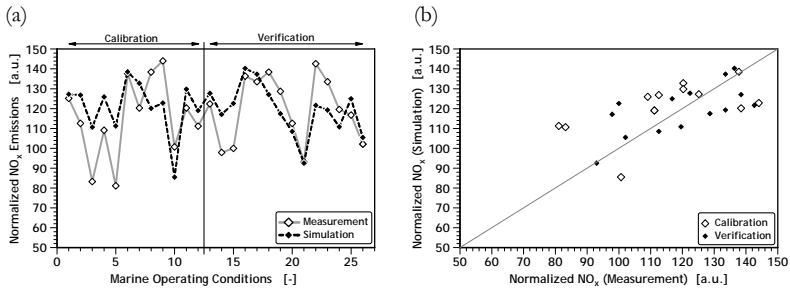


Fig. 5.8 Marine Diesel NO Model: Calibration & Verification

Given that absolute specific NO emissions from a marine diesel engine are slightly higher than from a heavy-duty or automotive engine, the deviations between measured and calculated NO emissions for the marine diesel engine are higher as well (peak relative deviations for all engines of the order of 25 %, c.f. Figure 5.8). According to Weisser [102], the quantitative inaccuracies in NO emission prediction are related to both the general chemistry model (i.e. extended Zeldovich mechanism) and the modeling approach for the turbulent mixing between hot combustion gases and surrounding fresh air (i.e. representative air/fuel ratio function). As the proposed air/fuel ratio function employs both ROHR and crank angle proportional mixing phases (c.f. Section 5.1.2), changes in the characteristic time strongly affect the model outcome (1 °CA corresponds to automotive: 50 μs, heavy-duty: 100 μs, and two-stroke marine diesel: 1.5 ms). Despite the deficiencies in quantitative predictions, the qualitative trends are well reflected.

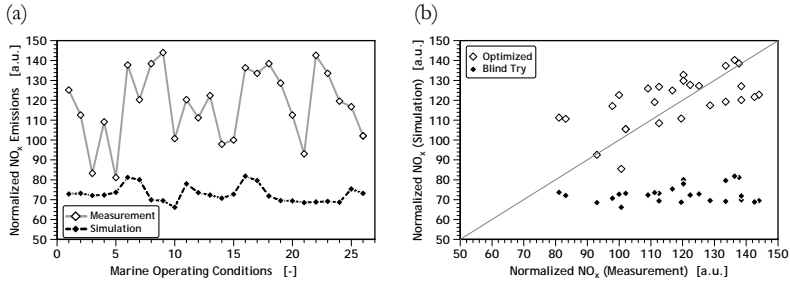


Fig. 5.9 Marine NO Emissions: Heavy-Duty Model Blind Try

In order to estimate the general applicability of the proposed NO model even for large two-stroke engines, the heavy-duty calibrated model is applied to the marine diesel operating conditions in a blind try, i.e. without changing any parameters. The comparison of the measured and blind try simulated NO emissions shown in Figure 5.9 does not imply a significant correlation. While the NO formation in the heavy-duty (and automotive) engine is strongly influenced by the premixed combustion and the initial increase in temperature and ROHR, the marine diesel NO formation is mainly affected by the turbulent mixing between hot combustion gases and surrounding fresh air, as the premixed combustion phase is negligible for standard operation conditions ( $m_{\text{Prmx}} < 2\text{-}3\%$ ).

The NO model statistics given in Table 5.4, in particular the low correlation coefficient ( $r < 0.2$ ) and flat linear regression slope ( $m = 0.04$ ) for the blind try model, confirm the absence of a correlation between measured and blind try simulated results as shown in Figure 5.9.

		OPTIMIZED	BLIND TRY
<i>Pearson's Correlation Coefficient <math>r</math></i>	[-]	0.7143	0.1919
<i>Linear Regression Slope <math>m</math></i>	[-]	0.51	0.04
<i>Linear Regression Intercept <math>b</math></i>	[-]	59.95	67.55

Tab. 5.4 Marine Engine Optimized vs. Blind Try Statistics

## 5.4 Conclusions

The developed phenomenological nitrogen oxide emissions model is capable of both qualitative and quantitative NO<sub>x</sub> emission predictions of automotive and heavy-duty engine operating conditions. The quantitative deviations between measured and simulated NO emissions for the two-stroke marine diesel engine are



related to both the general chemistry model and the modeling approach used to describe the turbulent gas mixing.

As noted during the sensitivity study of the model parameters, positive and negative parameter variations have a marked influence on the model output. Despite this sensitivity on the model parameter settings, the NO model allows for fast and reliable emission predictions over a range of more than an order of magnitude for the medium and high speed engines (heavy-duty and automotive engine, respectively). The (chemical) residence time ratio between the heavy-duty and marine diesel engine setup of 15 though makes it impossible for this model/parameter combination to predict the marine diesel NO emissions based on the heavy-duty engine calibration.



# 6 SOOT EMISSION

In addition to the ROHR and NO models proposed in Chapters 4 and 5, a phenomenological soot model is presented in the subsequent sections. Combined with the NO emissions model presented in Chapter 5, this model allows for addressing one of the most important topics in current diesel engine R&D: the simultaneous reduction of both  $\text{NO}_x$  and soot emissions to meet stringent emission regulations.

## 6.1 Model Description

Along with nitrogen oxide ( $\text{NO}_x$ ), soot<sup>1</sup> is considered as a major pollutant emitted by diesel engines under regular operating conditions.

Due to the both complex and governing physical/chemical processes in the formation and oxidation of soot, the quantitative operating-map-wide prediction of specific soot emissions is one of the most challenging topics in IC engine combustion calculations. Even without limitations on the computational time and implementing the most sophisticated models known (e.g. detailed PAH<sup>2</sup> chemistry), quantitative soot emission predictions are still limited only to particular operating map regions or engine operating conditions [15][27][94].

Recent studies on numerous Common-Rail DI diesel engines showed, that two step approaches (formation and oxidation, c.f. Figure 6.1), such as those presented by Hiroyasu et al. [46][48], Boulouchos et al. [87] or Gao [34], despite their limited accuracy, do provide the potential for qualitative predictions with low computational costs.

Using the model developed by Boulouchos et al. for the subsequent investigations, the following assumptions are made:

- No soot formation/oxidation occurs during premixed combustion phase
- Split-up of soot formation and oxidation into virtual combustion zones (c.f. Section 5.1.2) with corresponding characteristic temperature histories

### 6.1.1 Inputs & Outputs

Similar to the NO model presented in Chapter 5, the soot model is intended as an emission submodel in an engine process simulation program. Hence, the model uses

---

1. *Soot* - a.k.a. particulate matter (PM); agglomerations of elemental amorphous carbon particles with unburned hydrocarbons, acids, elemental sulfur, and metal oxides  
2. *PAH* - Polycyclic Aromatic Hydrocarbons

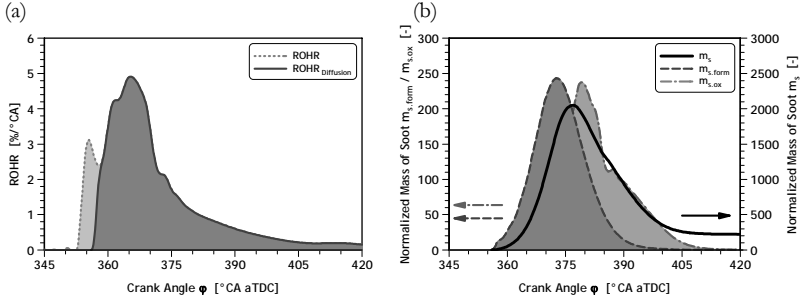


Fig. 6.1 Representative Heavy-Duty Engine Operating Condition: (a) ROHR, (b) Soot Formed, Oxidized and Total Mass of Soot Histories

the temporally resolved state of the global combustion process (ROHR, temperature, pressure, etc.), the representative virtual formation and oxidation combustion zones, as well as the “ $\phi$  - T” map by Akihama et al. [2] as inputs.

The temporally resolved soot formation and oxidation histories are provided as outputs by the model.

### 6.1.2 “Two Step - Two Zone” Approach

Whereas common two step models consider the soot formation process as involving two reaction steps in one zone, Boulouchos et al. use discrete virtual combustion zones to model the formation and oxidation processes. A detailed description of both, the model and virtual combustion zone concept are given in [99].

The net rate of change in soot mass  $m_s$  is the difference between the rates of soot formed  $m_{s,form}$  and oxidized  $m_{s,ox}$ .

$$\frac{dm_s}{dt} = \frac{dm_{s,form}}{dt} - \frac{dm_{s,ox}}{dt} \quad (6.1)$$

The formation of soot is given as function of the mass of fuel burned in the diffusion controlled combustion phase  $m_{FuelBurnDiff}$ , the normalized in-cylinder pressure  $p/p_0$  and the “ $\phi$  - T” map function  $f$ .

$$\frac{dm_{s,form}}{dt} = c_{form} \cdot \frac{dm_{FuelBurnDiff}}{dt} \cdot \left(\frac{p}{p_0}\right)^{c_1} \cdot f(\phi_{form}, T_{form}) \quad (6.2)$$

The results of the complex chemistry, “ $\phi$  - T” map calculations carried out by Akihama et al. are integrated in the phenomenological two step model with the approximation function  $f$  given in Equations (6.3) and (6.4), and shown in Figure 6.2.

$$f(\phi_{form}, T_{form}) = \left(\frac{0.75 - (1/\phi_{form})}{0.65}\right)^{1.5} \cdot \exp\left(-\frac{(T_{form} - \mu_0)^2}{2 \cdot \sigma_0^2}\right) \quad (6.3)$$

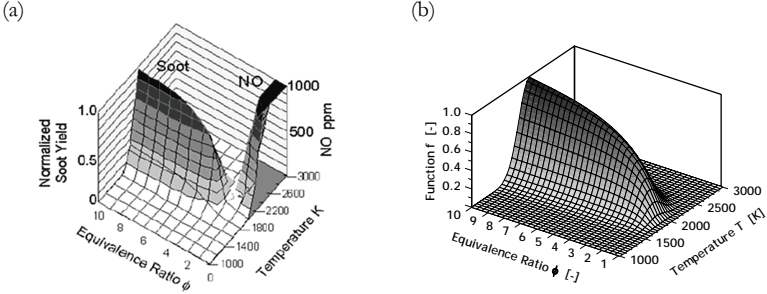


Fig. 6.2 Equivalence Ratio - Temperature Map for Soot Formation: (a) Original Akihama et al [2], (b) Mathematical Approximation

$$\mu_0 = 2160 - 400 \cdot (1/\phi_{\text{form}}), \text{ and } \sigma_0 = 210 - 100 \cdot (1/\phi_{\text{form}}) \quad (6.4)$$

The oxidation of soot particles by molecular oxygen is modeled using an exponential temperature term (i.e. Arrhenius functional form), the mass of soot accumulated  $m_s$ , the characteristic mixing frequency of the diffusion controlled combustion  $\tau_{\text{char}}$  and the current normalized oxygen partial pressure  $p_{O_2}/p_{O_2,\text{ref}}$ .

$$\frac{dm_{s,\text{ox}}}{dt} = c_{\text{ox}} \cdot \frac{1}{\tau_{\text{char}}} \cdot m_s^{c_2} \cdot \left(\frac{p_{O_2}}{p_{O_2,\text{ref}}}\right)^{c_3} \cdot \exp\left(-\frac{T_{A,\text{ox}}}{T_{\text{ox}}}\right) \quad (6.5)$$

Table 6.1 gives the eight empirical parameters used in the Boulouchos et al. soot model along with their according units and size ranges.

PARAMETER		UNIT	SIZE RANGE
$\phi_{\text{form}}$	Soot formation: (fuel/air) equivalence ratio	[-]	1.0 .. 2.5
$c_{\text{form}}$	Soot formation: scaling factor	[-]	0.0 .. $1 \cdot 10^5$
$c_1$	Soot formation: exponential pressure factor	[-]	0.5 .. 2.0
$\phi_{\text{ox}}$	Soot oxidation: (fuel/air) equivalence ratio	[-]	$\phi_{\text{global}}^a$ .. 1.0
$c_{\text{form}}$	Soot oxidation: scaling factor	[-]	0.0 .. $1 \cdot 10^5$
$c_2$	Soot oxidation: exponential mass factor	[-]	0.5 .. 2.0
$c_3$	Soot oxidation: exponential O <sub>2</sub> pressure factor	[-]	0.5 .. 2.0
$T_{A,\text{ox}}$	Soot oxidation: activation temperature	[K]	$1 \cdot 10^3$ .. $1 \cdot 10^5$

Tab. 6.1 Soot Emission Model Parameters

a.  $\phi_{\text{global}}$  - global (in-cylinder) fuel/air ratio;  $\phi_{\text{global}} = 1/\lambda_{\text{global}}$

## 6.2 Model Parameter Sensitivity Study

In order to estimate the relative influence of the individual parameters on the soot model results, a sensitivity study on 19 heavy-duty engine operating conditions is performed (“calibrating” operating conditions Table A.2). Analog to the NO model parameter sensitivity study presented in Section 5.2, the sensitivity  $\chi$  of the mass of soot  $m_s$  on the model parameter  $x_i$  (Table 6.1) is thereby defined as average of the relative changes in mass of soot normalized with the imposed variations in  $x_i$ :

$$\chi_{(m_s, x_i)} = \frac{1}{n_{oc}} \cdot \sum_{n_{oc}} \frac{\Delta m_s}{\Delta x_i} = \frac{1}{n_{oc}} \cdot \sum_{n_{oc}} \frac{|m_s - m_{s,0}| / m_{s,0}}{|x_i - x_{i,0}| / x_{i,0}} \quad (6.6)$$

To illustrate the variations in sensitivity on both operating conditions and positive/negative step size, Figure 6.3 (a) shows the  $\pm 5\%$  variations of the soot oxidation scaling factor  $c_{ox}$  and activation temperature  $T_{A,ox}$  for the 19 operating conditions considered. Whereas the minor changes in sensitivity for the  $\pm 5\%$  variations of  $c_{ox}$  reflect the linear equation form, the discrepancies between the positive ( $\chi_{mean} \approx 75$ ) and negative ( $\chi_{mean} \approx 15$ ) step size variations of  $T_{A,ox}$  are caused by the exponential temperature term in Equation (6.5). The variations among specific operating conditions for both  $c_{ox}$  and  $T_{A,ox}$  further reveal the complex influence of operating condition parameters - such as engine speed and load, injection parameters and EGR rates - on the soot formation.

When comparing the mean sensitivities for both the soot model (Figure 6.3 (b)) and the NO model (Figure 5.3 (b)), the higher than unity sensitivities for all parameters, except for  $\phi_{ox}$ , indicate the large influence of the input parameters on the model output. Given the two step reaction mechanism, the soot formation parameters  $\phi_{form}$  and  $c_1$  (via the  $p/p_0$  term in Equation (6.2), and the ideal gas law) affect the amount of soot formed by changes in the “ $\phi - T$ ” map function  $f$ , whereas the soot oxidation parameter  $c_2$  is directly linked to the mass of soot already formed.

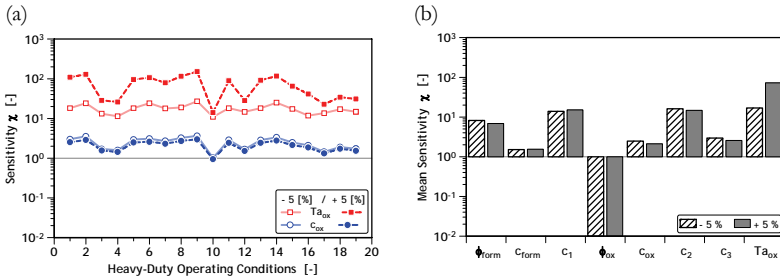


Fig. 6.3 Operating Condition Specific Sensitivities: (a) Oxidation Activation Temperature  $T_{A,ox}$  and Scaling Factor  $c_{ox}$ , (b) Soot Model Mean Sensitivities for  $\pm 5\%$  Step Size Parameter Variations

### 6.3 Model Study on Different Engine Sizes

Similar to the model studies on different engine sizes for the ROHR and NO models in the previous chapters, the proposed soot model is applied to the heavy-duty, automotive and marine diesel engine in order to evaluate the general applicability of the approach. The heavy-duty engine is again used as the reference engine. In addition to the engine specific model calibrations for the automotive and marine diesel engine, the heavy-duty model is applied to both engines without modifications (blind try).

#### 6.3.1 “Heavy-Duty” Diesel

Figure 6.4 shows the results using an Evolutionary Algorithm with a population size  $n_{pop}$  of 50 ( $n_{parent} = 25, n_{offspring} = 75$ ) to calibrate the eight parameters of the soot model (c.f. Table 6.1). Given a mean calculation time of one third of a second, the calibration based on the 19 operating conditions takes approximately 6 hours.

Figure 6.4 indicates that the correlation, or rather linear regression statistics, for both the calibration and verification are not as good as those for the NO emission model (Figure 5.4). While the correlation coefficient  $r$  for the calibration indicates a good qualitative agreement between measured and simulated soot emission values ( $r > 0.9$ ), the low linear regression slope ( $m < 0.8$ ) is a sign of the low sensitivity of the two step soot model (Table 6.2). The model over- and underestimates low and high experimental soot emissions, respectively, even if the experimental uncertainties of  $\pm 0.03$  [g/kWh] (Section 3.5.2) are taken into account.

Despite the deficiencies in quantitative terms, the model correctly reproduces the trends (i.e. qualitative variations) among individual operating conditions, such as the characteristic decrease of soot emissions for an increase in injection pressures shown for the operating conditions # 4, 5, and 6 (400, 700, and 1000 [bar], respectively).

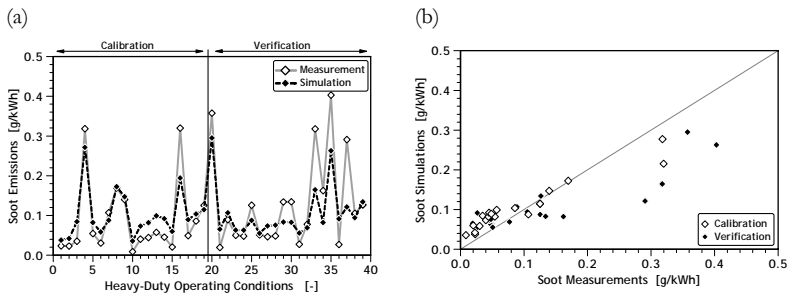


Fig. 6.4 Heavy-Duty Diesel Soot Model Calibration & Verification: (a) Sequential Operating Conditions Plot, (b) “1-to-1” Scatter Plot

		CALIBRATION	VERIFICATION
<i>Pearson's Correlation Coefficient <math>r</math></i>	[-]	0.9181	0.8216
<i>Linear Regression Slope <math>m</math></i>	[-]	0.79	0.49
<i>Linear Regression Intercept <math>b</math></i>	[-]	0.05	0.04

Tab. 6.2 Heavy-Duty Soot Model: Calibration & Verification Statistics

### 6.3.2 “Automotive” Diesel

The identical Evolutionary Algorithm implemented in Section 6.3.1 ( $n_{\text{pop}} = 50$ ,  $n_{\text{parent}} = 25$ ,  $n_{\text{offspring}} = 75$ ) is used to calibrate the soot model based on 20 out of the 57 representative automotive diesel engine operating conditions given in Table A.2.

Except for the overestimation of low experimental values for high load, no EGR operating conditions (BMEP > 11 [bar] and EGR < 0.5 [%]; # 8, 11, 27, 33, 38/39, and 45/46), a good correlation between the measured and calculated soot emissions for both calibration and verification cases is observed (c.f. Figure 6.5). Furthermore the absolute deviations between measured and calculated soot emissions observed for the verification operating conditions back up the low model sensitivity mentioned in Section 6.3.1. However, trends among different operating conditions are still correctly reproduced for both the calibration and verification cases.

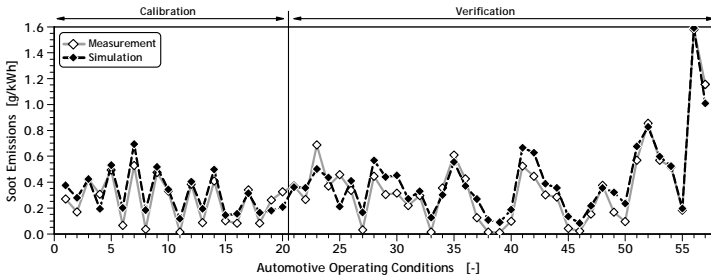


Fig. 6.5 Automotive Diesel Soot Model Calibration & Verification

To illustrate the low model sensitivity, Figure 6.6 and Table 6.3 provide a sample of six out of the 57 automotive operating conditions, showing a variation in engine load BMEP, injection pressure  $p_{\text{Inj}}$  and EGR rate at a constant piston speed  $c_m$ . Whereas the simulation slightly underestimates the experimental values for the low engine load with low injection pressure - and thus high soot emissions - operating conditions (# 34 - 36), it overestimates the values for the high engine load, high injection pressure and low EGR rate operating conditions (# 37 - 39) significantly.



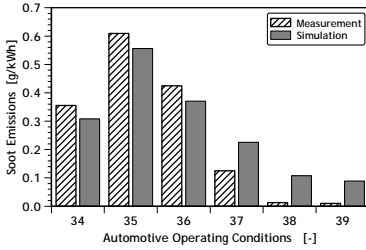


Fig. 6.6 Automotive Soot Model: Variation of Engine Load

#	$c_m$ [m/s]	BMEP [bar]	$p_{inj}$ [bar]	EGR [%]
34	6.199	4.00	567	19.16
35	6.199	9.00	869	16.70
36	6.199	10.00	913	16.48
37	6.199	11.00	957	11.10
38	6.199	12.99	1101	0.37
39	6.199	14.00	1174	0.33

Tab. 6.3 Variation of Engine Load Operating Condition Data

In order to estimate the general applicability of the proposed soot model, the calibrated parameter set from the heavy-duty diesel engine is used to simulate automotive operating conditions without changing any parameters (blind try).

Whereas calculated soot emissions do match experimental values for 6 out of the first 8 operating conditions shown in Figure 6.7, the blind try simulations for operating conditions with a measured specific soot emission higher than 0.1 [g/kWh] (32 out of 49) significantly underestimate the experimental values. Despite the absolute errors between simulated and measured emissions, the trends among individual operating conditions are well reflected and qualitative predictions of soot emissions for a different engine size and application using a two step soot model without parameter recalibration are possible.

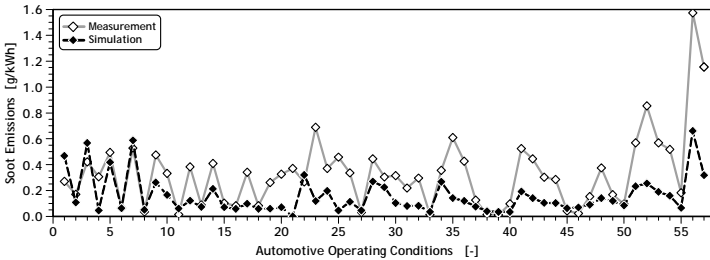


Fig. 6.7 Automotive Soot Emissions: Heavy-Duty Model Blind Try

The Pearson’s correlation coefficients and linear regression statistics given in Table 6.4, confirm the previously “visual” derived statements. While the qualitative prediction capabilities of the model are demonstrated by correlation coefficients of approximately 0.8 and 0.7 for the optimized (calibration/verification) and blind try model, respectively, the low linear regression slopes ( $m \leq 0.6$ ) reflect the low model sensitivity.

		<i>Calibration</i>	<i>Verification</i>	<i>Blind Try</i>
<i>Pearson's Correlation Coefficient <math>r</math></i>	[-]	0.9317	0.8373	0.6987
<i>Linear Regression Slope <math>m</math></i>	[-]	0.93	0.81	0.32
<i>Linear Regression Intercept <math>b</math></i>	[-]	0.11	0.14	0.05

Tab. 6.4 Automotive Optimized vs. Blind Try Soot Model Statistics

### 6.3.3 “Marine” Diesel

A scaled down version of the EA used to calibrate the soot model for the heavy-duty engine is applied to 12 out of the 26 representative marine diesel engine operating conditions given in Table A.4 ( $n_{\text{pop}} = 30$ ,  $n_{\text{parent}} = 15$ ,  $n_{\text{offspring}} = 60$ ).

To ensure the confidentiality of the marine diesel data, the soot emissions shown in Figure 6.8 and Figure 6.9 are normalized using the measured soot mass from operating condition # 15 as reference ( $m_{\text{s.meas}} = 100$  [a.u.]). As the specific soot emissions of the marine diesel engine are determined using filter smoke number (FSN) measurements and an experimentally derived correlation, this study focuses on qualitative rather than quantitative results due to the contradicting experimental FSN and gravimetric results obtained for particular operating conditions (c.f. Section 3.5.2).

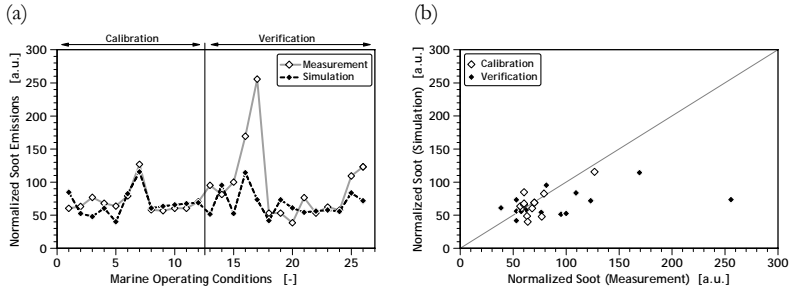


Fig. 6.8 Marine Diesel Soot Model Calibration & Verification

The measured and simulated soot emissions calculated using the calibrated model are given in Figure 6.8. The most significant discrepancies are at low load low speed operating conditions (# 16, 17), whereas the trends among single operating conditions are well reflected.

To assess the general applicability and gain further insights on the proposed soot model, the heavy-duty calibrated model is applied to the marine diesel operating conditions in a blind try, i.e. without any parameter changes.

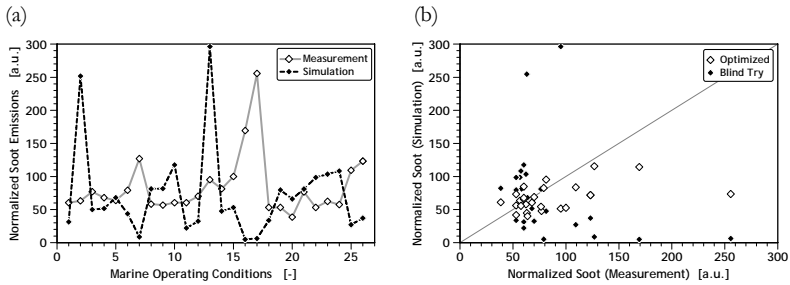


Fig. 6.9 Marine Soot Emissions: Heavy-Duty Model Blind Try

No distinct correlation is evident when the measured and blind try simulated soot emissions given in Figure 6.9 are compared. The correlation and regression statistics given in Table 6.5 indicate a negative correlation for the blind try model ( $r = -0.31$ ), implying, that for an increase in measured soot emissions the model predicts a decrease.

		<i>OPTIMIZED</i>	<i>BLIND TRY</i>
<i>Pearson's Correlation Coefficient <math>r</math></i>	[-]	0.4586	-0.3065
<i>Linear Regression Slope <math>m</math></i>	[-]	0.20	-0.47
<i>Linear Regression Intercept <math>b</math></i>	[-]	47.37	111.96

Tab. 6.5 Marine Engine Optimized vs. Blind Try Statistics

## 6.4 Conclusions

Despite the limitations in quantitative predictions, the phenomenological “two step - two zone” soot model accurately reproduces the qualitative variations between individual operating conditions. When the experimental uncertainties are taken into account, even quantitative agreements for particular automotive and heavy-duty diesel engine operating conditions are possible.

Beyond the reduced chemistry and the fact, that the model only accounts for carbon-soot, the application of the “two step - two zone” approach does not account for the existence of very hot and cold regions in an IC engine combustion chamber at the same time, causing for example a lack of oxidation of the soot produced due to low temperatures or similar effects (reduced model sensitivity).



# 7 ENGINE PROCESS SIMULATIONS

Engine process simulations are conducted to investigate practical applications of the proposed phenomenological models. After describing the general setup, both measured and simulated cylinder pressures and temperatures, as well as process characteristics and engine design parameters, such as maximum pressure, exhaust temperature, and indicated efficiency, are compared. To determine the influence of differences between measured and simulated ROHRs on engine-out emission simulations, nitrogen oxide emissions based on measured and simulated ROHRs are computed in this chapter.

## 7.1 Setup

Besides the comparison of both measured and simulated ROHR characteristics given in Chapter 4, engine process simulations based on measured and simulated rates of heat release are used to investigate the practical application of the proposed modeling approach.

Given the geometry and mechanical properties of the engine, as well as the operating condition settings, fluid and gas properties, and actual heat release rates, the engine process simulation program can be used for both steady-state and transient engine operation calculations. Using the 19 calibration operating conditions of the heavy-duty diesel engine as a basis (c.f. Table A.2), only steady-state simulations are performed.

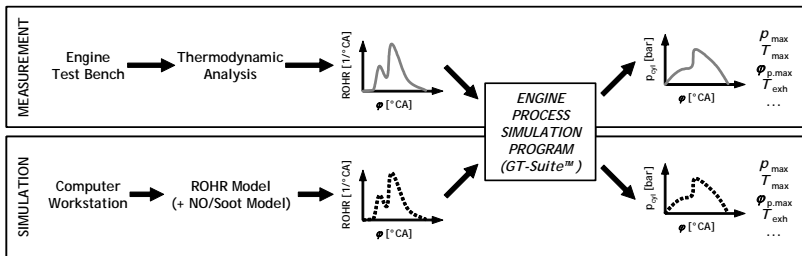


Fig. 7.1 Engine Process Simulation Comparative Study Setup

Derived from a thermodynamic analysis of engine test bench experiments (details see Chapter 4), the so-called “measured” rates of heat release are used as reference case for the engine process simulations. In order to be able to both quantify the discrepancies in the rates of heat release and gain further insights in the key aspects of ROHR modeling, “measured” instead of raw in-cylinder pressure histories are used

as the reference<sup>1</sup> in this study. The test case simulations are performed using the rates of heat release predicted by the phenomenological model proposed in Chapter 4 (Figure 7.1).

An outline of the engine model configuration and simulation program specifications are given in Table 7.1.

<i>PROGRAM</i>	GT-Suite™ 6.1
<i>LAYOUT</i>	Multi-cylinder turbocharged DI diesel engine (incl. high-pressure EGR-path with inter-cooler)
<i>GAS EXCHANGE</i>	1-D gas dynamics (entire manifold & exhaust)
<i>COMBUSTION</i>	Input: measured & simulated ROHR (“burn rates”) Two-zone temperature modeling (heat transfer: Woschni)
<i>INJECTION</i>	Experimental injection profiles
<i>EMISSIONS</i>	Built-in standard NO <sub>x</sub> and soot models

Tab. 7.1 *GT-Power Characteristics*

## 7.2 Simulations

In addition to cylinder pressure and temperature, standard engine characteristics, such as maximum pressure and temperature, maximum pressure location, and exhaust temperature are used to compare engine process simulation results.

### 7.2.1 Cylinder Pressure and Temperature

As an initial indication of the practical applicability of the proposed ROHR model, Figure 7.2 shows both the measured and simulated cylinder pressures and ROHRs (left side), as well as the corresponding mean and burned gas temperatures (right side) for three representative operating conditions (specifications are given in Table 7.2).

#	$c_m$ [m/s]	BMEP [bar]	$p_{Inj}$ [bar]	SOI [°CA]	EGR [%]
2	5.936	4.95	1400	356	23
5	5.936	4.89	700	350	0
15	8.699	8.79	1600	352	0

Tab. 7.2 *Selected Operating Conditions Specifications (c.f. Figure 7.2)*

- Figure A.1 compares the measured and experimental cylinder pressures for six out of the 19 operating conditions used in this study, generally showing negligible variations with maximum deviations of less than 2 [bar] or 3.5 %.

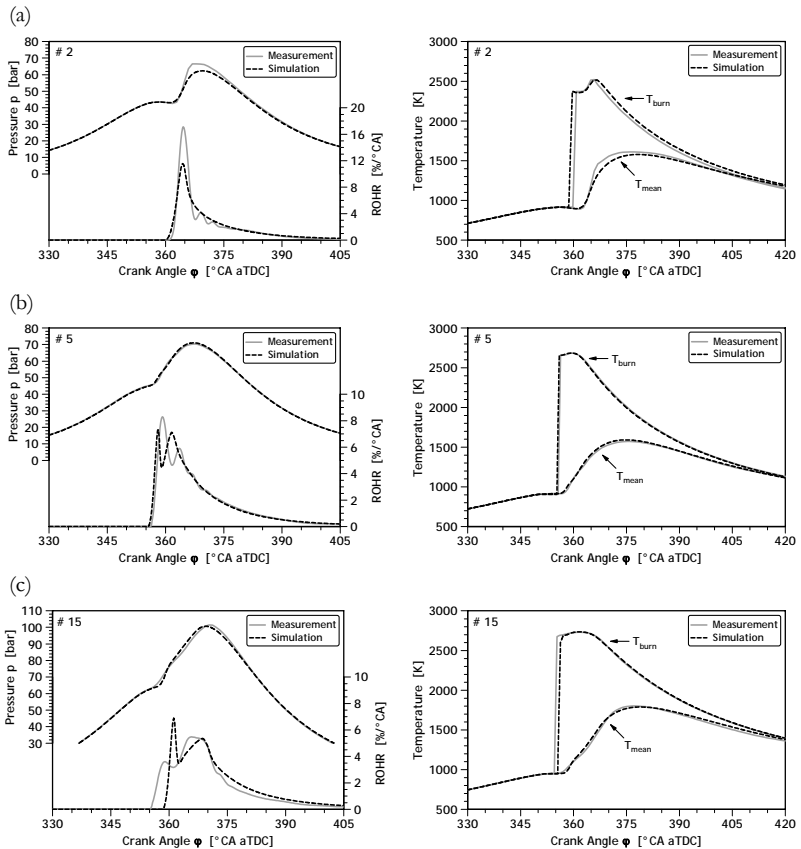


Fig. 7.2 Comparison of Cylinder Pressures and ROHRs (left side), Burned Gas and Mean Temperatures (right side) for Three Selected Heavy-Duty Diesel Operating Conditions; (a) # 2, (b) # 5, and (c) # 15

From Figure 7.2 (a), it can be seen that the discrepancy in peak rate of heat release values influences key process simulation outputs, such as cylinder pressure and mean temperature (errors: approx. 4 % of the maximum values), whereas burned gas temperatures and other ROHR characteristics (except the maximum rate of pressure increase) are much less affected. Regarding operating condition # 5 (Figure 7.2 (b)) and # 15 (Figure 7.2 (c)), deviations between measured and simulated cylinder pressures and temperatures are smaller than 1 % of the maximum values, although the maximum ROHR values and the start of combustion can differ significantly (e.g. operating condition # 15).

The comparison of cylinder pressures and temperatures for representative heavy-duty engine operating conditions thus indicates, that the proposed model is able to predict ROHRs with sufficient accuracy for use with common engine process simulation programs.

### 7.2.2 Combustion Characteristics

Common engine process simulation characteristics are used to investigate the performance of the model for all 19 operating conditions given. As an example, Figure 7.3 shows measured and simulated values of maximum cylinder pressure and its location (a), as well as maximum burned gas and mean temperature (b).

Whereas there are only minor discrepancies noted in the maximum cylinder pressure, and burned gas and mean temperatures, the values for the maximum cylinder pressure location at operating condition # 9 differ by almost 13 °CA. Upon closer inspection of both the measured and simulated cylinder pressures for this operating condition (c.f. Figure 7.4), it is revealed, that the discrepancy is caused by minor differences between the two characteristic maxima<sup>1</sup> of the pressure histories. While the location of the maxima for the simulated pressure history is due to the (late) combustion process (at approximately 372 [°CA aTDC]), it is due to cylinder compression/expansion only for the measured pressure history (at 360 [°CA aTDC], i.e. the combustion process maxima is smaller than the compression/expansion maxima)..

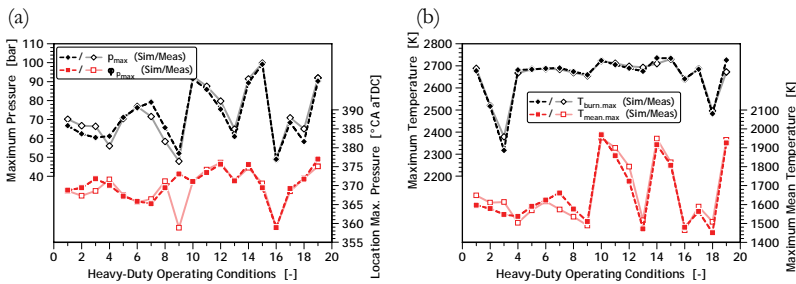


Fig. 7.3 Comparison of Engine Process Simulation Characteristics:  
 (a) Maximum Pressure and Location of Maximum Pressure,  
 (b) Maximum Temperature and Maximum Mean Temperature

As measures related to mechanical strains and turbocharger efficiency for example, the maximum and exhaust pressure and temperature are key factors in modern engine R&D. These engine process simulation outputs and their corresponding relative errors are given in Figure 7.5 (left and right side, respectively), where it can be

1. 1<sup>st</sup> Maxima: geometrically defined by the “compression/expansion” transition at TDC  
 2<sup>nd</sup> Maxima: pressure increase due to late combustion (SOC after TDC)



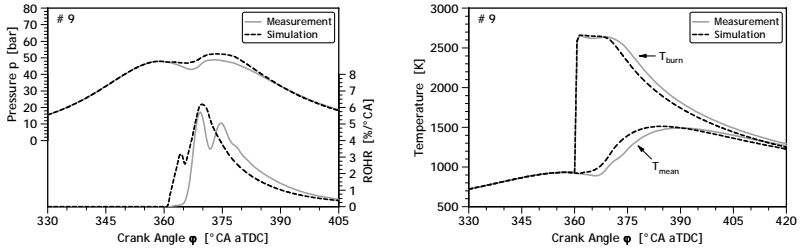


Fig. 7.4 Comparison of Cylinder Pressures and ROHRs (left side), Burn and Mean Temperatures (right side) for Operating Condition #9

seen, that the measured and simulated values are well correlated. Although errors in maximum pressure up to 12 % are noted (with an average error of approximately 5 % or 3.5 [bar] in absolute values), deviations in the exhaust pressure are smaller than 1 % (with an average error of approximately 0.3 %). Furthermore, errors in both the exhaust and maximum mean temperatures are less than 5 % (or 30 K and 65 K in absolute values, respectively), clearly indicating the good performance of the proposed ROHR model in terms of engine process characteristics.

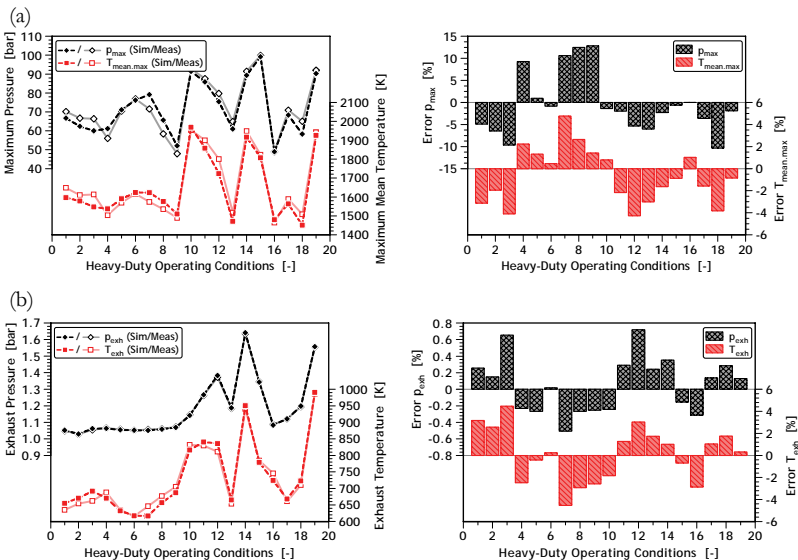


Fig. 7.5 Comparison of Engine Process Simulation Characteristics (left side: Absolute Values, right side: According Relative Errors):  
 (a) Maximum Pressure and Maximum Mean Temperature  
 (b) Exhaust Pressure and Exhaust Temperature

The largest deviations between measured and simulated pressure maxima are noted for operating conditions with either high EGR rates (# 2, 3 and 18) or low injection pressures (# 4, 7, 8 and 9). Whereas errors at high EGR rate operating conditions are caused by the underestimation of the maximum ROHR (c.f. # 2, Figure 7.2 (a)), the low injection pressure operating condition errors are due to the too short ignition delays simulated (c.f. # 9, Figure 7.4). Discrepancies in the maximum ROHR and short ignition delays for specific operating conditions strongly influence the accuracy of simulation results, such as the maximum rate of pressure increase (c.f. Figure 7.6).

While there are significant deviations in both pressure maxima and maximum rate of pressure increase, errors in global process characteristics, such as the indicated efficiency  $\eta$  generally are smaller than 2.5 %.

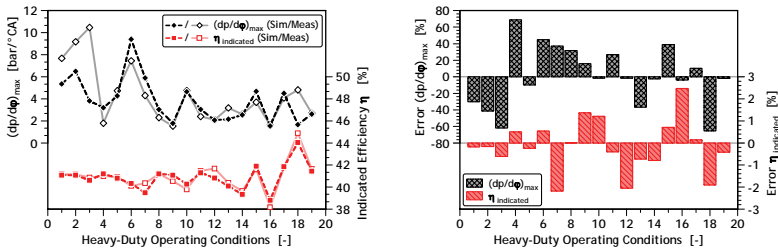


Fig. 7.6 Comparison of Maximum Pressure Increase and Indicated Efficiency (left side: Absolute Values, right side: According Relative Errors)

### 7.2.3 Emissions

To demonstrate the influence of errors in cylinder pressure and temperature on engine-out emissions, specific  $NO_x$  emissions for both measured and simulated engine process simulations - determined using the standard GT-Power built-in  $NO_x$  model - are given in Figure 7.7.

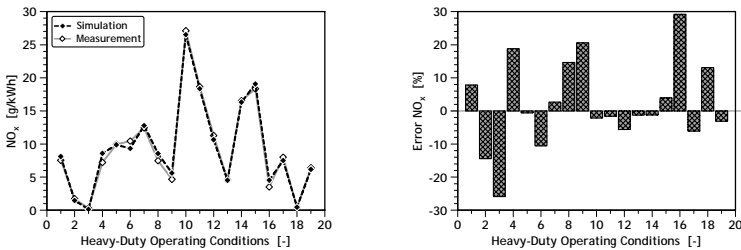


Fig. 7.7 Comparison of Nitrogen Oxide Emissions (left side: Absolute Values, right side: According Relative Errors)

Besides the large relative errors due to low absolute values of  $\text{NO}_x$  (e.g. operating conditions # 2, 3, and 18), significant errors for operating conditions with low injection pressures, such as # 4, 8, 9, and 16, can be observed. Whereas the simulated maximum cylinder pressure and mean temperature for operating conditions # 4, 8, and 9 are considerably higher than their corresponding measured values, the errors in maximum cylinder pressure and mean temperature for operating condition # 16 are less than 0.5 %. Akin to the measured operating condition # 9 (c.f. Figure 7.4), the late combustion during the expansion stroke in operating condition # 16 causes the first of the two characteristic maxima in cylinder pressure (“geometrically” defined) to be higher than the second maxima for both cases (measurement and simulation). When considering only the second maxima, the simulated pressure maxima - though lower than the first maxima - is substantially higher than measured pressure maxima and thus accounts for the overestimation of the measured nitrogen oxide emissions.

### **7.3 Conclusions**

The engine process simulation results using the ROHRs determined by the phenomenological model are in good agreement with the experimental data. Despite the substantial differences between measured and simulated maximum rates of cylinder pressure rise, as well as minor errors in the maximum cylinder pressure and mean temperature, the good agreements of both temperature and pressure at exhaust valve opening are not affected.

Considering the nitrogen oxide emission modeling as an example, the effects of the differences between the measured and simulated ROHRs for an engine process simulation are shown. While the relative NO emission prediction error is significant for operating conditions with low NO exhaust emissions or low injection pressures, the majority of the simulated NO emissions from the measured ROHR NO emissions differ by less than 0.2 [g/kWh].

The engine process simulation investigation indicates that the general application of the (phenomenological) model/knowledge based approach for fast, accurate, engine operating map wide simulations of Common-Rail DI diesel engines is indeed possible.



# 8 ARTIFICIAL NEURAL NETWORKS

In order to evaluate the performance of the investigated phenomenological models, this chapter compares the modeling outputs with Artificial Neural Network (ANN) results. After a description of the comparative study setup, both the ANN and corresponding results for all three models (i.e. rate of heat release, nitrogen oxide and soot emissions) and engines are shown.

## 8.1 Comparative Study Setup

Previous to the comparison of modeling outputs with ANN results, the neural networks are trained and verified on the identical operating conditions used for the phenomenological modeling (c.f. Chapters 4 to 6, Appendix A.1). Given that common results from ANNs (single values) and phenomenological models (data traces or functions) differ in form, the output characteristics for phenomenological models derived in Section 4.1.1 et sqq. are used in this comparison (Figure 8.1).

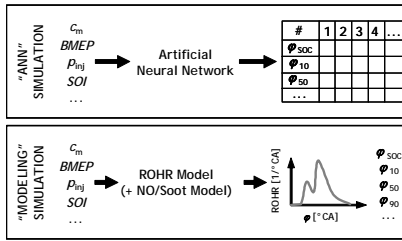


Fig. 8.1 Comparison of Simulation Schemes (ANN vs. Modeling)

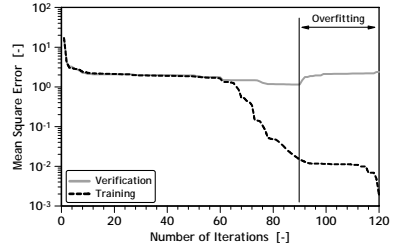


Fig. 8.2 Training vs. Verification: Overfitting Criteria

Table 3.2 gives an outline of the configuration of the ANNs used. In order to avoid an overfitting of these ANNs during training phase, both training and verification mean square errors are determined for each iteration. As a first order approximation, training is stopped as soon as the verification mean square error starts increasing (c.f. Figure 8.2).

## 8.2 Rate of Heat Release

An identical network architecture with seven key operating condition parameters as inputs ( $c_m$ , BMEP,  $p_{inj}$ ,  $\Delta t_{inj}$ ,  $\varphi_{SOI}$ ,  $x_{EGR}$ ,  $\lambda_{global}$ ) and ten ROHR characteristics as outputs ( $\varphi_{SOC}$ ,  $\varphi_{10}$ ,  $\varphi_{50}$ ,  $\varphi_{90}$ ,  $Q_{max,p}$ ,  $Q_{max,d}$ ,  $\varphi_{Qmax,p}$ ,  $\varphi_{Qmax,d}$ ,  $m_{Prmx}$  and  $m_{Diff}$ ) is used for all three engines investigated.

### 8.2.1 “Heavy-Duty” Diesel

The results of the ANN training and verification are given in Figure 8.3, in a fashion similar to that used for the ROHR model results given in Chapter 4. Evident from an engineering point of view is the excellent agreement of measured and simulated  $\varphi_{SOC}$ ,  $\varphi_{10}$ ,  $\varphi_{50}$ , and  $\varphi_{90}$  characteristics for the training operating conditions (c.f. Figure 8.5 (a)). However, for approximately half of the verification operating conditions no correlation between the measured and simulated values is noted.

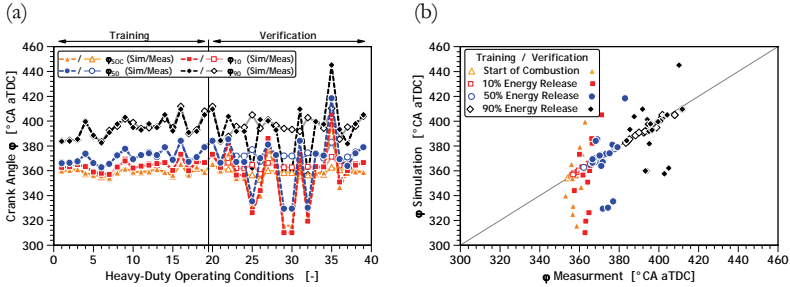
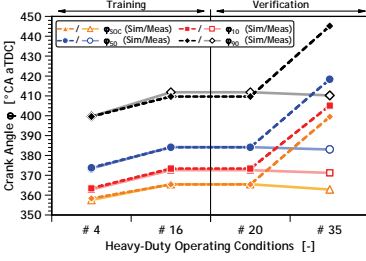


Fig. 8.3 Heavy-Duty Diesel ROHR ANN Training & Verification: (a) Sequential Operating Conditions Plot, (b) “1-to-1” Scatter Plot

From the correlation coefficients  $r$  given in Table 8.2, both the excellent agreement for ANN training ( $r > 0.95$ ) and the weak correlation for ANN verification ( $r < 0.5$ ) are confirmed. Although the correlation coefficients are smaller than 0.5 for the ANN verification, the fact that the measured and simulated results do agree for 10 out of the 20 verification operating conditions results in correlation coefficients significantly higher than 0<sup>1</sup>.

As an example of verification operating conditions with both good and poor agreement, the ROHR characteristics and operating condition data for four conditions - two training and two verification conditions - are given in Figure 8.4 and Table 8.1, respectively. The four operating conditions have identical engine speeds and brake mean effective pressures, as well as similar injection pressures ( $p_{Inj} = 350$  or  $400$  [bar]) and SOIs ( $SOI = 350, 356$  or  $357$  [°CA aTDC]). Whereas almost no discrepancy is noted between the measured and simulated characteristics for operating conditions # 4, 16, and 20, ROHR characteristics for operating condition # 35 determined from ANN simulations are delayed by approximately 40 °CA. Although the effects of an advanced SOI timing are correctly reproduced for # 4 ( $SOI = 350$  [°CA aTDC]), the one degree change in SOI from 357 to 356 [°CA aTDC] between # 20 and # 35 causes the neural network to fail.

1.  $r = 0$  : no linear correlation between two variables. The two variables are considered to be statistically independent.



#	$c_m$ [m/s]	BMEP [bar]	$p_{Inj}$ [bar]	SOI [°CA]
4	5.936	4.91	400	350
16	5.944	4.93	350	357
20	5.947	4.94	350	357
35	5.936	4.90	350	356

Fig. 8.4 Heavy-Duty ROHR ANN: Training vs. Verification

In order to compare the ANN and modeling results on a one-to-one basis, Figure 8.5 shows the measured and simulated ROHR characteristics for both approaches on the identical set of heavy-duty operating conditions (Table A.2). While the agreement between measured and simulated values is equally good for the entire set of operating conditions in the phenomenological modeling approach, a distinct decrease in simulation prediction quality is obvious between ANN training and verification operating conditions.

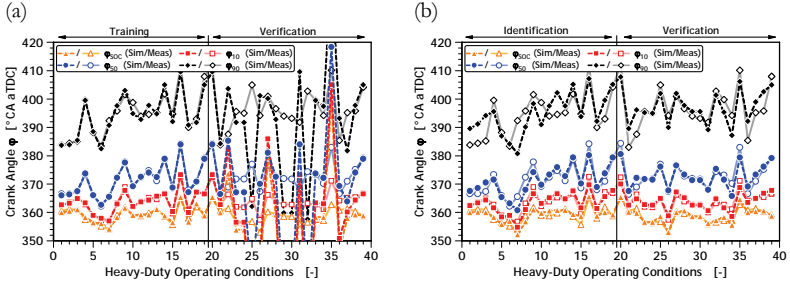


Fig. 8.5 Comparison of Heavy-Duty Engine ROHR Simulation Methods: (a) Artificial Neural Network, (b) Phenomenological Modeling

To quantify these visually observed statements, the correlation coefficients  $r$  of the ROHR characteristics for both ANN training and verification, as well as modeling calibration and verification are given in Table 8.2.

		$\varphi_{SOC}$	$\varphi_{10}$	$\varphi_{50}$	$\varphi_{90}$
<b>ANN Training</b>	[-]	0.9737	0.9880	0.9965	0.9716
<b>ANN Verification</b>	[-]	0.4750	0.4636	0.2663	0.2627
<b>Modeling Calibration</b>	[-]	0.8970	0.9248	0.9005	0.7111
<b>Modeling Verification</b>	[-]	0.9465	0.9194	0.9174	0.8178

Tab. 8.2 Heavy-Duty Engine Pearson's Correlation Coefficients  $r$

### 8.2.2 “Marine” Diesel

As was done for the heavy-duty engine investigation in the previous section, ANN and phenomenological modeling results for the marine diesel engine are given in Figure 8.6. Whereas the trained ANN in the heavy-duty investigation fails for half of the verification operating conditions given, the marine diesel trained ANN fails (clearly) only for operating condition # 19. However, the ANN fails for an operating condition setting which lies between two similar settings # 2 and 23 that are correctly reproduced (# 2/19/23 : SOI = 2.58/-3.87/-10.32 [a.u.]).

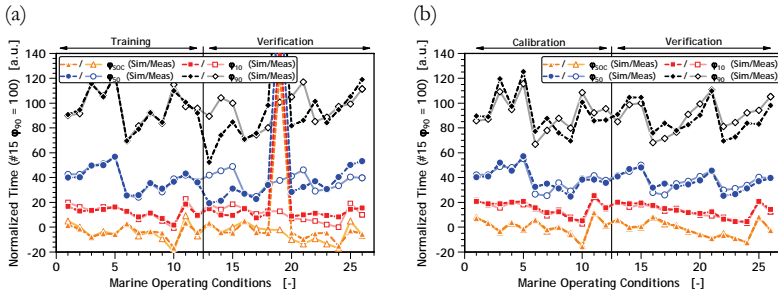


Fig. 8.6 Comparison of Marine Diesel Engine ROHR Simulation Methods: (a) Artificial Neuronal Network, (b) Phenomenological Modeling

In general, the agreement between the measured and simulated ROHR characteristics for the two approaches is similar to that seen in the heavy-duty engine investigation. While the correlation is almost perfect for the ANN training conditions and significantly lower for the ANN verification conditions (even if the outlier operating condition # 19 is excluded), the corresponding values for the phenomenological modeling approach are constant over the entire set of operating conditions (c.f. Table 8.3). Whereas the exclusion from outlier operating condition # 19 in the ANN verification set has a significant positive impact on the correlation of both  $\varphi_{SOC}$  and  $\varphi_{10}$ , the low overall correlation coefficients for the  $\varphi_{50}$  and  $\varphi_{90}$  verification characteristics are largely unaffected.

		$\varphi_{SOC}$	$\varphi_{10}$	$\varphi_{50}$	$\varphi_{90}$
<b>ANN Training</b>	[-]	0.9494	0.9679	0.9493	0.9647
<b>ANN Verification</b>	[-]	0.0119	-0.0127	-0.0059	0.1852
<b>ANN Verification (w.o. # 19)</b>	[-]	0.8303	0.5228	0.0402	0.3781
<b>Modeling (Optimized)</b>	[-]	0.9959	0.9683	0.9775	0.8432

Tab. 8.3 Marine Engine Pearson’s Correlation Coefficients  $r$



In order to estimate the general applicability of the ANN and phenomenological modeling approach, the heavy-duty engine trained network and calibrated model are applied to the marine diesel operating conditions in a blind try, i.e. without recalibration. While the blind try ANN simulation cannot predict any of the combustion characteristics, the phenomenological model simulation, except for the short combustion durations, accurately predicts trends and variations in  $\varphi_{10}$ ,  $\varphi_{50}$  and  $\varphi_{90}$  values (c.f. Figure 8.7 and Section 4.4.3).

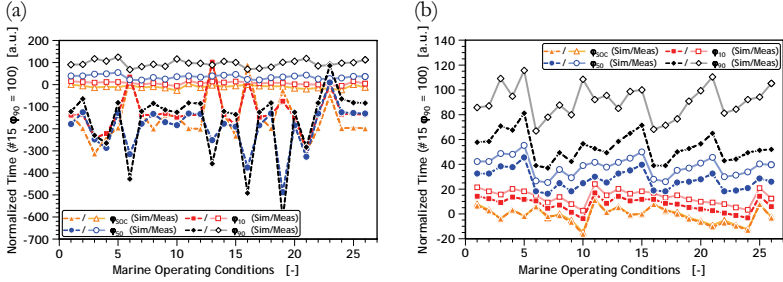


Fig. 8.7 Comparison of Blind Try Marine Diesel Engine ROHR Simulations: (a) Artificial Neuronal Network, (b) Phenomenological Modeling

## 8.3 Nitrogen Oxide & Soot Emissions

In addition to the ROHR characteristics investigation above, the ANN approach is used to simulate both emissions of nitrogen oxide and soot for all three engines. Common network architectures as described in Section 3.4.2 are used, with the seven key operating condition parameters  $c_m$ , BMEP,  $p_{Inj}$ ,  $\Delta t_{Inj}$ ,  $\varphi_{SOI}$ ,  $x_{EGR}$ , and  $\lambda_{global}$  as inputs, and the specific nitrogen oxide and soot emissions  $m_{NO}$  and  $m_{soot}$  as outputs.

### 8.3.1 “Heavy-Duty” Diesel

Both measured and simulated specific nitrogen oxide and soot emissions for the standard heavy-duty diesel operating conditions (Table A.2) are given in Figure 8.8. Whereas in the training sets there are only minimal variations noted between the measured and simulated emissions, distinct deviations are observed for several verification operating conditions. While the deviations in specific nitrogen oxide emissions are caused only by operating condition settings outside the range of the trained settings (e.g. # 23/24, 29/30/32), deviations in specific soot emissions appear for operating conditions even within the range of the trained settings (e.g. # 37).

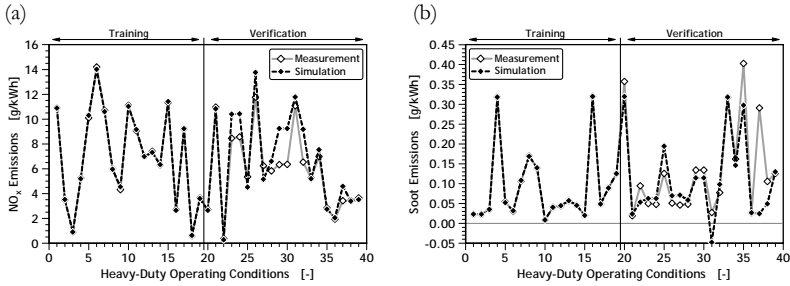


Fig. 8.8 Heavy-Duty Diesel Emissions ANN Training & Verification: (a) Nitrogen Oxide Emissions, (b) Soot Emissions

Besides the negative specific soot mass predicted for operating condition # 31, a large discrepancy between the measured and simulated soot emissions for operating condition # 37 is noted. The operating condition settings and measured, ANN, and phenomenological model simulated specific soot emissions for the operating conditions # 13, 18, and 37 given in Table 8.4 indicate, that an increase in specific soot emissions with increasing EGR rate is expected. Whereas this is true for the measured and the simulated values for the operating conditions # 13 and 18, only the model prediction for the operating condition # 37 shows this behavior. While the measured emission for # 37 (EGR = 17 %) is more than 300 % of the value measured for # 18 (EGR = 27 %), the ANN predicted emission for # 37 is even 50 % lower than that for # 13 (no EGR), implying that the ANN does not capture the influence of EGR. Although the experimental soot measurements of operating condition # 37 are suspected to be statistical outliers, the decrease in soot emissions for an increase in EGR from 0 to 17 %, as predicted by the ANN, is even less plausible.

#	$c_m$ [m/s]	BMEP [bar]	$p_{inj}$ [bar]	SOI [°CA]	EGR [%]	SOOT [g/kWh]		
						Measured	ANN	Model
13	8.696	4.40	1400	356	0	0.0572	0.05714	0.0988
18	8.702	4.35	1400	356	27	0.0891	0.08909	0.1212
37	8.693	4.40	1400	356	17	0.29074	0.02436	0.1035

Tab. 8.4 Heavy-Duty Diesel Specific Soot Emission Details

### 8.3.2 “Marine” Diesel

Similar to the heavy-duty results given in Figure 8.8 (a), the ANN nitrogen oxide emission simulations for the two-stroke marine diesel engine show an almost perfect agreement between measured and simulated values for training operating conditions and a qualitatively correct prediction of the measured values for all verification operating conditions (Figure 8.9 (a) and (b)).

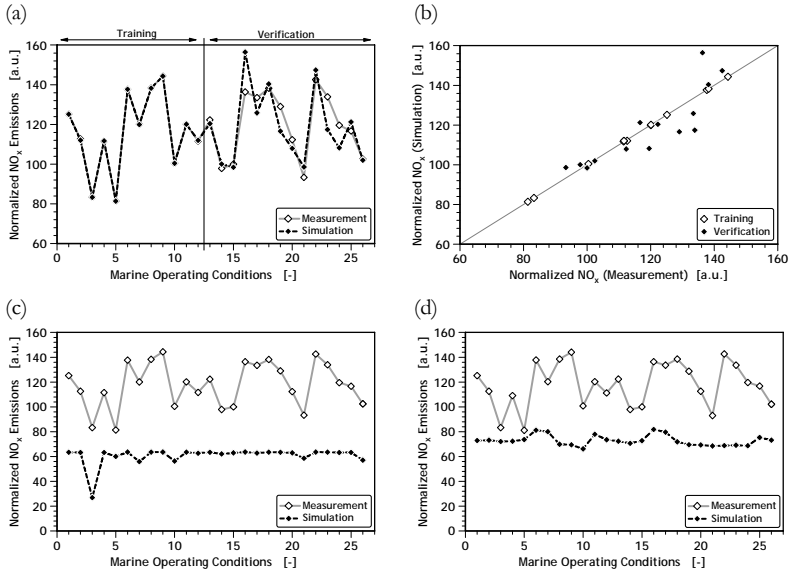


Fig. 8.9 Marine Diesel Nitrogen Oxide Emission Simulation: (a) ANN Sequential Operating Conditions Plot, (b) ANN "1-to-1" Scatter Plot, (c) ANN Blind Try, (d) Phenomenological Modeling Blind Try

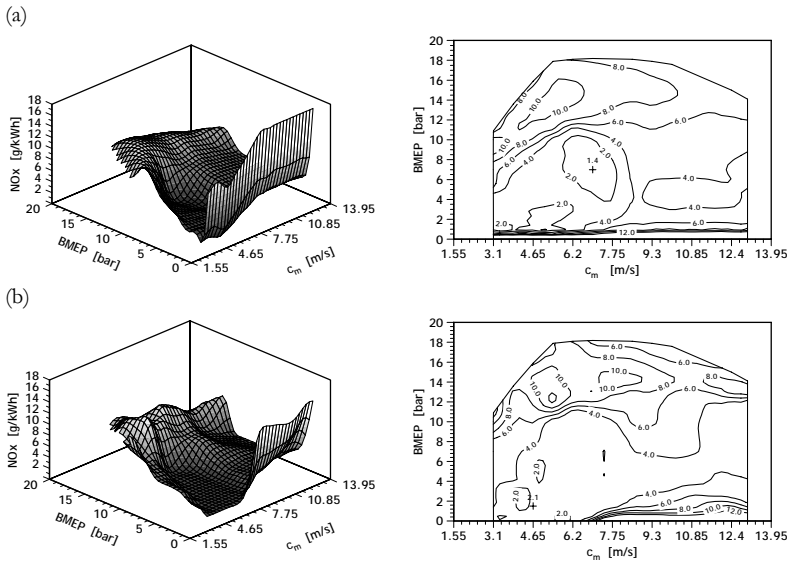


Fig. 8.10 Automotive NO Emissions: (a) Measurements, (b) ANN Simulation

Given the difficulties with the blind try application of the heavy-duty calibrated nitrogen oxide emission model to marine diesel operating conditions (Section 5.3.3), the use of the heavy-duty nitrogen oxide ANN for marine diesel operating conditions was investigated. Except for the low injection pressure ( $p_{Inj} = 450$  [bar]) operating conditions # 3, 7, 10, 21, and 26, the blind try ANN simulated NO emissions vary between 60 and 65 [a.u.] only (c.f. Figure 8.9 (c)). Thus, neither the nitrogen oxide ANN nor the phenomenological NO model are capable to predict the emissions of the marine diesel engine correctly without a recalibration.

### 8.3.3 “Automotive” Diesel

In order to demonstrate both the assets and drawbacks of the ANN approach, the 57 automotive calibration and verification operating conditions (c.f. Table A.1) are used to train a specific nitrogen oxide emissions ANN which subsequently is verified for the entire engine operating map with more than 300 operating conditions  $n_{OC}$ .

The measured and simulated NO emissions given in Figure 8.10 indicate a qualitatively correct prediction of the experimental values over the entire operating map. When considering only the ANN training operating conditions, a quantitatively correct prediction of the experimental values is possible (c.f. Figure 8.11 (a)), as indicated by Pearson’s correlation coefficients of 0.9121 and 0.6309 for the training and verification operating condition sets, respectively<sup>1</sup>.

From the configuration of the specific nitrogen oxide emission residuals shown in Figure 8.11 (b), a significant dependence of the ANN prediction quality on the range of parameters used during network training is seen. Despite minor errors in the absolute NO emission values, the ANN approach is able to accurately predict the major effects and trends for an entire engine operating map, given sufficient and comprehensive training data.

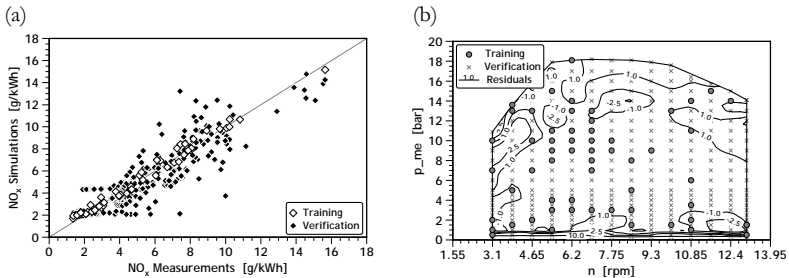


Fig. 8.11 Automotive NO Emissions: (a) “1-to-1” Plot of Training and Verification Operating Conditions, (b) NO Emission Residuals

1. Phenomenological Model: Calibration  $r = 0.9593$  ( $n_{OC} : 20$ ), Verification  $r = 0.7428$  ( $n_{OC} : 37$ )  
 ANN : Training  $r = 0.9121$  ( $n_{OC} : 57$ ), Verification  $r = 0.6309$  ( $n_{OC} : 256$  ! operating conditions)

## 8.4 Conclusions

The comparison of the ANN and phenomenological model results for Common-Rail DI diesel engine combustion and emissions clearly demonstrates the advantages and disadvantages of both approaches. While the ANN approach yields fast and accurate training results, it may implicate errors for verification operating conditions outside of the training range<sup>1</sup>. Alternatively, the phenomenological (model/knowledge based) approach needs fundamental knowledge about the governing processes and advanced calibration methods, but allows for accurate predictions for verification operating condition and engine setups even outside of the training range.

From the heavy-duty diesel ROHR, NO and soot emission model comparison, it is noted that the emission ANNs show better agreement with the measured values than the ROHR ANN. This behavior is particularly evident for operating conditions outside of the training range, as well as for the verification operating conditions (although to a lesser degree). In spite of this, neither the ROHR nor the NO emission ANNs allow for reliable predictions when switching from one engine to another, such as from a heavy-duty diesel to a two-stroke marine diesel.

Given an appropriate number of experimental measurements for training, it is possible for the ANN to generate a rough estimate of the NO emissions for an entire engine operating map within minutes. This is a major advantage of the ANN over other, for example phenomenological model based methods.

---

1. *Training range* - range of operating condition parameters used used for the model calibration



## 9 CONCLUSIONS AND OUTLOOK

In this work, a model/knowledge based and a black-box approach for the simulation and optimization of the combustion in Common-Rail DI diesel engines are compared, based on their ability to predict the rates of heat release, and the nitrogen oxide and soot emissions. The focus of the investigation is on the applicability of the two different approaches, the advanced optimization/calibration methods and the phenomenological/ANN models to three distinct engines: an automotive, a heavy-duty, and a two-stroke marine diesel engine.

### 9.1 Summary & Conclusions

After an literature overview of the various IC engine models and calibration/optimization methods, the following phenomenological models are derived for the model/knowledge based approach and systematically evaluated against comprehensive experimental data from the three engines.

- *RATE OF HEAT RELEASE*

Fast and accurate engine operating map wide predictions of ROHR characteristics are determined using the simplified yet physically and chemically coherent phenomenological ROHR model in combination with an Evolutionary Algorithm (EA) to calibrate the model parameters. Motivated by the successful calibration and verification of the model for the three distinct engines, the general applicability of the model is investigated using the heavy-duty engine calibrated model to simulate both automotive and marine diesel engine operating conditions without any parameter changes (i.e. blind try). Despite deviations in the absolute values, both blind trials correctly reproduce the variations among single operating conditions, and can be adjusted to yield correct absolute values using basic knowledge about the tested engine. An advanced fuels survey further shows that the calibrated ROHR model is capable of predicting the effects of water-in-diesel emulsion and diesel-butylal blended fuels on ROHR characteristics.

- *NITROGEN OXIDE EMISSIONS*

The developed phenomenological nitrogen oxide emissions model allows for both qualitative and quantitative predictions of specific NO emissions for the automotive and heavy-duty engine operating conditions. The quantitative deviations between measured and simulated NO emissions for the two-stroke marine diesel engine can be related to both the general chemistry model and the modeling approach used for the turbulent gas mixing.

- *SOOT EMISSIONS*

Despite the limitations in quantitative predictions, the phenomenological “two step - two zone” soot model accurately reproduces the variations between individual operating conditions. Taking the experimental measurements uncertainties into account, even a quantitative agreement for particular automotive and heavy-duty diesel engine operating conditions is possible.

Artificial Neural Networks (ANN) are used as the black-box approach alternative to the phenomenological model/knowledge based approach. While the ANN approach yields fast and accurate training results, it may implicate errors for verification operating conditions outside of the training range. Alternatively, the phenomenological model/knowledge based approach needs fundamental knowledge about the governing processes and advanced calibration methods, but allows for accurate predictions for verification operating condition and engine setups even outside of the training range.

## 9.2 Outlook

The following list contains possible questions and topics for future research that arised during this work:

- *PHENOMENOLOGICAL MODELING*

Although the characterization of the model quality using single objective approximation functions allow for fast and accurate calibrations and verifications, the engine process simulation results given in Chapter 7 indicate the need for a comprehensive study on the fitness/objective functions used (including multi-objective optimization approaches). Whereas the deviation between the measured and simulated maximum ROHR significantly affects the in-cylinder peak pressure for operating conditions with high EGR rates, there is no influence detectable for high load, high speed operating conditions (with no EGR).

Regarding the formulation of the individual models, the influence of the EGR rate on the ROHR history, the impact of the Fenimore NO formation for low nitrogen oxide emission operating conditions, and the low sensitivity of the “two steps - two zone” soot model on engine operating condition parameters might be interesting topics for future investigations.

Furthermore, the coupling of both in-cylinder and exhaust gas aftertreatment models, real-time engine (emissions!) modeling, and adaption/extension of existing models according to the future demands (e.g. number size distribution, particulate matter models rather than specific soot mass models) are important topics in future engine modeling.



- *ANN MODELING*

Given the uncertainties noted during the ANN model verification (c.f. Chapter 8), promising topics for future IC engine related research may focus on large experimental data analyses, such as production engine testing (e.g. in combination with Design of Experiments) or online modeling (e.g. onboard diagnosis, “virtual” sensors, or measurement and control applications).

- *CALIBRATION & OPTIMIZATION*

With a change from the single objective approximation functions to multi-objective optimization functions in order to characterize the model quality, an in-depth comparison of the various multi-objective optimization methods for engine modeling specific applications would provide valuable insights.

Considering the potential of the advanced optimization methods as shown for the phenomenological model/knowledge approach, a direct application of these optimization methods on an automated engine test-bed would be an additional step towards shorter IC engine development times.

- *FUTURE ENGINE SIMULATIONS*

The development of an integrated engine simulation concept, accounting for both the system level (e.g. powertrain configuration, gas exchange, or auxiliaries) and the module level aspects (e.g. combustion, exhaust gas aftertreatment, etc.), is perhaps the most challenging topic in future IC engine R&D. As a first step, exemplary investigations on subproblems, such as the combination of in-cylinder soot formation and particulate filter modeling, could be used to determine the potential gains that exist when the various modeling resolutions (empirical, phenomenological, detailed/complex) are combined.

As a scenario for the near-term future in engine R&D, an engine development procedure may start with a qualitative numerical evaluation of various technologies and concepts, using previously calibrated phenomenological models (blind try). After this initial design phase and the construction/production of the new engine for test purposes, a small number of reference measurements for the new engine are conducted (approx. 100 operating conditions; time exposure: 1 or 2 days, depending on the complexity of the system). Given these measurements, a calibration of the model parameters using an Evolutionary Algorithm, for example, (time exposure: one night) and an exhaustive evaluation of all possible engine parameter combinations are carried out (time exposure: one to ten days, depending on the number of setups and CPU's used). After choosing the most promising configurations, the verification on the test bench completes the procedure. Compared to a standard all “test-bench based” scenario, i.e. measuring 1.5 million combinations (engine parameter setups), for example, the future scenario offers a decrease in time by at least two orders of magnitude.



# REFERENCES

- [1] ACEA (European Automobile Manufacturers Association) Statistics, <http://www.acea.be>, accessed October 2005.
- [2] Akihama K., et al.: "Mechanism of the Smokeless Rich Diesel Combustion by Reducing Temperature," *SAE paper 2001-01-0655*, 2001.
- [3] Aufdenblatten S., et al.: "Charakterisierung der Partikelemission von modernen Verbrennungsmotoren," *Motortechnische Zeitschrift (MTZ)*, vol. 63, pp. 962-974, 2002.
- [4] Aufdenblatten S., Personal Communication, 2005.
- [5] Bäck T.: *Evolutionary Algorithms in Theory and Practice*, Oxford University Press, New York, 1996.
- [6] Bäck T., Fogel D.B., and Michalewicz Z. (eds.): *Handbook of Evolutionary Computation*, Computational Intelligence Library, IOP Publishing Ltd and Oxford University Press, London, 1997.
- [7] Barba C.: *Erarbeitung von Verbrennungskennwerten aus Indizierdaten zur verbesserten Prognose und rechnerischen Simulation des Verbrennungsablaufes bei Pkw-DE-Dieselmotoren mit Common-Rail-Einspritzung*, Ph.D. Thesis, ETH Zürich, Nr. 14276, 2001.
- [8] Barroso G., Schneider B., and Boulouchos K.: "An Extensive Parametric Study on Diesel Spray Simulation and Verification with Experimental Data," *SAE paper 2003-01-3230*, 2003.
- [9] Barroso G., et al.: "Simulation der Zündung und Energieumsetzung in Motoren mit HCCI-Brennverfahren mit Reaktornetzwerke," *1<sup>st</sup> Symposium "Motorprozesssimulation und Aufladung"*, pp. 53-75, 2005.
- [10] Bertola A.G.: *Technologies for Lowest NO<sub>x</sub> and Particulate Emissions in DI-Diesel Engine Combustion: Influence of Injection Parameters, EGR and Fuel Composition*, Ph.D. Thesis, ETH Zürich, Nr. 15373, 2003.
- [11] Bertola A.G., Li R., and Boulouchos K.: "Influence of Water-Diesel Fuel Emulsions and EGR on Combustion and Exhaust Emissions of Heavy-Duty, DI-Diesel Engines Equipped with Common-Rail Injection System," *SAE paper 2003-01-3146*, 2003.
- [12] Bilger R.W.: "Conditional Moment Closure for Turbulent Reacting Flow," *Physics of Fluids A: Fluid Dynamics*, vol. 5, pp. 436-444, 1993.
- [13] Bittermann A., et al.: "Emissionsauslegung des dieselmotorischen Fahrzeugantriebs mittels DoE und Simulationsrechnung," *Motortechnische Zeitschrift (MTZ)*, vol. 65, pp. 466-474, 2004.

- 
- [14] Blumberg P.N., Lavoie G.A., and Tabaczynski R.J.: "Phenomenological Models for Reciprocating Internal Combustion Engines," *Progress in Energy and Combustion Science*, vol. 5, pp. 123-167, 1979.
- [15] Bockhorn H. (ed.): *Soot Formation in Combustion: Mechanisms and Models*, Springer Series in Chemical Physics 59, Springer Verlag, Berlin, 1994.
- [16] Boulouchos K. and Papadopoulos S.: "Zur Modellbildung des motorischen Verbrennungsablaufes," *Motortechnische Zeitschrift (MTZ)*, vol. 45, pp. 324-335, 1984.
- [17] Boulouchos K., Obrecht P., and Warth M.: "Kennfeldtaugliche Vorausberechnungen beim Dieselmotor," *Motortechnische Zeitschrift (MTZ)*, vol. 65, pp. 924-931, 2004.
- [18] Box G.E.P., Hunter J.S., and Hunter W.G. (ed.): *Statistics for Experimenters: Design, Innovation, and Discovery (2<sup>nd</sup> Edition)*, Wiley Series in Probability and Statistics, Wiley-Interscience, Hoboken, NJ, 2005.
- [19] Bracco F.V.: "Introducing a New Generation of More Detailed and Informative Combustion Models," *SAE paper 741174*, 1974.
- [20] Büche D.: *Multi-Objective Evolutionary Optimization of Gas Turbine Components*, Ph.D. Thesis, ETH Zürich, Nr. 15420, 2003.
- [21] Bunn W., et al.: "A Reevaluation of the Literature Regarding the Health Assessment of Diesel Engine Exhaust," *Inhalation Toxicology*, vol. 16, pp. 889-900, 2004.
- [22] Chase M.W.: "NIST-JANAF Thermochemical Tables (Fourth Edition)," *Journal of Physical and Chemical Reference Data*, vol. Monograph No. 9 (Part I and Part II), pp. 1963, 1998.
- [23] Clark N.N., et al.: "Emissions Modeling of Heavy-Duty Conventional and Hybrid Electric Vehicles," *SAE paper 2001-01-3675*, 2001.
- [24] De Lucas A., et al.: "Modeling Diesel Particulate Emissions with Neural Networks," *Fuel*, vol. 80, pp. 539-548, 2001.
- [25] Delagrammatikas G.J. and Assanis D.N.: "Development of a Neural Network Model of an Advanced, Turbocharged Diesel Engine for Use in Vehicle-Level Optimization Studies," *Proceedings of the I MECH E Part D: Journal of Automobile Engineering*, vol. 218, pp. 521-533, 2004.
- [26] Desantes J.M., et al.: "Multi-Objective Optimization of Heavy-Duty Diesel Engines Under Stationary Conditions," *Proceedings of the I MECH E Part D: Journal of Automobile Engineering*, vol. 219, pp. 77-87, 2005.
- [27] Durán A., Carmona M., and Monteagudo J.M.: "Modelling Soot and SOF Emissions From a Diesel Engine," *Chemosphere*, vol. 56, pp. 209-225, 2004.

- 
- [28] Eichelberg G.: "Some New Investigations on Old-Combustion-Engine Problems," *Engineering*, vol. 148, pp. 463 and 567, 1939.
- [29] Eiglmeier C. and Merker G.P.: "Neue Ansätze zur phänomenologischen Modellierung des gaseitigen Wandwärmeübergangs im Dieselmotor," *Motortechnische Zeitschrift (MTZ)*, vol. 61, pp. 324-335, 2000.
- [30] Fogel D.B.: *Evolutionary Computation: Toward a New Philosophy of Machine Intelligence*, IEEE Press, Piscataway NJ, 1995.
- [31] Frenklach M. and Wang H.: *Detailed Mechanism and Modeling of Soot Particle Formation*, in: Bockhorn H. (ed.), *Soot Formation in Combustion*, pp. 165-192, Springer-Verlag, Berlin, 1994
- [32] Freunberger S., et al.: "1 + 1 Dimensional Model for PE Fuel Cells of Technical Size," *2<sup>nd</sup> European PEFC Forum*, pp. 299-308, 2003.
- [33] Frouzakis C.E., et al.: "From Diffusion to Premixed Flames in an H<sub>2</sub>/Air Opposed-Jet Burner: The Role of Edge Flames," *Combustion and Flame*, vol. 130, pp. 171-184, 2002.
- [34] Gao Z. and Schreiber W.: "A Phenomenologically Based Computer Model to Predict Soot and NO<sub>x</sub> Emission in a Direct Injection Diesel Engine," *International Journal of Engine Research*, vol. 2, pp. 177-188, 2001.
- [35] Goldberg D.E.: *Genetic Algorithms in Search, Optimization, and Machine Learning*, Addison-Wesley Professional, Reading MA, 1989.
- [36] Gosman A.D. and Watkins A.P.: "Predictions of Local Instantaneous Heat Transfer in Idealised Motored Reciprocating Engines," *Imperial College Fluid Section Report*, FS/79/28, 1979.
- [37] Hafner M.: "Steps Towards an Optimization of the Dynamic Emission Behavior of IC Engines: Measurement Strategies - Modelling - Model-Based Optimization," *SAE paper 2001-01-1793*, 2001.
- [38] Hansen N., Müller S.D., and Koumoutsakos P.: "Reducing the Time Complexity of the Derandomized Evolution Strategy with Covariance Matrix Adaptation (CMA-ES)," *Evolutionary Computation*, vol. 11, pp. 1-18, 2003.
- [39] Hawley J.G., Wallace F.J., and Khalil-Arya S.: "A Fully Analytical Treatment of Heat Release in Diesel Engines," *Proceedings of the I MECH E Part D: Journal of Automobile Engineering*, vol. 217, pp. 701-717, 2003.
- [40] Haykin S.: *Neural Networks: A Comprehensive Foundation*, 2<sup>nd</sup> ed., Prentice Hall Inc., Upper Saddle River NJ, 1999.
- [41] He Y. and Rutland C.J.: "Application of Artificial Neural Networks in Engine Modelling," *International Journal of Engine Research*, vol. 5, pp. 281-296, 2004.

- 
- [42] Heider G.: *Rechenmodell zur Vorausberechnung der NO-Emission von Dieselmotoren*, Ph.D. Thesis, TU München, 1996.
- [43] Hentschel R., Cernat R.-M., and Varchmin J.-U.: "In-Car Modeling of Emissions with Dynamic Artificial Neural Networks," *SAE paper 2001-01-3383*, 2001.
- [44] Heywood J.B.: *Internal Combustion Engine Fundamentals*, McGraw-Hill Book Company, New York, 1988.
- [45] Hikosaka N.: "A View of the Future of Automotive Diesel Engines," *SAE paper 972682*, 1997.
- [46] Hiroyasu H., Yoshimatsu A., and Arai M.: "Mathematical Model for Predicting the Rate of Heat Release and Exhaust Emissions in IDI Diesel Engines," *Proceedings of the I MECH E Part C - Journal of Mechanical Engineering Science*, vol. 102, pp. 207-213, 1982.
- [47] Hiroyasu H., Kadota T., and Arai M.: "Development and Use of a Spray Combustion Model to Predict Diesel Engine Efficiency and Pollutant Emissions (Part I+II)," *Bulletin of the JSME*, vol. 26, pp. 569-583, 1983.
- [48] Hiroyasu H.: "Diesel Engine Combustion and Its Modeling," *1<sup>st</sup> International Symposium on Diagnostics and Modeling of Combustion in Internal Combustion Engines*, pp. 53-75, 1985.
- [49] Hohlbaum B.: *Beitrag zur rechnerischen Untersuchung der Stickoxid-Bildung schnelllaufender Hochleistungsdieselmotoren*, Ph.D. Thesis, Universität Fridericana Karlsruhe (TH), 1992.
- [50] Holland J.H.: *Adaptation in Natural and Artificial Systems: An Introductory Analysis with Applications to Biology, Control, and Artificial Intelligence*, The MIT Press, Cambridge MA, 1975.
- [51] Hornik K., Stinchcombe M., and White H.: "Multilayer Feedforward Networks are Universal Approximators," *Neural Networks*, vol. 2, pp. 359-366, 1989.
- [52] Kalogirou S.A.: "Artificial Intelligence for the Modeling and Control of Combustion Processes: a Review," *Progress in Energy and Combustion Science*, vol. 29, pp. 515-566, 2003.
- [53] Kamimoto T. and Kobayashi H.: "Combustion Processes in Diesel Engines," *Progress in Energy and Combustion Science*, vol. 17, pp. 163-189, 1991.
- [54] Kee R.J., Rupley F.M., and Miller J.A.: "The CHEMKIN Thermodynamic Data Base," *Sandia National Laboratories Report*, SAND87-8215B, 1990.
- [55] Kennedy I.M.: "Models of Soot Formation and Oxidation," *Progress in Energy and Combustion Science*, vol. 23, pp. 95-132, 1997.

- 
- [56] Kesgin U.: "Genetic Algorithm and Artificial Neural Network for Engine Optimisation of Efficiency and NO<sub>x</sub> Emission," *Fuel*, vol. 83, pp. 885-895, 2004.
- [57] Khan I.M., Greeves G., and Probert D.M.: "Prediction of Soot and Nitric Oxide Concentrations in Diesel Engine Exhaust," *Proceedings of the I MECH E Part C: Journal of Air Pollution in Transport Engines*, vol. 142, pp. 205-217, 1971.
- [58] Kitamura T., Senda J., and Fujimoto H.: "Mechanism of Smokeless Diesel Combustion With Oxygenated Fuels Based on the Dependence of the Equivalence Ratio and Temperature on Soot Particle Formation," *International Journal of Engine Research*, vol. 3, pp. 223-248, 2002.
- [59] Koch T.: *Numerischer Beitrag zur Charakterisierung und Vorausberechnung der Gemischbildung und Verbrennung in einem direkteingespritzten, strahlgeführten Ottomotor*, Ph.D. Thesis, ETH Zürich, Nr. 14937, 2002.
- [60] Koza J.R.: *Genetic Programming: On the Programming of Computers by Means of Natural Selection*, The MIT Press, Cambridge MA, 1992.
- [61] Küng M., et al.: "LES of Turbulent Jet Flames Using the Approximate Deconvolution Model," *European Combustion Meeting*, Louvain-la-Neuve, Belgium, 2005.
- [62] Lämmle C.: *Numerical and Experimental Study of Flame Propagation and Knock in a Compressed Natural Gas Engine*, Ph.D. Thesis, ETH Zürich, Nr. 16362, 2005.
- [63] Lee K.B., Thring M.W., and Beéra J.M.: "On the Rate of Combustion of Soot in a Laminar Soot Flame," *Combustion and Flame*, vol. 6, pp. 137-145, 1962.
- [64] MacLean H.L. and Lave L.B.: "Evaluating Automobile Fuel/Propulsion System Technologies," *Progress in Energy and Combustion Science*, vol. 29, pp. 1-69, 2003.
- [65] Magnussen B.F. and Hjertager B.H.: "On Mathematical Modeling of Turbulent Combustion with Special Emphasis on Soot Formation and Combustion," *16<sup>th</sup> Symposium (International) on Combustion*, pp. 719-729, 1976.
- [66] The MathWorks Inc.: *Neural Network Toolbox User's Guide (For Use with MATLAB<sup>®</sup>)*, Demuth H. and Beale M. (eds.), v 4.0.5, 2005.
- [67] Merker G.P., et al.: *Verbrennungsmotoren - Simulation der Verbrennung und Schadstoffbildung*, 2. Auflage, Teubner Verlag, Stuttgart, 2004.
- [68] Miller J.A. and Bowman C.T.: "Mechanism and Modeling of Nitrogen Chemistry in Combustion," *Progress in Energy and Combustion Science*, vol. 15, pp. 287-338, 1989.

- 
- [69] Müller S.D.: *Bio-Inspired Optimization Algorithms for Engineering Applications*, Ph.D. Thesis, ETH Zürich, Nr. 14719, 2002.
- [70] NIST/Sematech: *e-Handbook of Statistical Methods*, Cambridge, 2005.
- [71] Nußelt W.: *Der Wärmeübergang in der Verbrennungskraftmaschine*, Heft 264, Verlag des Vereines deutscher Ingenieure, Berlin, 1923.
- [72] Obrecht P.: *WEG (Benutzerhandbuch und Programmdokumentation)*, LAV, ETH Zürich, 2005.
- [73] Ouenou Gamo S., Ouladsine M., and Rachid A.: “Diesel Engine Exhaust Emissions Modeling Using Artificial Neural Networks,” *SAE paper 1999-01-1163*, 1999.
- [74] Papadimitriou I., et al.: “Neural Network-Based, Fast-Running Engine Models for Control-Oriented Applications,” *SAE paper 2005-01-0072*, 2005.
- [75] Payri F., et al.: “Influence of Measurement Errors and Estimated Parameters on Combustion Diagnosis,” *Applied Thermal Engineering*, In Press, Corrected Proof, Online Available, 1 July 2005.
- [76] Peters N.: “Laminar Diffusion Flamelet Models in Non-Premixed Turbulent Combustion,” *Progress in Energy and Combustion Science*, vol. 10, pp. 319-339, 1984.
- [77] Pilley A.D., et al.: “Design of Experiments for Optimization of Engines to Meet Future Emissions Targets,” *27<sup>th</sup> International Symposium on Advanced Transportation Applications*, pp. 1-22, 1994.
- [78] Pohlheim H.: *Evolutionäre Algorithmen - Verfahren, Operatoren, Hinweise aus der Praxis*, Springer-Verlag, Berlin, 1999.
- [79] Rakopoulos C.D., Rakopoulos D.C., and Kyritsis D.C.: “Development and Validation of a Comprehensive Two-Zone Model for Combustion and Emissions Formation in a DI Diesel Engine,” *International Journal of Energy Research*, vol. 27, pp. 1221-1249, 2003.
- [80] Rask E. and Sellnau M.: “Simulation-Based Engine Calibration: Tools, Techniques, and Applications,” *SAE paper 2004-01-1264*, 2004.
- [81] Rechenberg I.: *Evolutionstrategie'94*, Frommann-Holzboog, Stuttgart, 1994.
- [82] Rhodes D.B. and Keck J.C.: “Laminar Burning Speed Measurements of Indolene-Air-Diluent Mixtures At High Pressures and Temperatures,” *SAE paper 850047*, 1985.
- [83] Schänzlin K.: *Experimenteller Beitrag zur Charakterisierung der Gemischbildung und Verbrennung in einem direkteingespritzten, strahlgeführten Ottomotor*, Ph.D. Thesis, ETH Zürich, Nr. 14939, 2002.



- 
- [84] Schreiner K.: "Der Polygon-Hyperbel-Ersatzbrennverlauf: Untersuchungen zur Kennfeldabhängigkeit der Parameter," *5<sup>th</sup> Symposium "Der Arbeitsprozess des Verbrennungsmotors"*, pp. 239-257, 1995.
- [85] Schröder A.: *Vorschlag einer Methode zur Berechnung der Stickoxid-Emission von Dieselmotoren*, Ph.D. Thesis, TU Braunschweig, 1975.
- [86] Schubert C., Wimmer A., and Chmela F.: "Advanced Heat Transfer Model for CI Engines," *SAE paper 2005-01-0695*, 2005.
- [87] Schubiger R.A.: *Untersuchungen zur Rußbildung und -oxidation in der dieselmotorischen Verbrennung: Thermodynamische Kenngrößen, Verbrennungsanalyse und Mehrfarbenendoskopie*, Ph.D. Thesis, ETH Zürich, Nr. 14445, 2002.
- [88] Schubiger R., Boulouchos K., and Eberle M.: "Rußbildung und Oxidation bei der dieselmotorischen Verbrennung," *Motortechnische Zeitschrift (MTZ)*, vol. 63, pp. 342-353, 2002.
- [89] Schwefel H.-P.: *Evolution and Optimum Seeking*, John Wiley & Sons, Inc., New York, 1995.
- [90] Senecal P.K., Pomraning E., and Richards K.J.: "Multi-Mode Genetic Algorithm Optimization of Combustion Chamber Geometry for Low Emissions," *SAE paper 2002-01-0958*, 2002.
- [91] Stiesch G., et al.: "Möglichkeiten und Anwendung der phänomenologischen Modellbildung im Dieselmotor," *Motortechnische Zeitschrift (MTZ)*, vol. 60, pp. 274-283, 1999.
- [92] Stiesch G.: *Modeling Engine Spray and Combustion Processes*, Springer-Verlag, Berlin Heidelberg, 2003.
- [93] Tan P.-Q., Deng K., and Lu J.-X.: "Predicting PM Emissions from Direct Injection Diesel Engines Using a Phenomenological Model," *Journal of the Energy Institute*, vol. 77, pp. 68-75, 2004.
- [94] Tao F., et al.: "Current Status of Soot Modeling Applied to Diesel Combustion Simulations," *6<sup>th</sup> International Symposium on Diagnostics and Modeling of Combustion in Internal Combustion Engines*, pp. 151-158, 2004.
- [95] Thiel M.P., Klingbeil A.E., and Reitz R.D.: "Experimental Optimization of a Heavy-Duty Diesel Engine Using Automated Genetic Algorithms," *SAE paper 2002-01-0960*, 2002.
- [96] Traver M.L., Atkinson R.J., and Atkinson C.M.: "Neural Network-Based Diesel Engine Emissions Prediction Using In-Cylinder Combustion Pressure," *SAE paper 1999-01-1532*, 1999.

- 
- [97] Van Veldhuizen D.A. and Lamont G.B.: "Multiobjective Evolutionary Algorithms: Analyzing the State-of-the-Art," *Evolutionary Computation*, vol. 8, pp. 125-147, 2000.
- [98] Vibe I.I.: *Brennverlauf und Kreisprozess von Verbrennungsmotoren*, VEB Verlag Technik, Berlin, 1970.
- [99] Warth M., et al.: "Vorausberechnung von Brennverlauf, NO- und Russemissionen beim Dieselmotor – Optimierung und Validierung eines neuen Ansatzes," *9<sup>th</sup> Symposium "Der Arbeitsprozess des Verbrennungsmotors"*, pp. 115-133, 2003.
- [100] Warth M., et al.: "Predictive Phenomenological C.I. Combustion Modelling - Optimization on the Basis of Bio-Inspired Algorithms," *SAE paper 2005-01-1119*, 2005.
- [101] Weisser G.A. and Boulouchos K.: "NOEMI - Ein Werkzeug zur Vorabschätzung der Stickoxidemissionen direkteinspritzender Dieselmotoren," *5<sup>th</sup> Symposium "Der Arbeitsprozess des Verbrennungsmotors"*, pp. 23-50, 1995.
- [102] Weisser G.A.: *Modelling of Combustion and Nitric Oxide Formation for Medium-Speed DI Diesel Engines: A Comparative Evaluation of Zero- and Three-Dimensional Approaches*, Ph.D. Thesis, ETH Zürich, Nr. 14465, 2002.
- [103] Wimmer A. and Glaser J.: *Indizieren am Verbrennungsmotor - Anwenderhandbuch*, AVL List GmbH, Graz, 2002.
- [104] Wolpert D.H. and Macready W.G.: "No Free Lunch Theorems for Search," *Santa Fe Institute Reports*, SFI-TR-95-02-010, 1995.
- [105] Wolpert D.H. and Macready W.G.: "No Free Lunch Theorems for Optimization," *IEEE Transactions on Evolutionary Computation*, vol. 1, pp. 67-82, 1997.
- [106] Woschni G.: "Universally Applicable Equation for the Instantaneous Heat Transfer Coefficient in the Internal Combustion Engine," *SAE paper 670931*, 1967.
- [107] Wright Y.M.: *Numerical Investigation of Turbulent Spray Combustion with Conditional Moment Closure*, Ph.D. Thesis, ETH Zürich, Nr. 16386, 2005.
- [108] Zacharias F.: *Analytische Darstellung der thermodynamischen Eigenschaften von Verbrennungsgasen*, Ph.D. Thesis, TU Berlin, 1966.
- [109] Zeldovich Y.A.: "The Oxidation of Nitrogen in Combustion and Explosions," *Acta Physicochimica*, vol. 21, pp. 577-628, 1946.

# A APPENDIX

## A.1 Operating Conditions

### A.1.1 “Automotive” Diesel

	#	$c_m$ [m/s]	BMEP [bar]	$p_{Inj}$ [bar]	$SOI_{pilot}$ [°CA]	$SOI_{main}$ [°CA]	EGR [%]
“CALIBRATION”	1	3.101	0.99	380	351.3	361.0	41.79
	2	3.097	9.99	538	326.3	353.0	0.28
	3	3.874	1.50	410	348.7	359.6	38.92
	4	3.874	13.01	747	320.2	353.9	0.17
	5	4.650	2.01	435	347.8	359.2	32.44
	6	4.650	10.00	660	329.5	354.5	0.42
	7	5.426	0.99	440	345.8	357.8	41.23
	8	5.426	11.01	891	323.2	354.6	0.41
	9	6.199	3.00	498	342.6	356.4	24.36
	10	6.975	3.00	492	341.5	355.8	14.06
	11	6.975	12.98	1121	318.0	350.5	0.38
	12	7.751	3.00	520	338.6	353.2	14.91
	13	7.751	10.00	962	318.2	353.7	5.09
	14	8.524	1.50	459	337.7	349.5	0.95
	15	9.304	9.01	960	318.3	350.5	0.38
	16	10.076	12.98	1349	317.0	347.6	0.36
	17	10.849	6.00	783	320.8	349.5	0.46
	18	10.849	14.00	1553	317.0	345.8	0.38
	19	10.849	11.00	1243	317.0	348.7	0.39
	20	12.401	14.00	1600	0.0	339.0	0.46
“VERIFICATION”	21	3.101	0.50	380	351.5	360.9	44.40
	22	3.101	2.00	381	349.6	361.3	30.07
	23	3.097	6.98	449	339.4	355.7	5.93
	24	3.874	5.00	444	343.8	360.4	13.28
	25	3.874	13.59	800	318.7	354.4	0.16
	26	4.650	7.00	545	337.4	358.9	9.56
	27	4.650	12.99	878	321.7	353.6	0.22
	28	5.426	3.02	482	344.5	358.4	26.22
	29	5.426	4.00	532	342.0	358.4	19.24
	30	5.426	8.00	734	330.6	357.1	12.52

Tab. A.1 Automotive Diesel Operating Conditions

... continued on next page

#	$c_m$ [m/s]	BMEP [bar]	$p_{Inj}$ [bar]	$SOI_{pilot}$ [°CA]	$SOI_{main}$ [°CA]	EGR [%]
31	5.426	9.00	804	326.7	356.0	11.35
32	5.426	10.01	838	325.0	355.4	11.32
33	5.426	15.00	1189	317.4	353.8	0.25
34	6.199	4.00	567	339.7	356.8	19.16
35	6.199	9.00	869	321.3	356.6	16.70
36	6.199	10.00	913	320.0	356.0	16.48
37	6.199	11.00	957	319.7	354.8	11.10
38	6.199	12.99	1101	318.7	352.3	0.37
39	6.199	14.00	1174	318.1	352.2	0.33
40	6.199	18.11	1504	317.0	354.2	0.26
41	6.975	7.00	748	327.9	356.3	20.01
42	6.975	8.00	854	321.4	356.3	19.36
43	6.975	9.00	940	319.0	355.9	17.79
44	6.975	10.00	984	318.6	354.3	17.41
45	6.975	11.00	1004	318.4	353.6	5.79
46	6.975	12.00	1044	318.2	352.3	0.46
47	7.751	9.01	930	318.9	354.2	10.05
48	8.524	3.01	523	336.7	350.2	0.64
49	8.524	5.00	671	331.7	351.9	0.48
50	8.524	8.00	842	322.0	352.6	0.38
51	10.076	1.49	497	330.6	347.3	1.00
52	10.849	1.01	468	329.8	345.8	1.19
53	10.849	2.01	508	325.8	346.2	0.87
54	10.849	3.50	576	323.3	348.1	0.62
55	11.625	15.01	1600	0.0	341.2	0.44
56	13.020	0.50	499	318.2	342.3	1.20
57	13.020	1.50	556	317.0	343.6	0.90

"VERIFICATION"

Tab. A.1 Automotive Diesel Operating Conditions (cont.)

A.1.2 “Heavy-Duty” Diesel

	#	$c_m$ [m/s]	BMEP [bar]	$P_{Inj}$ [bar]	SOI [°CA]	EGR [%]
“CALIBRATION” / “TRAINING”	1	5.944	4.91	1400	356	0
	2	5.936	4.95	1400	356	23
	3	5.936	4.85	1400	356	36
	4	5.936	4.91	400	350	0
	5	5.936	4.89	700	350	0
	6	5.938	4.86	1000	350	0
	7	5.941	4.94	500	346	0
	8	5.944	4.95	500	352	0
	9	5.944	4.94	500	357	0
	10	5.938	9.81	1400	356	0
	11	7.333	9.94	1400	356	0
	12	8.702	8.88	1400	356	0
	13	8.696	4.40	1400	356	0
	14	8.707	13.29	1400	356	0
	15	8.699	8.79	1600	352	0
	16	5.944	4.93	350	357	0
	17	7.319	4.97	1000	352	0
	18	8.702	4.35	1400	356	27
	19	8.707	13.26	1400	356	7
“VERIFICATION”	20	5.947	4.94	350	357	0
	21	5.947	4.79	1400	356	0
	22	5.947	4.92	1400	356	41
	23	7.350	9.91	1000	352	0
	24	7.322	9.91	1000	352	0
	25	7.324	9.94	700	352	0
	26	7.324	9.87	1000	348	0
	27	7.324	9.95	1000	356	0
	28	7.322	9.89	1400	356	6
	29	7.322	4.97	700	352	0
	30	7.319	4.97	700	352	0
	31	5.941	9.86	1000	352	0
	32	8.699	8.84	1000	352	0
	33	5.936	4.91	400	350	0
	34	5.938	4.91	500	350	0
	35	5.936	4.90	350	356	0
	36	5.938	4.89	1400	356	30
	37	8.693	4.40	1400	356	17
	38	8.699	8.82	1400	356	10
	39	8.707	13.24	1400	356	7

Tab. A.2 Heavy-Duty Diesel Operating Conditions

APPENDIX

	#	$c_m$ [m/s]	BMEP [bar]	$p_{inj}$ [bar]	SOI [°CA]	EGR [%]	$\mu_{H_2O}$ [%]	$\mu_{O_2}$ [%]	
"CALIBRATION"	1	I	5.933	4.88	500	346	0	0	0
	2	II	5.933	4.91	500	352	0	0	0
	3	III	5.936	4.93	1100	356	0	0	0
	4	IV	5.936	4.92	1100	356	43	0	0
	5	V	5.936	4.91	400	350	0	0	0
	6	VI	5.938	9.81	1400	356	0	0	0
	7	VII	8.702	8.88	1400	356	0	0	0
	8	VIII	7.319	4.97	1000	352	0	0	0
	9	XIX	5.936	4.82	560	346	0	12.89	10.15
	10	XX	5.938	4.88	1200	356	0	12.89	10.15
	11	XXI	5.941	9.86	1220	356	11	12.89	10.15
	12	XXII	5.950	19.64	1260	356	0	12.89	10.15
	13	XXVII	5.930	4.95	600	346	0	20.89	15.36
	14	XXVIII	5.930	4.91	600	352	0	20.89	15.36
	15	XXIX	5.930	4.95	600	346	0	20.89	15.36
	16	XXX	5.927	4.92	1300	356	0	20.89	15.36
	17	XXXIV	5.933	4.96	1300	356	0	0	11.98
	18	XXXV	5.933	5.04	1300	356	38	0	11.98
	19	XXXVI	5.938	9.77	1270	356	15	0	11.98
	20	XXXVII	5.933	4.96	1300	356	0	0	11.98
"VERIFICATION"	21	IX	5.944	4.93	350	357	0	0	0
	22	X	5.936	4.91	400	350	0	0	0
	23	XI	5.938	4.91	500	350	0	0	0
	24	XII	5.947	4.92	1400	356	41	0	0
	25	XIII	5.941	9.89	1100	356	0	0	0
	26	XIV	5.944	9.78	1100	356	0	0	0
	27	XV	5.950	19.53	1100	356	0	0	0
	28	XVI	7.350	9.91	1000	352	0	0	0
	29	XVII	8.699	8.84	1000	352	0	0	0
	30	XVIII	8.699	8.82	1400	356	10	0	0
	31	XXIII	5.938	4.98	500	352	0	12.89	10.15
	32	XXIV	5.938	4.92	560	352	0	12.89	10.15
	33	XXV	5.941	9.79	1220	356	0	12.89	10.15
	34	XXVI	5.947	14.70	1220	356	0	12.89	10.15
	35	XXXI	5.930	4.95	600	346	0	20.89	15.36
	36	XXXII	5.930	4.91	600	352	0	20.89	15.36
	37	XXXIII	5.927	4.92	1300	356	0	20.89	15.36
	38	XXXVIII	5.930	5.07	610	352	0	0	11.98
	39	XXXIX	5.933	4.96	1300	356	0	0	11.98
	40	XL	5.923	5.05	1300	356	37	0	11.98

Tab. A.3 Heavy-Duty Advanced Fuels Survey Operating Conditions

A.1.3 “Marine” Diesel

	#	$c_m$ [m/s]	BMEP [bar]	$P_{inj}$ [bar]	SOI <sup>(a)</sup> [a.u.]	EGR [%]
“CALIBRATION”	1	7.683	15.70	1100	6.13	0
	2	7.683	15.70	800	2.58	0
	3	7.683	15.70	450	-3.87	0
	4	8.456	19.02	1000	2.90	0
	5	8.456	19.02	600	-2.26	0
	6	5.315	7.55	800	5.16	0
	7	5.315	7.55	450	-2.90	0
	8	7.683	15.70	1000	-1.29	0
	9	7.683	15.70	1100	-6.77	0
	10	7.683	15.70	450	-16.77	0
	11	6.716	11.98	1000	10.00	0
	12	6.716	11.98	600	0.65	0
“VERIFICATION”	13	7.683	15.70	1000	5.16	0
	14	7.683	15.70	600	-0.65	0
	15	8.456	19.02	800	0.00	0
	16	5.315	7.55	1000	7.42	0
	17	5.315	7.55	600	2.58	0
	18	7.683	15.70	1100	-0.32	0
	19	7.683	15.70	800	-3.87	0
	20	7.683	15.70	600	-7.10	0
	21	7.683	15.70	450	-10.32	0
	22	7.683	15.70	1000	-7.74	0
	23	7.683	15.70	800	-10.32	0
	24	7.683	15.70	600	-13.55	0
	25	6.716	11.98	800	7.10	0
	26	6.716	11.98	450	-3.87	0

Tab. A.4 Marine Diesel Operating Conditions

a. Normalized Time (Reference Operating Condition # 15: SOI = 0 and  $\phi_{90} = 100$ )

## A.2 Kinetics of NO Formation

The kinetic data refer to the standard Arrhenius rate constant formulation

$$k_{Arr} = A \cdot T^b \cdot \exp\left[\frac{-E_A}{\mathfrak{R}T}\right] \quad (\text{A.1})$$

where  $E_A$  is the activation energy in [J/mole],  $A$  is the frequency or preexponential factor [(m<sup>3</sup> · K<sup>b</sup>)/(mole · s)],  $\mathfrak{R} = 8.314472$  [J/(mole · K)] is the universal gas constant and  $b$  the dimensionless temperature exponent.

	PATTAS	WRAY	BAULCH BRACCO	URLAUB	HEYWOOD
<i>O + N<sub>2</sub> ↔ NO + N</i>					
$A_{\text{fwd}}$	4.93 · 10 <sup>7</sup>	7.00 · 10 <sup>7</sup>	1.36 · 10 <sup>8</sup>	1.30 · 10 <sup>8</sup>	7.60 · 10 <sup>7</sup>
$A_{\text{rev}}$	1.60 · 10 <sup>7</sup>	1.55 · 10 <sup>7</sup>	3.10 · 10 <sup>7</sup>	2.80 · 10 <sup>7</sup>	1.60 · 10 <sup>7</sup>
$b_{\text{fwd}}$	0.0472	0	0	0	0
$b_{\text{rev}}$	0	0	0	0	0
$E_{\text{Afwd}}$	316'480	316'100	315'680	317'850	316'000
$E_{\text{Arev}}$	0	0	1'400	0	0
<i>N + O<sub>2</sub> ↔ NO + O</i>					
$A_{\text{fwd}}$	1.48 · 10 <sup>2</sup>	1.33 · 10 <sup>4</sup>	6.40 · 10 <sup>3</sup>	6.40 · 10 <sup>3</sup>	6.40 · 10 <sup>3</sup>
$A_{\text{rev}}$	1.25 · 10 <sup>1</sup>	3.20 · 10 <sup>3</sup>	1.50 · 10 <sup>3</sup>	1.50 · 10 <sup>3</sup>	1.50 · 10 <sup>3</sup>
$b_{\text{fwd}}$	1.50	1.0	1.0	1.0	1.0
$b_{\text{rev}}$	1.612	1.0	1.0	1.0	1.0
$E_{\text{Afwd}}$	23'780	29'640	26'170	26'150	26'150
$E_{\text{Arev}}$	157'800	163'700	161'780	163'250	163'250
<i>N + OH ↔ NO + H</i>					
$A_{\text{fwd}}$	4.22 · 10 <sup>7</sup>	4.00 · 10 <sup>7</sup>	4.20 · 10 <sup>7</sup>	4.20 · 10 <sup>7</sup>	4.10 · 10 <sup>7</sup>
$A_{\text{rev}}$	6.76 · 10 <sup>8</sup>	1.30 · 10 <sup>8</sup>	1.30 · 10 <sup>8</sup>	1.30 · 10 <sup>8</sup>	2.00 · 10 <sup>8</sup>
$b_{\text{fwd}}$	0	0	0	0	0
$b_{\text{rev}}$	-0.212	0	0	0	0
$E_{\text{Afwd}}$	0	0	0	0	0
$E_{\text{Arev}}$	206'580	190'100	190'100	190'100	196'600

Tab. A.5 Rate Constants for the NO Formation Mechanism



### A.3 Correlation & Linear Regression Statistics

		GAOPT	EAOPT	CMA-ES	GADS
<i>Error Function</i>	$f_{Err}$	11854	11336	13124	15585
	$r$	0.9100	0.9523	0.9562	0.9384
<i>Start of Combustion</i>	$m$	0.9167	1.0363	1.1238	0.9776
	$b$	2.99	-1.29	-4.43	0.81
$\varphi_{SOC}$	$r$	0.9224	0.9357	0.8592	0.9340
	$m$	1.0085	0.9562	1.0243	1.0453
	$b$	-0.30	1.57	-0.83	-1.66
<i>10% Heat Release</i>	$r$	0.9098	0.9268	0.7677	0.8252
	$m$	1.0126	0.9437	0.7889	0.8097
	$b$	-0.46	2.05	7.80	6.99
$\varphi_{10}$	$r$	0.7648	0.8272	0.5513	0.7322
	$m$	0.8939	0.8020	0.6066	0.7379
	$b$	4.17	7.73	15.92	10.79
<i>50% Heat Release</i>	$r$	0.6426	0.7117	0.6403	0.4984
	$m$	1.0087	0.7455	0.7539	0.5765
	$b$	0.79	2.01	2.02	3.45
$\varphi_{50}$	$r$	0.8540	0.8383	0.6932	0.6812
	$m$	0.7955	0.7748	0.7176	0.6172
	$b$	7.60	8.37	10.53	14.19
<i>90% Heat Release</i>	$r$	0.6426	0.7117	0.6403	0.4984
	$m$	1.0087	0.7455	0.7539	0.5765
	$b$	0.79	2.01	2.02	3.45
$\varphi_{90}$	$r$	0.8540	0.8383	0.6932	0.6812
	$m$	0.7955	0.7748	0.7176	0.6172
	$b$	7.60	8.37	10.53	14.19
<i>Maximum ROHR</i>	$r$	0.8540	0.8383	0.6932	0.6812
	$m$	0.7955	0.7748	0.7176	0.6172
	$b$	7.60	8.37	10.53	14.19
$ dQ/d\varphi _{\max}$	$r$	0.8540	0.8383	0.6932	0.6812
	$m$	0.7955	0.7748	0.7176	0.6172
	$b$	7.60	8.37	10.53	14.19
<i>Position max. ROHR</i>	$r$	0.8540	0.8383	0.6932	0.6812
	$m$	0.7955	0.7748	0.7176	0.6172
	$b$	7.60	8.37	10.53	14.19
$\varphi(dQ/d\varphi)_{\max}$	$r$	0.8540	0.8383	0.6932	0.6812
	$m$	0.7955	0.7748	0.7176	0.6172
	$b$	7.60	8.37	10.53	14.19

Tab. A.6 Comparative Algorithm Study Statistics :  
( $r$ ) Pearson's Correlation Coefficient, ( $m$ ) Linear Regression Slope and ( $b$ ) Linear Regression Intercept

		$\varphi_{SOC}$	$\varphi_{10}$	$\varphi_{50}$	$\varphi_{90}$	
<i>Optimized</i>	<i>Pearson's Correlation Coefficient <math>r</math></i>	[-]	0.9959	0.9683	0.9775	0.8432
	<i>Linear Regression Slope <math>m</math></i>	[-]	1.02	0.98	0.91	0.98
	<i>Linear Regression Intercept <math>b</math></i>	[-]	0.06	0.35	0.90	0.55
<i>Blind</i>	<i>Pearson's Correlation Coefficient <math>r</math></i>	[-]	0.9948	0.9912	0.9164	0.8025
	<i>Linear Regression Slope <math>m</math></i>	[-]	1.03	0.99	0.96	0.74
	<i>Linear Regression Intercept <math>b</math></i>	[-]	-0.14	-1.88	-2.95	-3.12
<i>Adjusted</i>	<i>Pearson's Correlation Coefficient <math>r</math></i>	[-]	0.9951	0.9624	0.8690	0.8295
	<i>Linear Regression Slope <math>m</math></i>	[-]	1.02	0.92	0.87	1.01
	<i>Linear Regression Intercept <math>b</math></i>	[-]	-0.12	0.35	1.21	0.69

Tab. A.7 Marine Diesel Engine ROHR Model Statistics for the EA Optimized, the Heavy-Duty Blind Try, and the Adjusted Case

## A.4 Cylinder Pressures

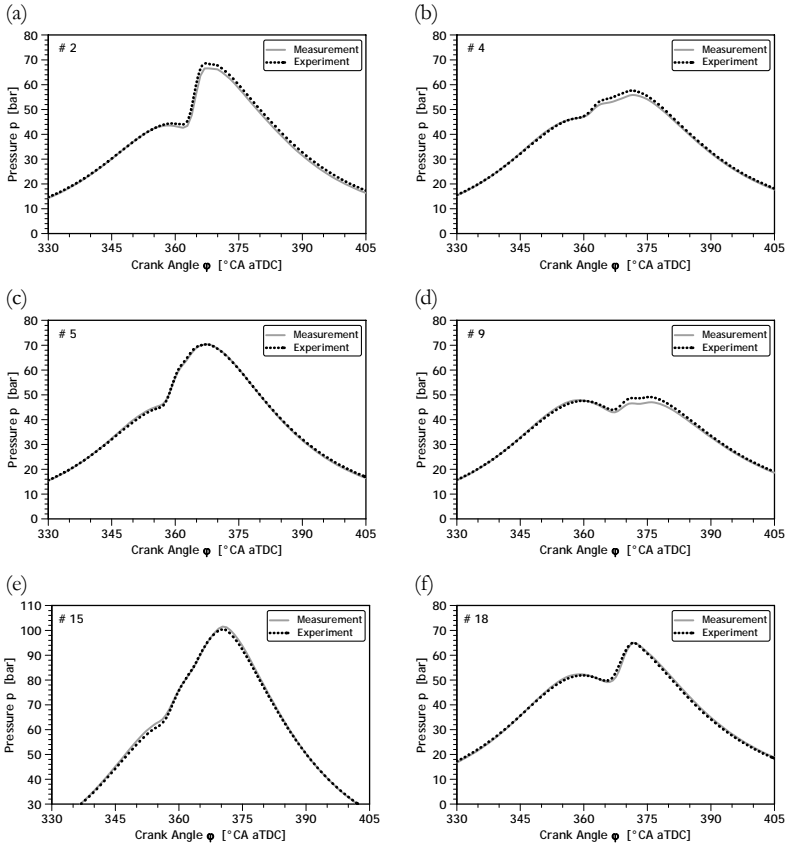


Fig. A.1 Comparison of Measured and Numerical Cylinder Pressures for Six Selected Heavy-Duty Diesel Operating Conditions; (a) # 2, (b) # 4, (c) # 5, (d) # 9, (e) # 15, and (f) # 18

# *CURRICULUM VITAE*

## *Personal Data*

Name: Marco Warth  
Date of Birth: April 10<sup>th</sup>, 1976  
Hometown(s): Ruswil and Gunzwil, LU

## *Education*

1983 - 1989 Primary School, Ruswil LU  
1989 - 1996 Secondary School, Willisau & Sursee LU  
*Matura Typus C*  
1997 - 2002 Diploma Studies in Mechanical Engineering  
ETH Zurich  
*Topics: IC Engines & Composites Technologies*

## *Career Development*

01.1997 - 10.1997 SF Emmen, Bereich Flugzeuge und Drohnen  
*Internship*  
01.1997 - 10.2001 Securitas AG, Direktion Luzern  
*Security*  
11.2001 - 05.2002 Daimler-Chrysler AG, Research and Technology  
*Diploma Thesis and Internship*  
06.2002 - present Aerothermochemistry and Combustion Systems Laboratory  
(LAV), Institute of Energy Technology, ETH Zurich  
*Research Associate and Ph.D. Student*

## *Military Service*

06.1996 - 10.1996 Basic Military Service (Rekrutenschule)  
*Pioneer*



*“All models are wrong. Some are useful.”*

George E. P. Box, Professor of Statistics, University of Wisconsin